Rheology and drying characteristics of sludge in the region of Liege

Auteur : Al Sayed, Mohamad Wael
Promoteur(s) : Léonard, Angélique
Faculté : Faculté des Sciences appliquées
Diplôme : Master : ingénieur civil en chimie et science des matériaux, à finalité spécialisée en Chemical Engineering
Année académique : 2022-2023
URI/URL : http://hdl.handle.net/2268.2/18322

University of Liege

Faculty of applied sciences

Year 2022-2023

Rheology and drying characteristics of sludge in the region of Liege

Master Thesis

Partial fulfilment of the requirements for the Master's degree in:

Chemical Engineering And Materials Sciences

Student:

AL SAYED Mohamad Wael

Professors and Supervisors:

LÉONARD Angélique

PARRA ANGARITA Sergio

August 2023

Acknowledgement

I am pleased to express my sincere gratitude to Prof. Leonard Angelique and Mr. Parra Angarita Sergio for their constructive support, orientation, and contributions throughout the completion of this master's thesis. Prof. Leonard Angelique, your extraordinary expertise, and delightful feedback have been distinctive in shaping my thesis. Your academic excellence and your willingness to continuously give away knowledge enriched my understanding of the topic. I am deeply grateful not just for reviewing my work, refining my ideas, and providing suggestions but also for all your efforts and contribution to my overall academic education. Mr. Parra Angarita Sergio, I am incredibly thankful for your support, encouragement, and care throughout the thesis journey. Your practical insights, and unique willingness to share your experiences have been instrumental in expanding my knowledge and putting my research methodology, experiments, and analysis on track. Your enthusiasm and passion for the topic were nothing but a source of joy and motivation. I would like to thank Mr. Wathieu Andy, Mr. Piette Michel, and Mr. Remacle Stéphane, the responsible individuals of the wastewater stations considered in this thesis, for their cooperation and for facilitating sample gathering, as well as for their valuable insights.

Abstract

This study delves into the drying behavior and rheological properties of sludge in the Liege region, focusing on characterising essential parameters to contribute to the optimization of sludge management by understanding the influencing characteristics and properties. A series of experiments is conducted on sludge samples from wastewater treatment plants to explicate the diversity of sewage sludge in the Liege region, covering the possible factors that can alter sludge drying, and rheology such as origins, history of treatment, mechanical traits, and others. Five wastewater treatment stations in Liege were covered, each utilizing similar or different treatment and mechanical methods. Experiments cover dry matter content determination, volatile matter content analysis, convective micro-drying, convective macro-drying, texture profile analysis (TPA), penetrometry, volume and area change during drying, and amplitude sweep. The study contributes valuable insights into sludge behavior during drying and highlights parameters critical for effective sludge management. By characterizing properties such as adhesiveness, cohesiveness, hardness, viscoelastic and rheological behavior, relate them to the drying performance illustrated by the drying flux, duration and moisture content change. This research provides a contribution for a better future, adding knowledge to a field that still have rooms for optimization. The findings may empower wastewater treatment facilities to make decisions regarding sludge handling by presenting the impact of rheological and texture properties on the drying behavior, aiming to enhance operational efficiency, reduce environmental impacts, and align with sustainable waste management practices.

Résumé

Cette étude porte sur le comportement de séchage et les propriétés rhéologiques des boues dans la région Liègoise, dans le but de caractériser les paramètres essentiels pour contribuer à l'optimisation de la gestion des boues, en comprenant les caractéristiques et les propriétés sous-jacentes qui les influencent. Une série d'expériences est menée sur des échantillons de boues provenant de stations d'épuration afin d'expliquer la diversité des boues d'épuration dans la région de Liège, couvrant les facteurs possibles qui peuvent altérer le séchage et la rhéologie des boues, tels que les origines, l'historique du traitement, les caractéristiques mécaniques, etc. Cinq stations d'épuration des eaux usées de Liège ont été couvertes, chacune utilisant des méthodes de traitement et des méthodes mécaniques similaires ou différentes. Les expériences comprennent la détermination de la teneur en matière sèche, l'analyse de la teneur en matières volatiles, le micro-séchage convectif, le macro-séchage convectif, l'analyse du profil de texture (TPA), la pénétrométrie, le changement de volume et de surface pendant le séchage et le balayage d'amplitude. l'étude apporte des informations précieuses sur le comportement des boues pendant le séchage et met en évidence les paramètres critiques pour une gestion efficace des boues. En caractérisant les propriétés telles que l'adhésivité, la cohésion, la dureté, le comportement viscoélastique et rhéologique, on peut les relier à la gestion efficace des boues En caractérisant les propriétés telles que l'adhésivité, la cohésion, la dureté, le comportement viscoélastique et rhéologique, on les relie aux performances de séchage illustrées par le flux de séchage, le temps de séchage et le changement de surface des boues pendant le séchage.

Contents

List of Figures

List of Tables

1 Literature Review

1.1 Sewage sludge

Eight billion is the current population on earth, estimated to reach 8.5 billion in 2030 and ten billion in 2100 (United-Nations, 2022). Human being expansion, surge more urbanization. Consequently, higher water demand will be needed. Wastewater treatment resembles an important recycled source of "the life liquid" and a source of renewable energy. Sewage contains over 99 % of water. There exist three phases in which sewage can be found in a typical wastewater treatment plant. It is found in a liquid phase during pre-treatment, primary treatment, secondary treatment, Tertiary treatment and during thickening, coagulation and flocculation. It is only after mechanical dewatering, sludge is found in a pasty mud-like phase, and following thermal treatment, sludge becomes finally granular in a solid-like phase. To elaborate on this idea and understand the origin of the material of interest, figure 1 shows the different sludge phases during the treatment process and indicates at what stage the sewage becomes pasty sludge. Sewage becomes solid only after thermal drying, where granular sludge formation is due to water evaporation (Pambou, 2016).

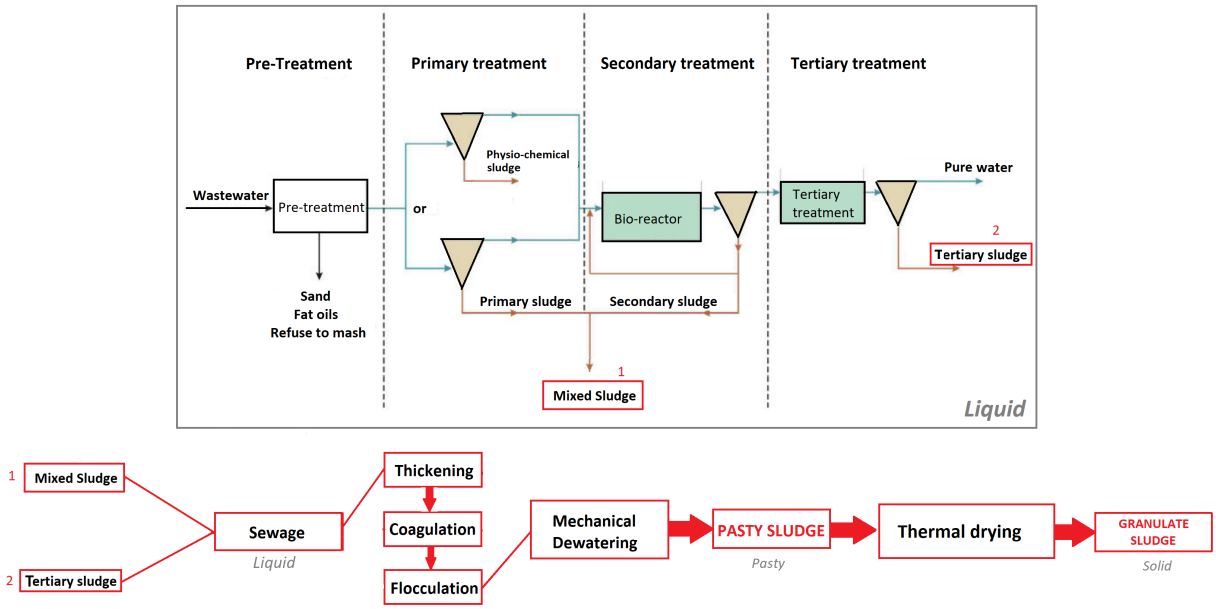

Figure 1: Pasty sludge source (Pambou, 2016)

Pasty sludge is neither a solid nor a liquid. In other words, it is a muddy material that still contains water. The magnified interest in the environment well being, along with the valorization of water and energy, urged sludge drying mainly to reduce the required storage volume, energy, costs, and pathogenic content (Andreoli et al., 2007). Figure 1 gives the general idea of the wastewater treatment process. However, Figure 2 gives a better example of a typical wastewater treatment facility, showing the different so-called sludge history treatments from collection to incineration, passing through thickening, stabilization, and water removal. The figure also shows the various stages at which sludge can be valuable such as the stage where nutrients can be recovered and the stage where sludge can be collected for agricultural use. Although, the di-

agram does not show the coagulation, flocculation, and liming stages. Coagulation and flocculation happen before filtration. The benefits of both additives are to improve dewatering, increase solid-liquid separation efficiency, enhance pollutants/pathogens removal, and reduce odors. Whereas, lime can be added during the treatment of primary sludge, which is obtained from the initial wastewater treatment, and during the treatment of secondary sludge, generated during the biological treatment phase. Lime serves to increase the pH level, diminish volatile characteristics, enhance the dewatering process, and minimize odor, pathogens, and volatile organic compounds (Đurđević et al., 2022).

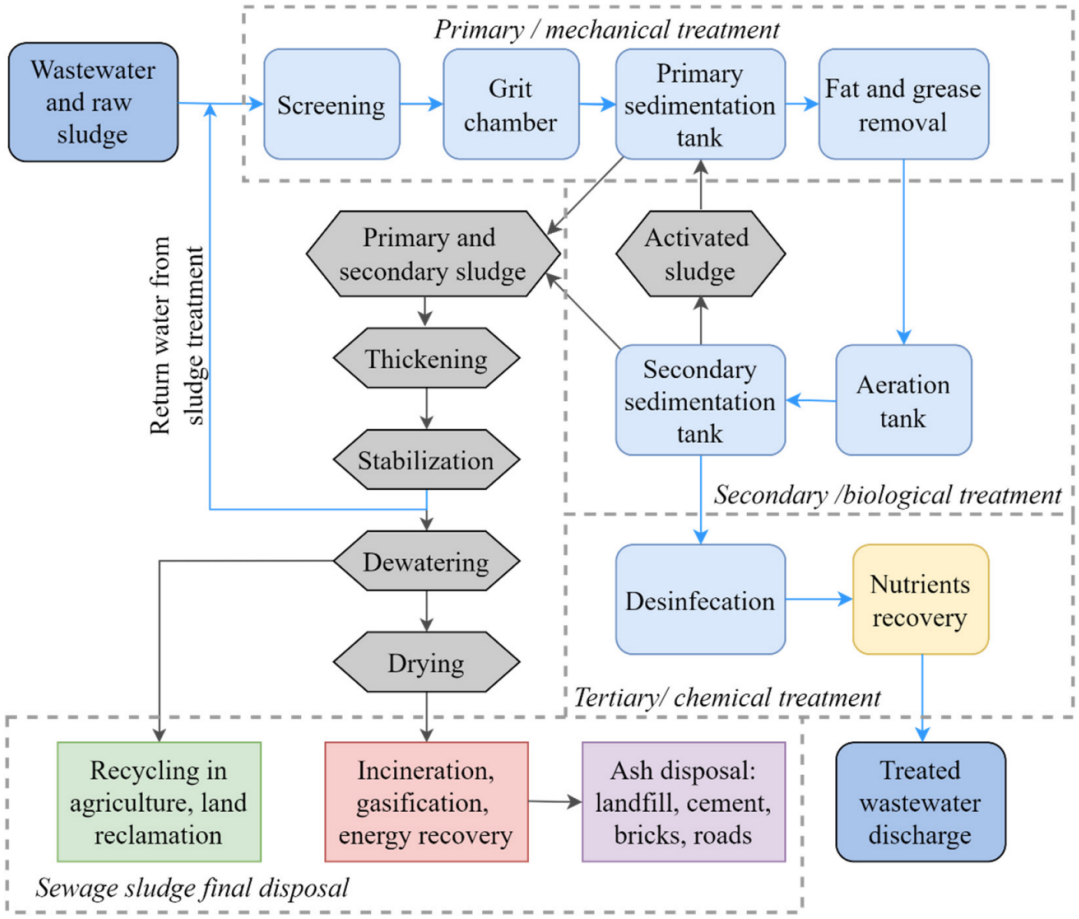

Figure 2: Pasty sludge source (Đurđević et al., 2022)

Sludge drying represents 1 % to 2 % of the post-treatment of wastewater. The attributed cost of drying adds up to 60 % of the operational cost. The nutrient-rich by-product of wastewater treatment typically contains 0.25 to 7 % solids by weight. When the residue follows adequate treatment, the result is a product often known as bio-solids. Bio-solids have many beneficial uses, such as cropland application, intending to improve soil quality due to the richness of nutrients and organic matter. Into the bargain, the possible use to improve soil drainage or as landfill cover. In conclusion, sludge is simply the byproduct of wastewater treatment. It is a mixture of organic matter derived from food, humans, and industries wastes, containing microorganisms and traces of inorganic matter. Table 1 represents the main elements contained in the

sludge. However, quantities vary depending on the sources and the treatment process (Turovskiy & Mathai, 2006). Although, Table 2 presents the findings of the physico-chemical composition and metal concentrations, along with their respective ranges of variation for a specific primary, and secondary municipal sludge. (Bennamoun et al., 2013).

Carbon	Hydrogen	Nitrogen	Oxygen	Phosphorus	Sulfur	Inorganic matters	Microorganisms

Table 1: Wastewater sludge main elements

Parameter	**Primary**	**Secondary**
Total solids (TS) (%)	3.0–7.0	0.5–2.0
Volatile solids (% of TS)	60–80	50–60
Nitrogen (N, % of TS)	1.5–4.0	2.4–5.0
Phosphorus ($P_2O_5, \%ofTS$)	0.8–2.8	0.5–0.7
Potash ($K_2O, \%ofTS$)	0–1.0	0.5–0.7
Heat value ($kJ.kg^{-1}$, dry basis)	23,000–30,000	18,500–23,000
pH	5.0–8.0	6.5–8.0
Alkalinity ($mg.l^{-1}$ as $CaCO_3$)	500–1,500	580–1,100
Metal contents ($mg.kg^{-1}db$)	**Range**	**Median**
Arsenic	1.1–230	10
Cadmium	1–3,410	10
Chromium	10–99,000	500
Copper	84–17000	800
Lead	13–26000	500
Mercury	0.6–56	6
Molybdenum	0.1–214	4
Nickel	2–5,300	80
Selenium	1.7–17.2	5
Zinc	101–49,000	1,700
Iron	1,000–154,000	17,000
Cobalt	11.3–2,490	30
Tin	2.6–329	14
Manganese	32–9870	26

Table 2: Specific sludge composition and characteristics (Bennamoun et al., 2013)

1.2 Sludge management

When it comes to sludge management different technologies exist, table 3 list the existing technologies based on the sludge treatment process (Mihelcic, 2019).

Treatment process	Technologies	Objective
Stabilization	Aerobic/anaerobic digestion and alkaline stabilization	Reduce odor, putrescence and pathogenic organisms. Using biological, chemical, and/or thermal processes, they minimize organic matter, water content, odors and pathogens
Thickening and dewatering	Lagoons, reed beds, drying beds, centrifugation, mechanical belt presses, thickening	Minimize sludge volume, increase solid concentration, stabilize dewatering, reduce pathogens
Others	Composting, heat drying, combustion	Reduce volume, kill pathogens, increase solid concentration

Table 3: Sludge management technologies (Mihelcic, 2019)

1.3 Wastewater treatment in Belgium

Belgium is in line with the sewage treatment legislation in Europe, having at about 95 % of the wastewater treatment, within the EU acceptable standards. This is well above the EU compliance average of 76 %. However, there is no accessible data for Belgium that shows the sewage sludge production statistics. Although, according to (Eurostat, 2023) all the European countries showed an increase in sludge production in the past years, due to the fact that more and more areas are being connected to the treatment networks. According to (European-Comission et al., 2019) over 158 tonnes of wastewater sludge were produced in Belgium in 2018. Also, industries and urban areas in Belgium generate up to 1.84 million m^3/day of wastewater. As wastewater needs to be treated prior to discharge to prevent environmental pollution, Belgium relies on a total of 399 treatment plants with 339 equipped for nitrogen and phosphorus removal as shown in Figure 3. Nitrogen and phosphorus removal are essential to prevent algal blooms and environmental harm. However, urban areas with less than 10,000 population equivalent (PE) are non-compulsory to remove nitrogen and

phosphorus before discharge. In terms of wastewater sludge management, Belgium reuses 31.3 % of the produced sludge with 20.5 % reuse in agriculture, incinerates 67.4 %, and disposes of 1.3 % in other manners (European-Comission et al., 2019).

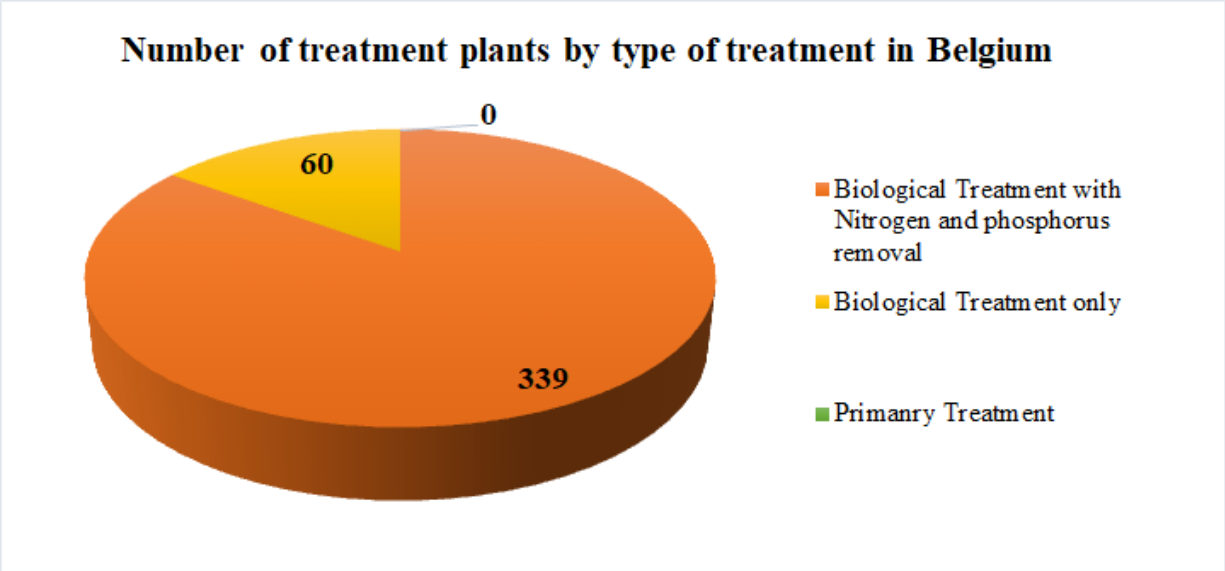

Figure 3: Number of treatment plants by type of treatment in Belgium

The wastewater treatment process contributes to the greenhouse effect. The CO_2 emission due to wastewater treatment was stabilized in Belgium since 2019, at a rate of 348 Kt CO_2 eq. This number was initially 517 Kt CO_2 eq in 2010, as shown in Figure 4. It is unexpected to see a further decrease or increase any time soon as the country is already in compliance with European legislation (European-Comission et al., 2019).

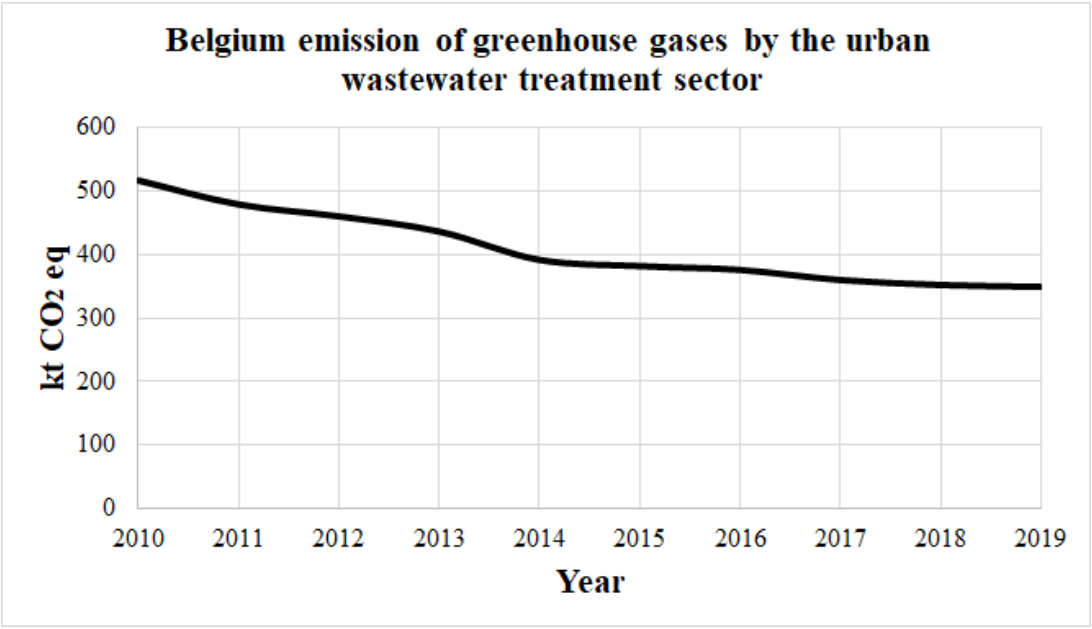

Figure 4: Belgium emission of greenhouse gases by the urban waste water treatment sector (European-Comission et al., 2019)

Within the European Union, approximately 45% of sludge is employed in agriculture either directly or after undergoing composting. This application often involves verifying its composition without any pre-

liminary processing. The secondary concern pertains to the process of incineration. (European-Comission et al., 2019).

1.4 Sludge hazards

Sludge hazards are manifested by the containment of contaminants such as heavy metals, chemicals, and pathogens. In this section, we will cover the environmental, vital, and hazardous dangers of sludge. Firstly, sludge imposes a flammability hazard. High moisture content sludge is less likely to burn. However, a lower moisture content with high organic content can pose a fire hazard (Manchester, 2017). Also, odor and nuisance are very common inconveniences when dealing with Sludge, due to the involved unpleasant odors resulting from the decomposition of organic matter, potentially causing discomfort to nearby communities if not properly managed. Moreover, minor physical hazards can be mentioned especially because sludge can be heavy and difficult to handle, causing falls, injuries from lifting, or equipment malfunctions. Adding to the flammability and physical hazards, sludge imposes concerns on health. Direct contact with untreated or poorly treated sludge might cause skin irritation, dermatitis, and chemical burns. In the case of skin absorption, the toxic substances present can lead to serious health issues. Inhalation is another type of exposure, dust or aerosols generated during sludge handling, drying, or incineration processes may contain hazardous substances and microorganisms. These particles can cause respiratory problems, allergies, and severe infections. Accidental ingestion can also lead to gastrointestinal issues, infections, and toxic chemical exposure (Dorn et al., 1985). From an environmental perspective, the impacts are represented firstly by eutrophication. Secondly, poorly treated or unwisely applied sludge provokes soil degradation, fertility reduction, pH imbalance, and heavy metals or organic pollutants contamination. Thirdly, improper sludge management, particularly during anaerobic decomposition or incineration, can release methane and carbon dioxide, contributing to climate change. Finally, discharging untreated sludge into natural environments can disrupt ecological balances, harm biodiversity, and negatively impact plants, animals, and microorganisms (Cabral et al., 1998). It is crucial to implement effective sludge treatment methods, adhere to regulations, and follow best practices in sludge management to minimize these hazards, protect human health, and reduce environmental impacts. It is crucial to value sludge to reduce the disposal cost, and the environmental impact, as well as to recycle water. Valorization can be done with different approaches, such as bio-gases production by an anaerobic or aerobic digestion process. This process transforms wastewater byproducts into a renewable source of energy and heat. Also, sludge thermal treatment, in which it is incinerated or subjected to processes like pyrolysis, and gasification leads yet again energy-rich products (Turovskiy & Mathai, 2006). Moreover, after sludge treatment and toxicants removal, resulting bio-solids rich in nutrients can be used as soil amendments to improve soil quality and aid in plant growth. Furthermore, extraction and preparation of plant growth essential nutrients can be realized (Grekhova & Gilmanova, 2016), such as phosphorus acid derived salts (fertilizer) obtained by acidic leaching phosphorus recovery (Shariff et al.,

2023). Also, in Wallonia, direct land application can be done with only a composition check conducted before utilization, without any preceding processing. Other uses can be mentioned, like extracting valuable metals and making construction materials.

1.5 Sludge drying

There is a difference between mechanical drying and thermal drying. Mechanical drying, like thickening and dewatering, is performed before thermal drying by mechanically removing moisture. While on the other hand, thermal drying is either conductive, convective, solar, or super-heated steam drying.

Thermal drying technologies

- Convective drying:

  Convective drying involves hot air or steam passing through the product, allows direct contact, and evaporation of the product water. Industrial-scale convective dryers can use direct or indirect heating through fossil fuel, biogas, biomass burners, heat exchangers, or a combination of these methods. For smaller-scale convective dryers, electrical resistances can be employed as heating sources. Industrial convective dryers include belt dryers, flash dryers, fluidized bed dryers, and rotary dryers, each with varying specific energy consumption and drying rates (Bennamoun et al., 2013).

- Conductive drying:

  Conductive drying involves heating the dryer's surface, which transfers heat to the sludge. Thermal oil or saturated steam is used as heating fluids, generated from boilers, fired with fossil fuel or biomass. The three dominant technologies are disc, paddle, and thin film dryers, with the rotor design playing a crucial role in sludge conveying (Bennamoun et al., 2013).

- Solar drying:

  Solar drying takes place in open or closed tunnel greenhouses, where solar radiation heats the surface, while the sludge maintains in a deep bed. Implemented ventilation helps to refresh the air inside, and in some cases, robots are engaged to manage the sludge, ensuring proper surface exchange and preventing crust formation (Bennamoun et al., 2013).

- Microwave drying:

  The MW sludge drying process improves drying rates, reduces energy consumption, and increases throughput capacity. It achieves this by extending the constant rate drying period, with higher output powers leading to increased sludge power absorption densities, resulting in faster drying and shorter exposure times. Operating the system at maximum output power maximizes MW generation efficiency (Kocbek et al., 2020).

- Hybrid drying:

  It is possible to couple different drying methods to create hybrid or combined dryers.

Aspects of thermal drying

The behavior of wastewater sludge during drying is complex, with phenomena such as shrinkage and cracks observed during convective drying. Commonly, imaging techniques are employed to monitor these phenomena intensity (Bennamoun et al., 2013). The benefit of drying is to reduce the sludge water content and decrease its size, therefore minimizing the disposal cost and land occupation. Moisture lessens and increases the sludge calorific content by increasing the carbon concentration (Insel et al., 2013). In addition, drying helps in rendering sludge effective and suitable for further treatments like incineration and pyrolysis. On top of that, drying corroborate a stabilized product free of pathogens and disallows further decomposition or bacteria digestion (Leonard, 2003). With huge benefits come restrictions, and drawbacks. Sludge drying requires a tremendous amount of energy, which contributes to the carbon footprint and the process's operational and maintenance costs. Also, the drying process provokes losses of nutrients and organic matter, reducing the effectiveness of its valuable use in agriculture (European-Environment-Agency & ISWA, 1998). In addition, it is difficult to avert limitations such as the complexity requiring expertise, handling and storage, long drying times, and scalability issues.

Theory of thermal drying

In order to reach moisture levels ranging from 80% to 90%, beyond simply removing water through dehydration, it becomes essential to subject the product to a drying process. The fundamental scientific principles essential for achieving this objective are as follows (Pambou, 2016):

- Moisture content (X):

$$X = \frac{M_W}{M_S} = \frac{M_W}{M - M_W} \tag{1}$$

M_W: Water mass [g]

M_S: Solid mass [g]

M: Total mass = Water mass + solid mass [g]

- Moisture content on wet basis (X_wb):

$$X_{wb} = \frac{M_W}{M} \tag{2}$$

- Relation between equation 1 and 2:

$$X = \frac{X_{wb}}{1 - X_{wb}} \quad and \quad X_{wb} = \frac{X}{1 + X} \tag{3}$$

- Convective sludge drying kinetics: Using a mass loss curve plotted against time (Figure 5), the drying speed through a basic derivative calculation can easily determined. Traditionally, the drying speed (N, kg/s) is graphed against the moisture content of the product based on its dry weight (X, Kg_w/Kg_S), as shown in Figure 6. To delve into the mechanisms underlying drying kinetics, it's important to shift focus from drying speed to drying flux. This leads to the creation of the Krischer curve (Kemp et al., 2001), which portrays how the drying flux (F, kg/(m^2.s)) progress with respect to the moisture content on a dry basis (X, Kg_w/Kg_S). In cases where the material remains completely rigid and experiences no change in its surface such as volumetric shrinkage, the drying flux F can be directly derived from the mass loss curve. In such cases, it's approximately equivalent to the drying speed N (kg/s), with only a minor constant factor involved (Equation 4).

$$F = \frac{m_s}{A_0}(-\frac{dW}{dt}) = \frac{1}{A_0}(-\frac{dm}{dt}) = \frac{1}{A_0}N \tag{4}$$

On the other hand, if the wet material experiences contraction, it's crucial to have information about the external surface area (A(X), m^2) of the sample in order to construct the drying flux curve for the material (Equation 5).

$$F = \frac{1}{A(W)}N \tag{5}$$

With that being explained, all it takes is to measure the area change to visualize the change of the mass with respect to time and the change of water content with respect to the drying velocity as shown in Figures 5 & 6 respectively. Therefore, the faster the drying speed, the greater the moisture content, and it is evident that the mass decreases over time during the drying procedure.

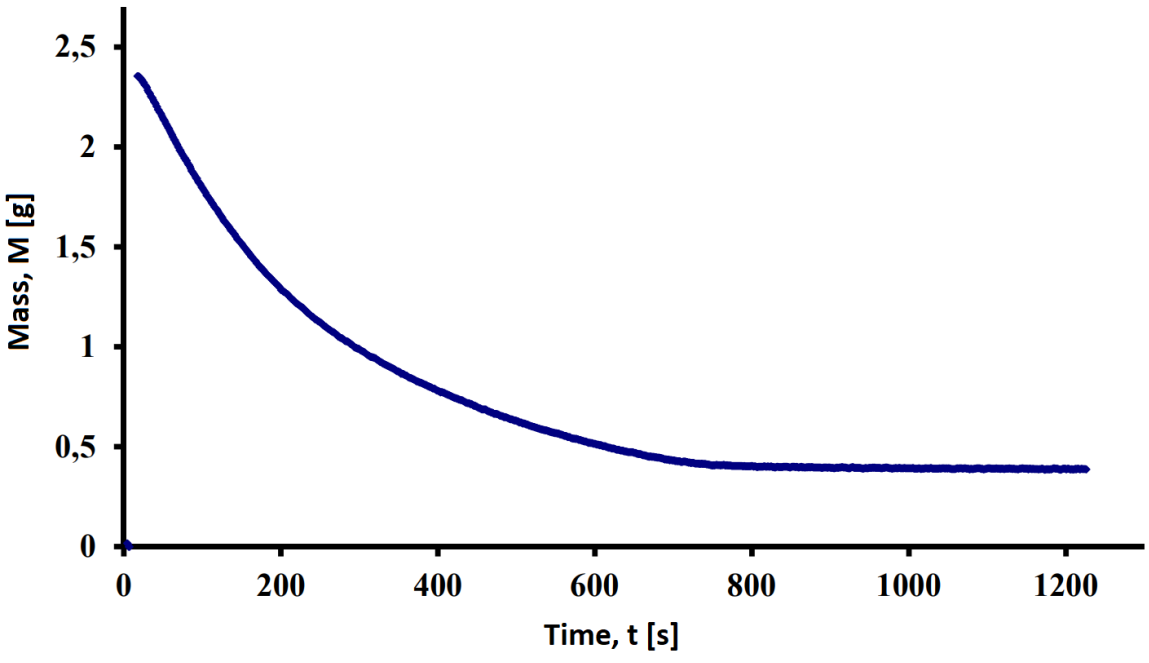

Figure 5: Example of a mass loss curve over time (Pambou, 2016)

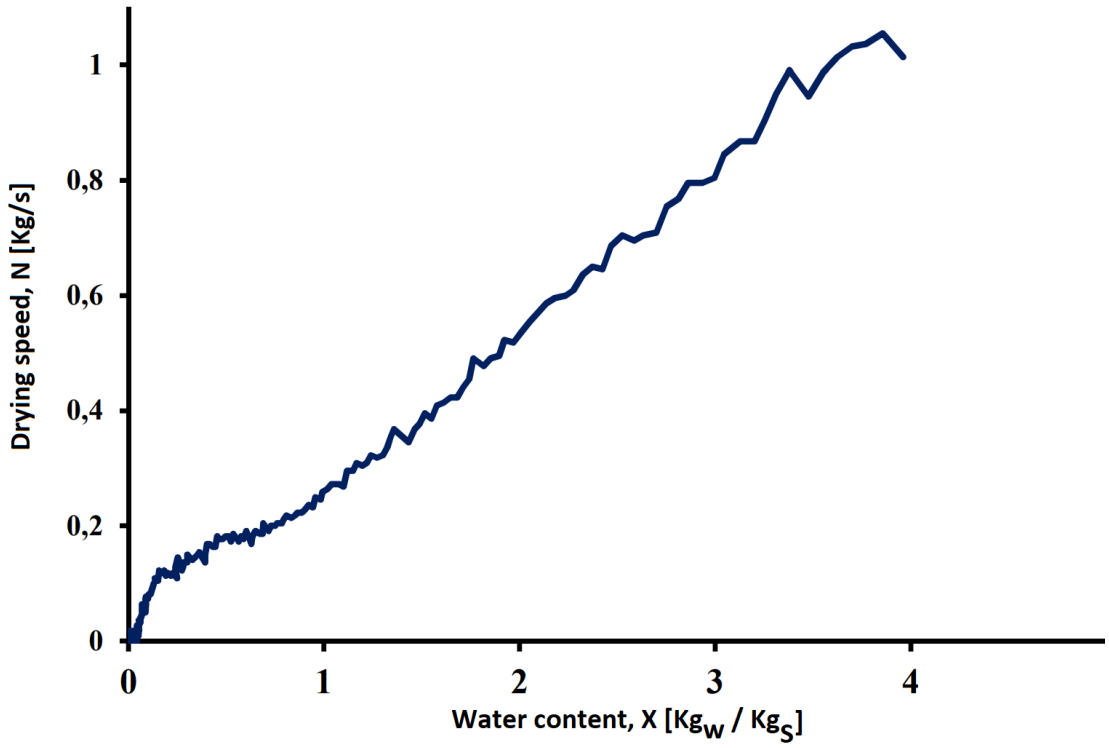

Figure 6: Example of a humidity change over time (Pambou, 2016)

Drying and Krischer's curve

The drying curve is the model used to understand how a product behaves during the drying process. Studies have revealed that a product goes through various phases during drying, and the number of these phases varies depending on the product, the drying method employed, and the operating conditions. To detect these phases, the most suitable approach to employ is Krischer's curve, which graphically represents the evaporation rate versus moisture content. An in-depth analysis of this graphical representation of the drying kinetics is fundamental, because changes in the sample occur after the adaptation phase. To effectively observe the constant drying phase, it is practical to use the evaporated flux per product surface in $(Kg.s^{-1}.m^{-2})$. Before initiating the drying process, dewatering the sludge by filtration, compression, or centrifugation is a common practice to reduce process costs. These steps typically decrease the initial product moisture content by around 5% (Bennamoun et al., 2013). Numerous investigations have presented a standard sludge drying pattern, which can be primarily categorized into two main phases: the constant drying rate and the falling drying rate, as depicted in Figure 7. In the constant drying rate phase (AB), the product's free water undergoes evaporation. As the moisture content decreases, the quantity of evaporated water diminishes during the falling rate phase. Initially, interstitial water (BC) is evaporated, followed by surface water (CD), and eventually, bound water is outstretched, marking the end of the drying process. Experimental findings have shown some deviations from theoretical expectations. Typically, the drying process initiates with a brief transient phase, known as the adaptation phase (Figure 8). During this stage, there is a significant increase in the evaporation rate until it reaches a maximum value, and the surface temperature corresponds to the

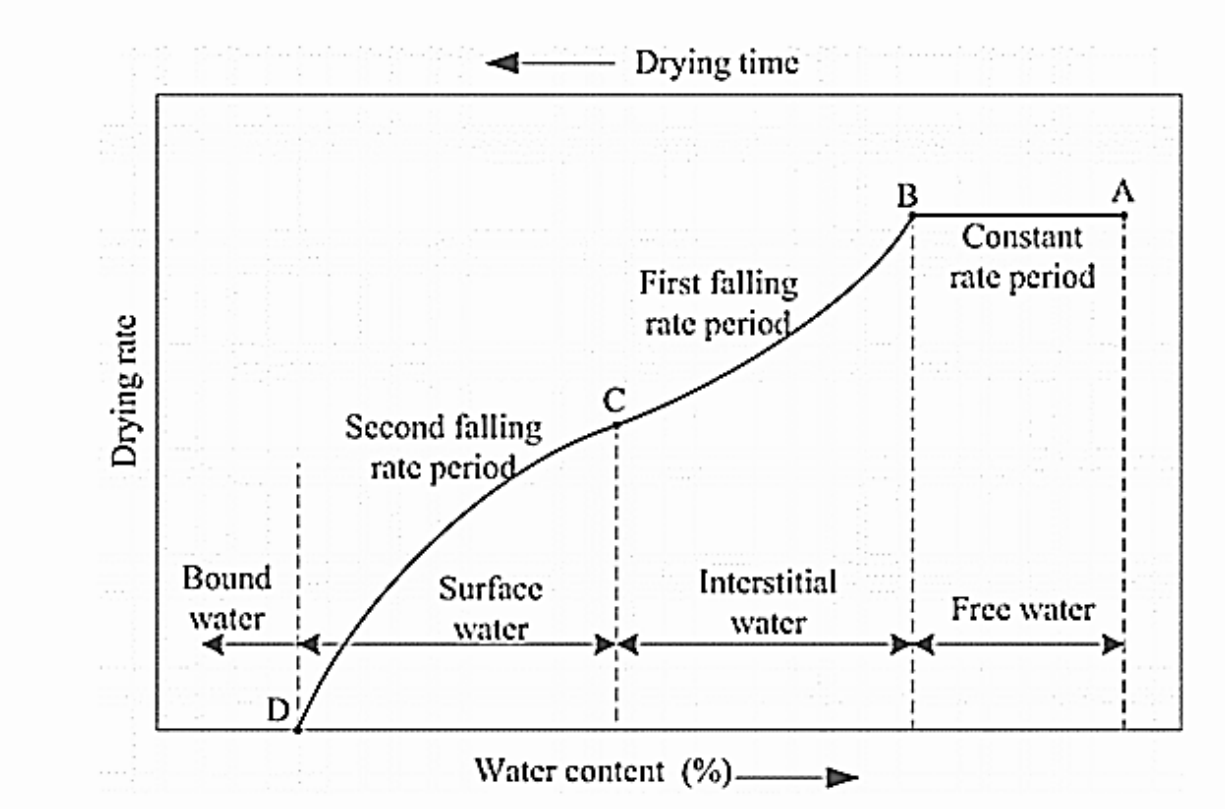

Figure 7: Wastewater sludge drying curve (Hovey et al., 2017)

wet-bulb temperature associated with the air temperature and humidity. Following this, the constant drying rate phase begins, where the evaporation rate remains steady. The duration of this period is influenced by the sludge's origin (Figure 9). Some sludge exhibit a very short constant drying phase, while back-mixing can also impact its duration. The final observed phase is the falling drying rate period, during which the evaporated flux decreases from the maximum value to zero. Generally, this phase can be divided into two or three distinct parts, as illustrated in Figures 8 and 9. The effect of operating conditions and the sludge's origin persists. Although, it is emphasized more in the constant drying rate phase (Hovey et al., 2017).

According to (Leonard, 2003; Pambou, 2016), during the drying process, different types of moisture are eliminated at different stages. The moisture removed during the constant-rate period was termed "free water," during the first falling-rate period, referred to as "interstitial water," and during the second falling-rate period, called "surface water." The remaining moisture observed during the equilibrium stage is categorized as "bound water". To analyze the moisture distribution in sludge more effectively, The standard drying curve shown in Figure 7 is used (Deng et al., 2011; Vaxelaire & Cézac, 2004). However, deriving experimental curves from raw data pose challenges, especially when dealing with noisy curves. Drying operations tended to accentuate noise, as seen in the drying curve (Figure 10, grey line), which is obtained using centered differences with a time step of 10 seconds. The blue curve displayed significant noise, necessitating a smoothing operation to mitigate or eliminate the noise.

To address this issue, (Lanczos, 1956) proposed a numerical derivation method for filtering and smoothing curves. By applying Lanczos's method to the raw data using MATLAB as the computational software,

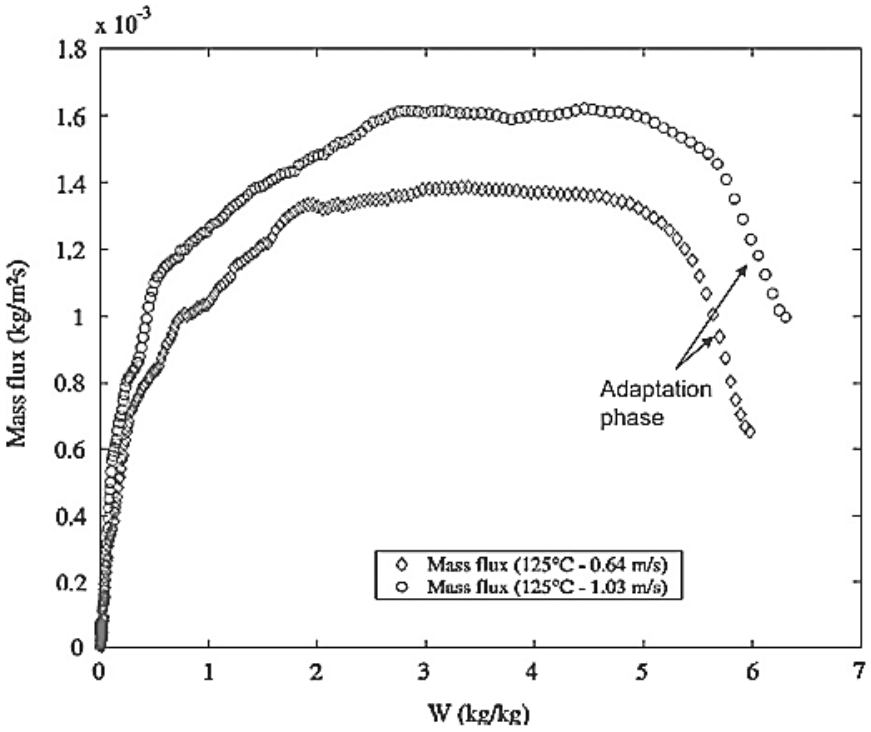

Figure 8: Sludge convective drying experimental data
for mass flux vs moisture content (Bennamoun et al., 2013)

researchers obtained the drying rate curves (Figure 10, red line). It's important to note that this method involved sacrificing the first and last points of the curve depending on the chosen filtering length. The MATLAB code is presented in annex-10.

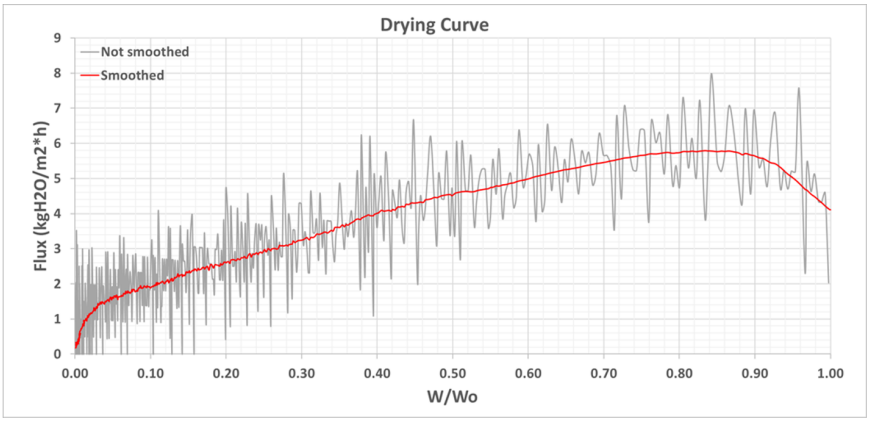

Figure 10: Smoothed Dryer curve (Lanczos, 1956)

In summary, the research led by (Lanczos, 1956) utilizes Krischer's curves to study drying processes, and identify different stages in the drying curve. They differentiated various types of moisture content and used the standard drying curve for analyzing moisture distribution in sludge. To overcome noise in experimental curves, they employed C. Lanczos's numerical derivation method, which is proved to be effective in obtaining smoother results, and this is exactly what was done in our study to obtain Kricher's curves.

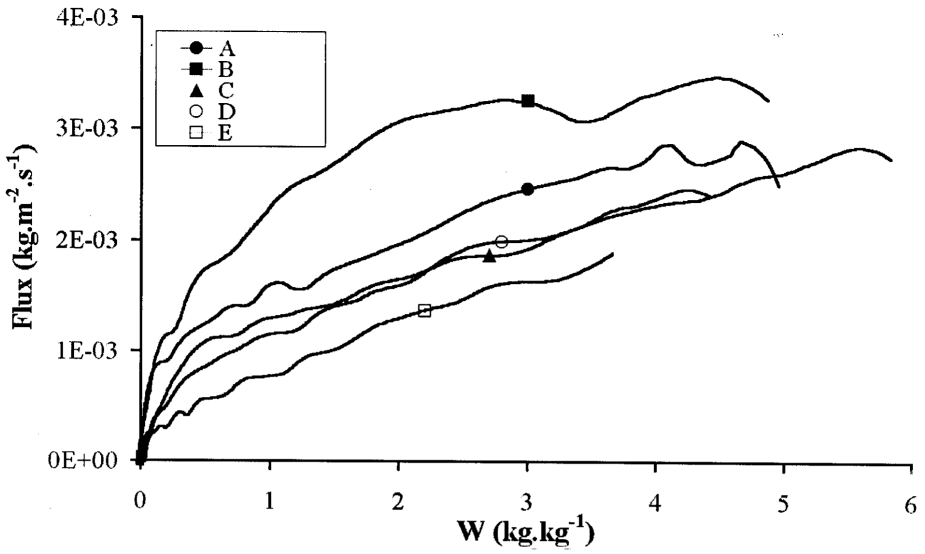

	B	A	C	D	E
Water evaporation capacity (kg m^{-2} s^{-1})	1.96 10^{-3}	1.46 10^{-3}	1.41 10^{-3}	1.34 10^{-3}	0.96 10^{-3}
Volatile solids (% DS)	57.4	58.7	66.4	68.9	74.7

WWTP	EH	Effluent	Tertiary Treatment	Other
A	8000	Domestic	None	Thickening + Belt filter
B	9000	Domestic	None	Thickening + Belt filter
C	18000	Industrial (agrofood)	None	Sludge digestion + Thickening + Belt filter
D	27000	Domestic	Nitrification-Denitrification (intermittent stage)	Thickening + Belt filter
E	110000	Domestic (50 %) + industrial (agrofood)	Nitrification-Denitrification Dephosphotation (precipitation)	Thickening + Centrifugation

Figure 9: Sludge origin influence on the convective drying behavior (Leonard, Vandevenne, et al., 2004)

1.6 Shrinkage phenomena

The process of observing changes in a material's structure as it dries involves measuring how much the material's volume decreases, which is known as volumetric shrinkage. This occurs because the different components of the material contract and become more tightly packed due to internal forces. This measurement is calculated as a ratio of volumes containing the same amount of dry material. In simpler terms, shrinkage indicates how much the volume of the sample changes as its moisture content decreases, compared to its initial volume. The formula to quantify this shrinkage, referred to as equation (Equation 6), gives insight into how much the sample contracts during the drying process:

$$R_V = \frac{V_S - V0}{V_0} \tag{6}$$

R_V: The volumetric shrinkage undergone by the sample [%]

V_S: The volume of the saturated sample

V_0: The volume of the anhydrous sample.

During the drying of flexible materials, various types of shrinkage, as discussed by (Kneule, 1964), can take place.

When a material can contract freely, it's called free shrinkage. On the other hand, if external forces restrict the contraction, it's termed restrained shrinkage. (Kneule, 1964) also introduces the concept of total or ideal shrinkage, which happens when the reduction in material volume exactly matches the volume of water that evaporates. Consequently, the relationship between volumetric shrinkage and moisture content follows an affine curve. If this shrinkage is uniform across all three spatial dimensions, it's known as isotropic shrinkage.

Several authors have elucidated the mechanisms of shrinkage in gels, leading to various explanations:

- The macroscopic approach: as proposed by (Kneule, 1964), likens the drying material to solid elements separated by layers of water with varying thickness. Stronger cohesion among the solid elements due to inter-molecular forces occurs when they are closer together. As drying progresses, these layers thin out, leading to a decrease in volume.

- The capillary approach: put forth by (Brinker & Scherer, 1990), attributes the shrinkage of porous flexible materials to capillary forces. This theory outlines three stages: Initially, a liquid film forms on the material's surface, which is removed by evaporation. At this stage, water departure leads to volume reduction, and the liquid-gas interface remains flat. As the system becomes more rigid, the liquid enters the pores. To minimize the internal energy of the pore-liquid system, menisci form to limit solid-air contact. This creates tension within the liquid due to capillary forces. Eventually, the material's structure resists this compression, halting shrinkage, and the menisci move further into the pores. This process generates stress that can damage the material.

- The colloidal approach: it suggests that shrinkage results from repulsive forces explained by the double electric layer theory.

In the context of sewage sludge, it seems that capillary forces primarily drive shrinkage. During drying, the dominant phenomenon involves water removal, without significant consideration of chemical reactions or osmotic forces.

Parameters affecting the drying behavior

Several parameters affect the drying process, it is important to understand their influence in order to optimize or relevantly characterize the drying process. When we talk about sludge drying influencing parameters, we

can differ between process parameters and material parameters. The different parameters are explained in Table 4, summarizing the influence in a handy manner.

Process parameters	**Influence**
Temperature	Temperature significantly affects sludge drying. Higher temperatures improve the drying rate, but they are also associated with an uptick in energy consumption. Remarkably, greater temperatures contribute to an improvement in thermal energy efficiency. Different sludge types respond differently to temperature. Raising the temperature, reduces drying time, yet excessive heat can result in a hardened surface on the sludge. Elevated temperatures are beneficial for managing odors and emissions. Equipment design and end-product quality are influenced by temperature (Zheng et al., 2021).
Air humidity	Humidity greatly affects the drying process of sludge, as it directly influences the rate at which water evaporates and the efficiency of the equipment used. High humidity leads to a slower drying rate and an increase in energy consumption. Also, it makes it challenging to achieve the desired end product level of moisture content. (Zheng et al., 2021).
Air velocity	The air velocity significantly affects the process of sludge drying. Higher air velocity uptick the drying rate, reduce drying time, but increase energy consumption. Adequate air distribution is crucial for uniform drying. However, too high air speeds can cause uneven drying and particle entrainment. The optimal air velocity is a parameter that requires optimization, depending on the nature of the sludge, and the drying method (Zheng et al., 2021).
Material parameters	**Influence**
Origin/history	The origin of sludge significantly affects the sludge drying process, as demonstrated by (Leonard, Vandevenne, et al., 2004). Different sludge types have varying moisture content, drying rates, and energy requirements. Sludge with higher volatile solids may dry more slowly and shows less evaporation capacity. Comprehending sludge origin characteristics, pre-treatment, and composition is needed to optimize drying efficiency.

Initial moisture content	The initial moisture content of sludge greatly impacts the drying process. Sludge with higher initial moisture content takes longer to dry and requires more energy. On the other hand, lower initial moisture content, leads to higher drying efficiency and better final product quality. Adequate pre-treatment or dewatering can reduce initial moisture content, optimizing the drying process for efficiency and quality (Huiliñir & Villegas, 2015).
Rheology in general	The rheological behavior of sludge is two-sided, in a way that the dewatering process or pre-treatment affects the rheological properties, and the rheological characteristics of sludge influence the drying process. Increased viscosity corresponds to a slower drying rate, whereas decreased viscosity leads to a faster rate of drying. (Eshtiaghi et al., 2013). Also, Non-uniform rheological properties cause uneven moisture distribution during drying (Mert et al., 2007).
Texture	This parameter includes particle size distribution, surface area, porosity, and structure. For example, smaller particles with high surface area, dry in a faster pace due to the emphasized moisture evaporation. Also, porosity has a direct impact on the airflow and on water mobility and therefore on the drying. For these reasons texture is managed usually in choosing mixing methods or by supplementing agents (Huron et al., 2010).

Table 4: Drying influencing parameters

In conclusion, when it comes to analyzing sludge drying, many single points of failure exist. Careful awareness of the involved parameters is required to understand and characterize such process. In fact, the direct influence results from the air humidity, speed, and temperature. The study made by (Zheng et al., 2021) offers a good understanding of the cross-influence as shown in Figure 11, the lower the airspeed, the poorer the drying. In other words, if the drying airspeed increases, lower moisture content can be achieved, even in a shorter time, thus with less energy consumption. Also, any temperature increase can shift the moisture content to the time curve backward, reducing the drying time and output moisture content.

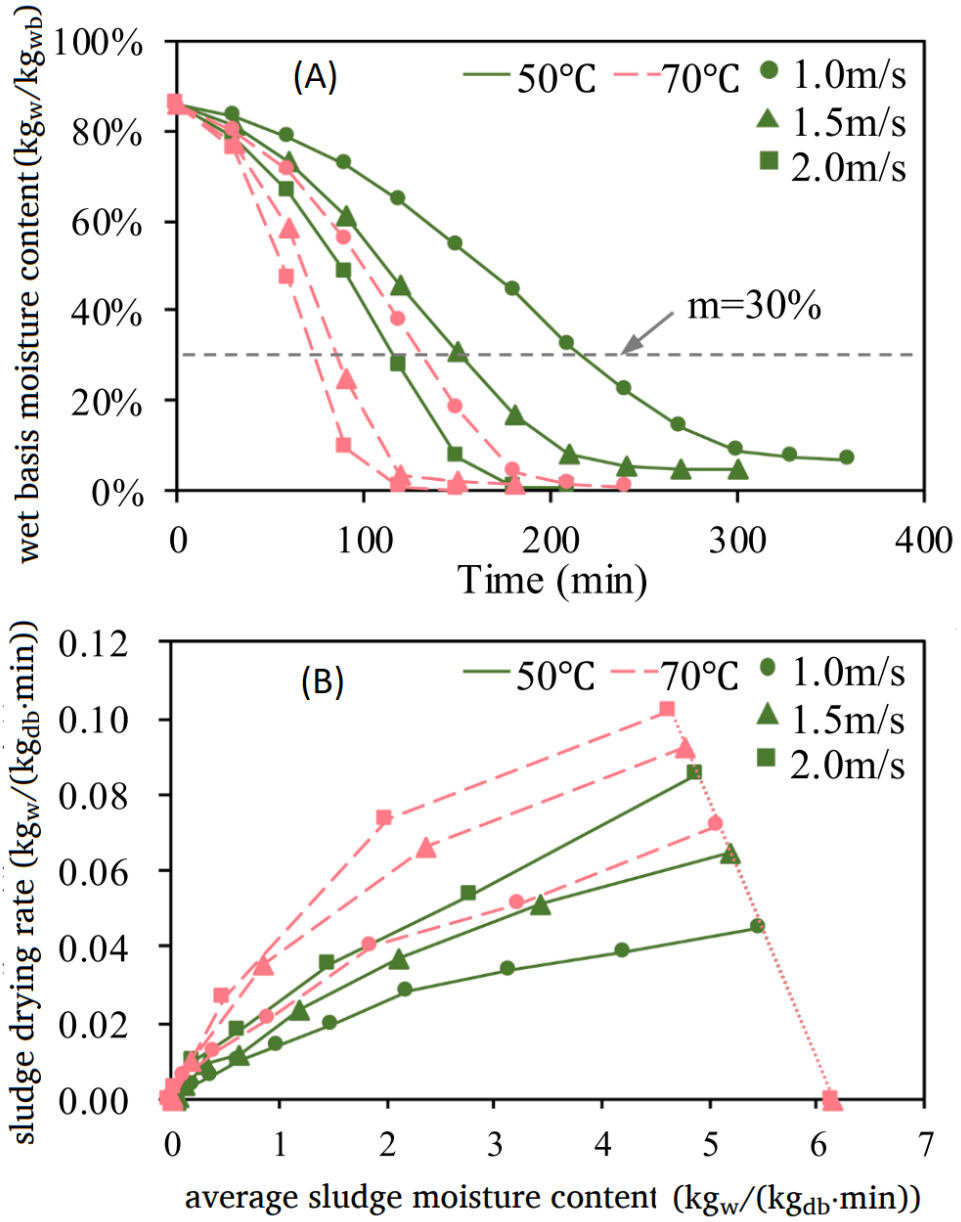

Figure 11: Sludge drying for different air velocities, temperatures, and relative humidity (Zheng et al., 2021)

In addition, the humidity climb causes a decrease in the drying rate (Zheng et al., 2021). As also proved, the gap between different humidity drying curves increases if the temperature or the air velocity increases. In a more rigorous analogy, the boundary layer theory can be referred to. It addresses the fluid behavior when moving close to a solid object, differentiating between laminar, turbulent and chaotic boundary layers and the effect of such parameters on the the behavior (Schlichting & Kestin, 1961). So, the drying rate is higher for lower humidity, and the impact of humidity on the drying rate will be larger if the temperature or the velocity of the drying air increases as shown in Figure 12.

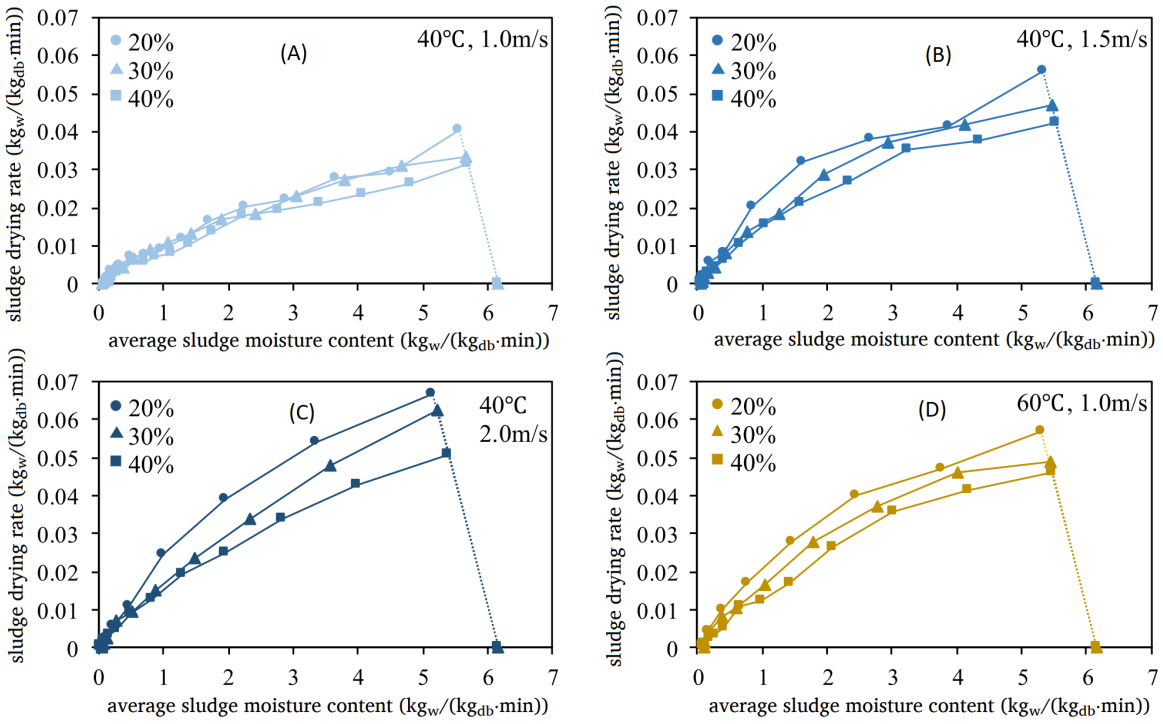

Figure 12: Sludge drying rate variation humidity, temperature and air speed. (Zheng et al., 2021)

1.7 Water sludge texture and rheology

- Rheology

The sludge of interest is a stage so-called viscoelastic solid. A viscoelastic solid is a substance that blends attributes of solids and fluids, manifesting traits of viscosity and elasticity when exposed to stress or deformation. It exhibits a behavior dependent on time, slowly altering its shape under stress while also releasing energy. In order to measure these changes in rheology, an oscillatory experiment can be conducted, namely amplitude sweep. these experiments allow us to determine the storage modulus or loss modulus change with respect to the strain. The typical results are depicted in Figure 13. where the curve starts with a constant modulus, which is the stage in which sludge responds linearly to any stress by restoring the original shape until the stress is big enough to reach the point of no return (viscoelastic limit), for which any stress higher will cause the material to permanently deforms. Also, the intersection between the storage and the loss modulus after the viscoelastic limit, indicates the flow point, regarding which the material is considered to have flowing ability. It is important to have an idea of the typical values of both modulus, in order to keep in mind the order of magnitude of these parameters. Hence, Figure 14, gives us an idea that the modulus is in the range of [10^3-10^5] Pa (Ofei & Saasen, 2019).

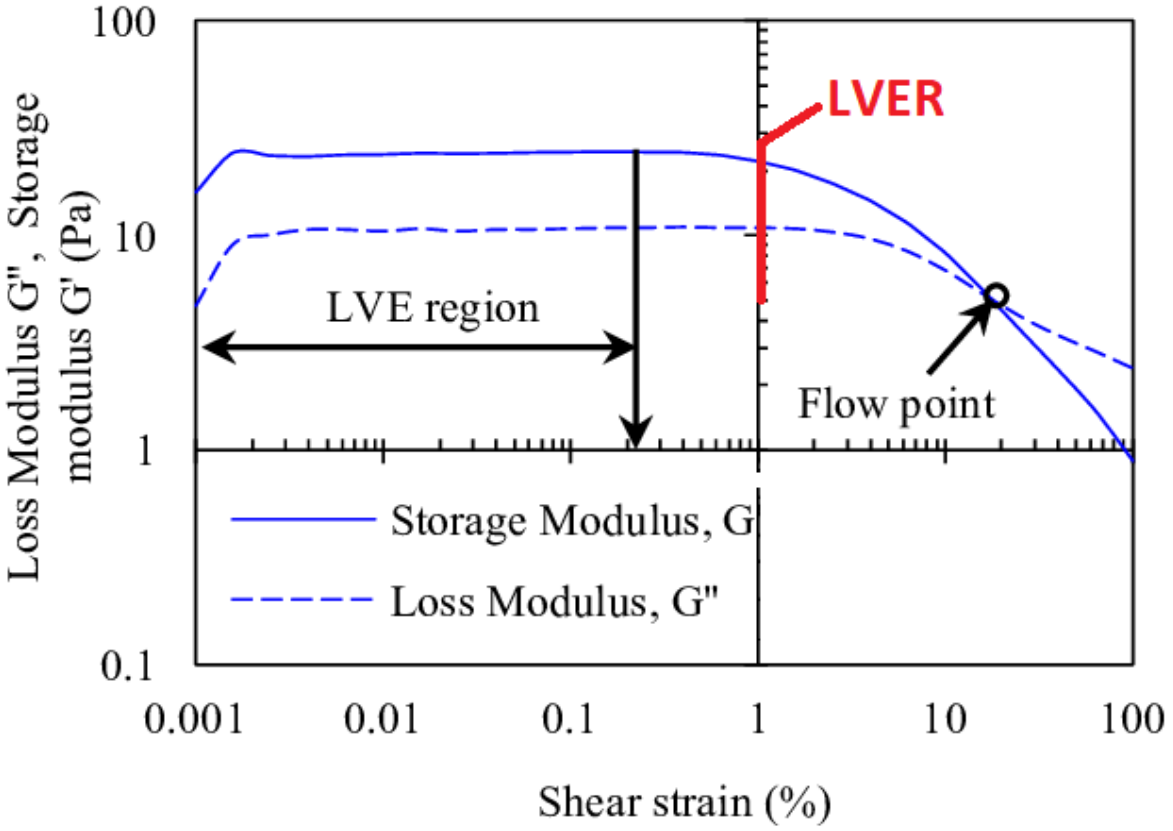

Figure 13: Storage and loss modulus vs the strain (Ofei & Saasen, 2019)

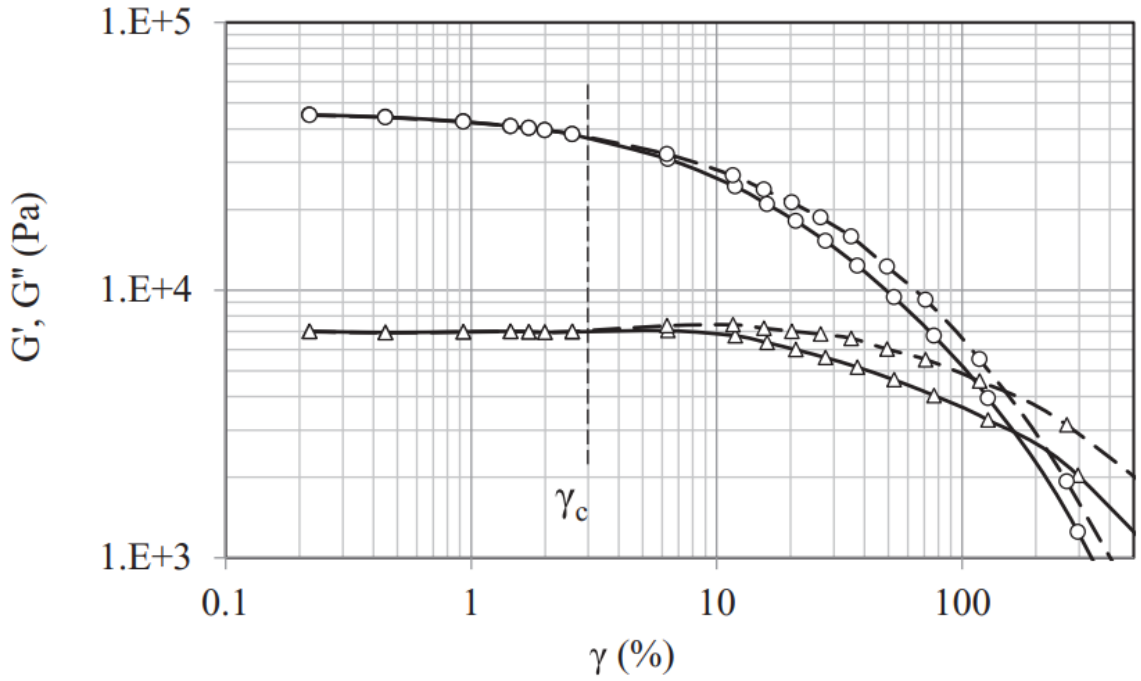

Figure 14: Modulus vs strain example with correction (Mouzaoui et al., 2018)

- Texture:

For the texture, it changes as mentioned in the drying progress. Figure 57 demonstrates two main points; initially, shrinkage becomes noticeable at the early stages of the process, evidenced by a decrease in volume at a consistent drying rate. Conversely, the visuals indicate that initial indications of cracks emerge later, coinciding with a declining drying rate as depicted by the white areas in the illustration. Both shrinkage and cracks are impacted by the sludge's source, resulting in shrinkage levels ranging from 60% to 80% and crack occurrence varying from 30% to over 50% by the conclusion of the drying procedure. In addition to texture, there are two important aspects to consider, namely cohesion and adhesivity. Sludge cohesion characterizes how well particles and components within sludge, a partially solid mixture of solids and liquids, hold together and prevent separation. It reflects the inner strength of the sludge and its capacity to resist deformation or disintegration. A higher cohesion enhances the stiffness of extrudates, resulting in a more permeable sludge bed with greater surface area for heat and mass exchange. As a result, drying rates are elevated. This is exemplified in Figure 15, which demonstrates the correlation between sludge cohesion and increasing lime dosage. Cone penetrometer testing can assess cohesion. A clear pattern emerges: greater cohesion corresponds to shorter drying times. Mixing equipment generating high shear stresses can lead to sludge breakdown, yielding low cohesion. Conversely, the texturizing impact of lime addition can heighten cohesion if mixing-induced shear stresses remain moderate (Leonard et al., 2011). A similar phenomenon is noted during backmixing of dried product prior to drying. (Leonard et al., 2002).

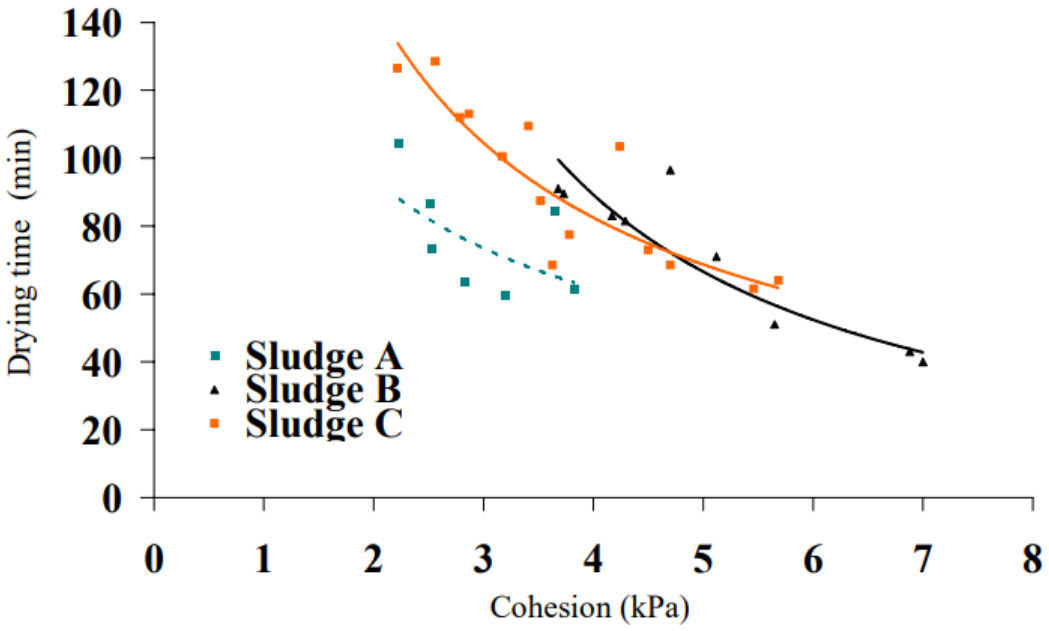

Figure 15: Drying time vs cohesion (Leonard et al., 2011)

Sludge adhesivity pertains to the capacity of sludge particles to adhere or stick to surfaces. This property indicates how likely sludge is to cling to various materials or structures, influencing processes like movement, treatment, and equipment functionality. The level of adhesion corresponds to the maximum force recorded when detaching the cone from the sludge after a penetration test. The results shown in Figure 16 can be interpreted in two ways. First, the increase in cohesion confirms the texturing effect of liming. Second, the decrease in cohesion and increase in adhesiveness are attributed to the disintegration caused by pumping. This mirrors the evident sticky nature of the disintegrated sludge, as depicted in Figure 17. The outcomes from the penetration tests allow us to comprehend the observed drying behaviors: heightened adhesiveness will impede the internal movement of water. However, the results suggest that a strong cohesion can partly counteract high adhesiveness. Specifically, disintegrated, pre-limed, dewatered sludges dry more swiftly than raw disintegrated sludge, yet they exhibit greater adhesiveness and cohesion (Huron et al., 2010).

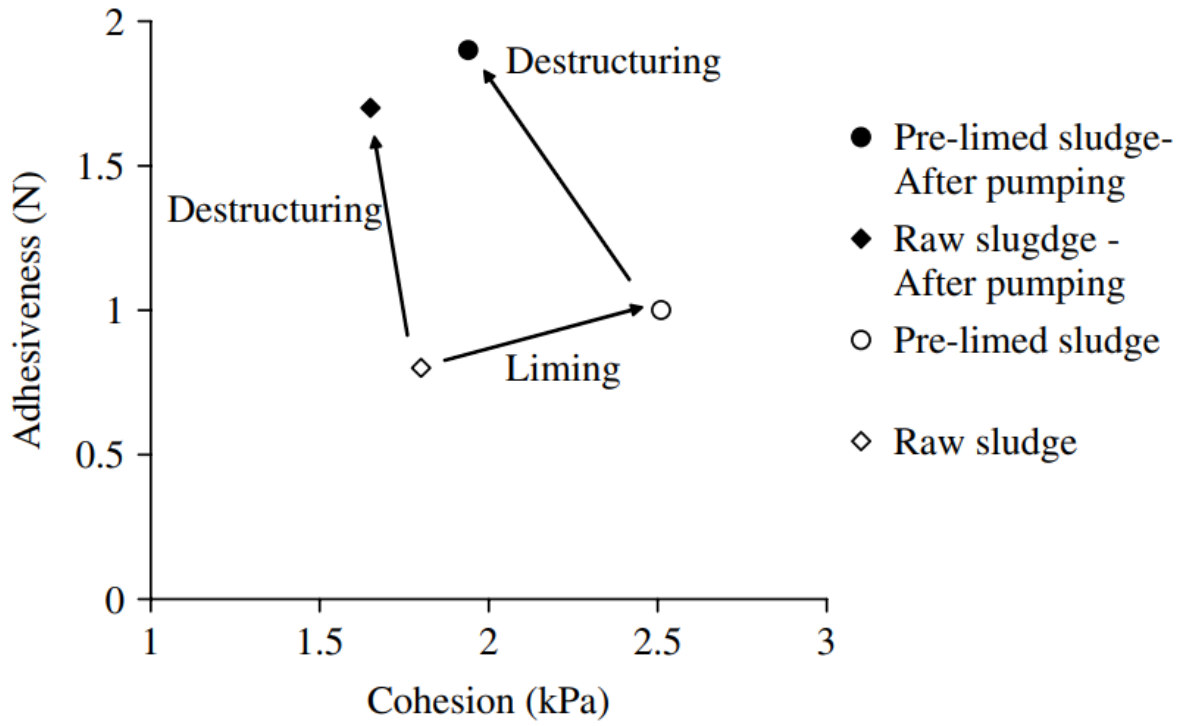

Figure 16: Pumping Influence on cohesion and adhesiveness of raw and pre-limed sludges.(Huron et al., 2010)

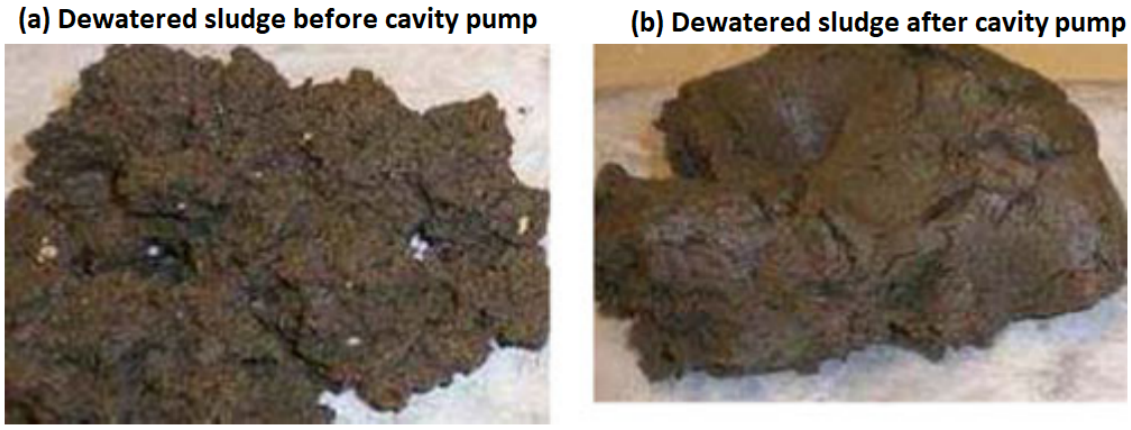

Figure 17: Dewatered sludge before and after cavity pump (Huron et al., 2010)

1.8 Liming

The well-established practice in wastewater treatment plants (WWTPs) involves the widespread use of alkaline chemicals and primarily lime for stabilization purposes. Lime is used to increase the pH of the sludge, effectively neutralizing or eliminating pathogens and microorganisms through adequate contact time and mixing. Moreover, the hydration reaction of lime helps improve sludge dryness. The process of sludge liming can take place either before or after dewatering, with specific objectives for each approach. While the texturing effect of lime in landspreading is well-known, its effects on subsequent drying processes have not been deeply explored. Nevertheless, drying is a crucial pre-treatment step after mechanical dewatering, as it reduces water content, waste mass, and volume, thereby lowering storage, handling, and transportation expenses. Additionally, drying transforms the sludge into a suitable combustible material when exposed to sufficiently high temperatures and yields a pathogen-free, stabilized substance that can be used as an agricultural soil amendment (Huron et al., 2010).

To visualize the impact of liming on the drying process, the study of (Huron et al., 2010) takes a different set of sludge based on their treatment techniques and analyzes the liming effect on the drying rate. The set that we will refer to is the one following an anaerobic digestion. We will look at the results for raw, pre-limed, and post-limed sludge. The difference between pre-limed and post-limed is manifested in the liming process stage, happening respectively before or after dewatering. Figure 18 shows that liming enhances drying, results in a higher drying rate, and leads to a lower product moisture content. Also, Figure 19 shows that liming reduces the drying time and therefore the cost. However, the study also proves that pre-liming is more effective than post-liming.

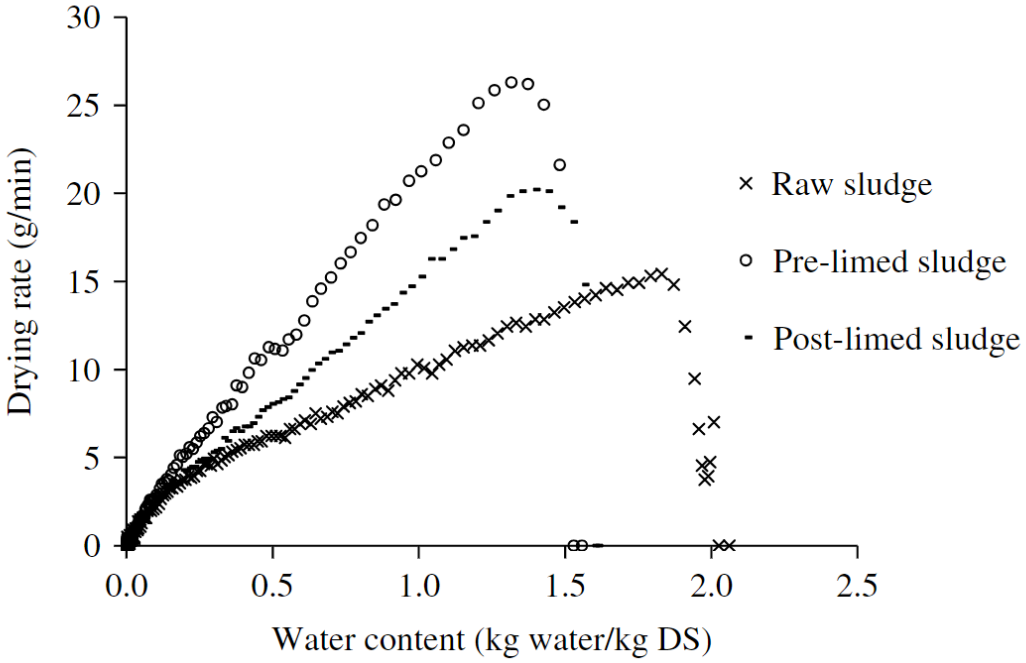

Figure 18: Krischer's curves illustrating the effect of liming on sludge (Huron et al., 2010)

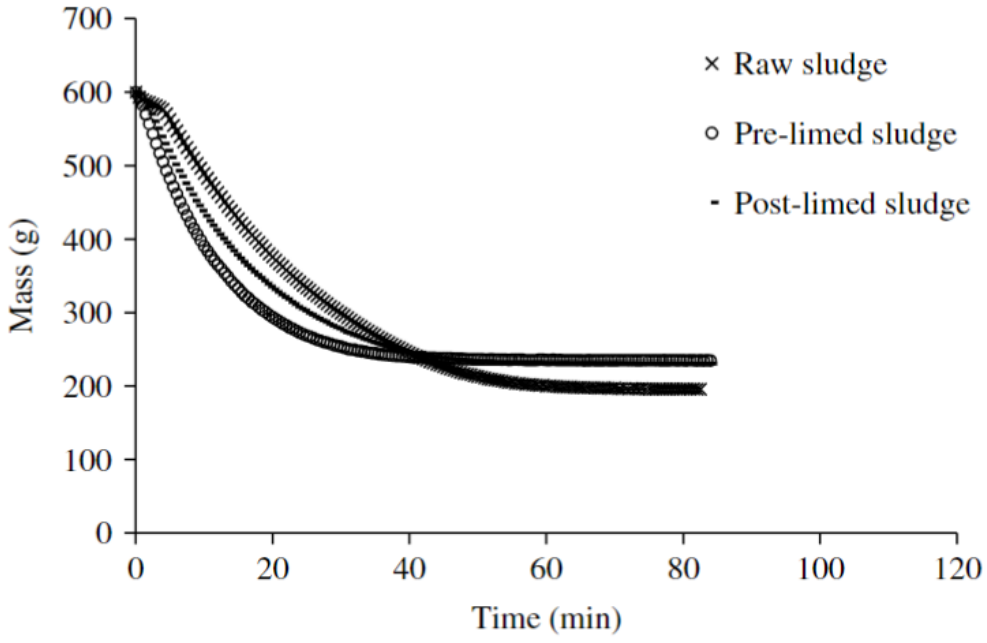

Figure 19: Effect of liming on the mass vs time curve (Huron et al., 2010)

2 Goal and scope of the study

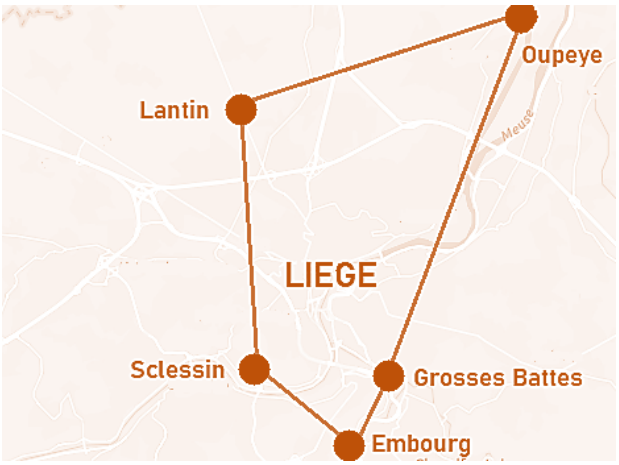

Figure 20: Map of Liege treatment plants considered in the study

The purpose of this thesis is to study the characteristics of drying and the rheology of sludge in the region of Liege. To do so several experiments are conducted as listed in Table 5. These experiments are fully described in the materials and methods section. The outcome is a list of characteristics and properties that allow us to understand the behavior of sludge following the biological and mechanical treatment. Five stations located around the region of Liege are considered for this study as shown on the map in Figure 20. Each station employs different or similar treatment and mechanical techniques with different load capacities. The importance of sampling as many stations as possible provides us with better adequacy, since as discussed in the literature review, sludge rheology and behavior during drying depends widely on its origin and therefore on the surrounding urban, and industrial distribution. For the sake of clarification, the study does not judge the station performance but takes various existing wastewater treatment facilities to illustrate the closest image of sludge rheology and characterization of the region in question. The benefits of studying the latter are mainly a contribution to the science of wastewater treatment and disposal, due to the fact that the drying characteristics and rheology of sludge play a major role in determining the energy, land occupation, cost, and environmental impacts attributed to wastewater post-treatment. There are six samples in total, four being sludge not subjected to liming and two subjected to liming, the plants and the corresponding samples are listed in Table 6. Assumptions are present in any study to facilitate navigation through complex or rigorous calculations. However, these assumptions also introduce a level of error and uncertainty. in our case, the main assumption is considering the striding sludge as perfect cylinders and assuming the sludge persists in this ideal shape during the process of drying. The mentioned assumptions allow us to estimate the area change with time and therefore with the drying rate in a simple mathematical model based on the height and the diameter of a cylinder. the sludge cylinders are obtained using a extruder as well be described later on in the material and method.

Number	Experiment
1	Total solid content
2	Total volatile content
3	Convective micro-drying
4	Convective macro-drying
5	Texture profile analysis
6	Penetrometry
7	Amplitude sweep

Table 5: Conducted experiments

Number	Station	Liming	Label
1a	Grosses battes	No	S1
1b	Grosses battes	yes	SL1
2	Embourg	No	S2
3	Oupeye	No	S3
4	Lantin	No	S4
5	Sclessin	Yes	SL5

Table 6: Stations, samples, and labels

3 Plants description

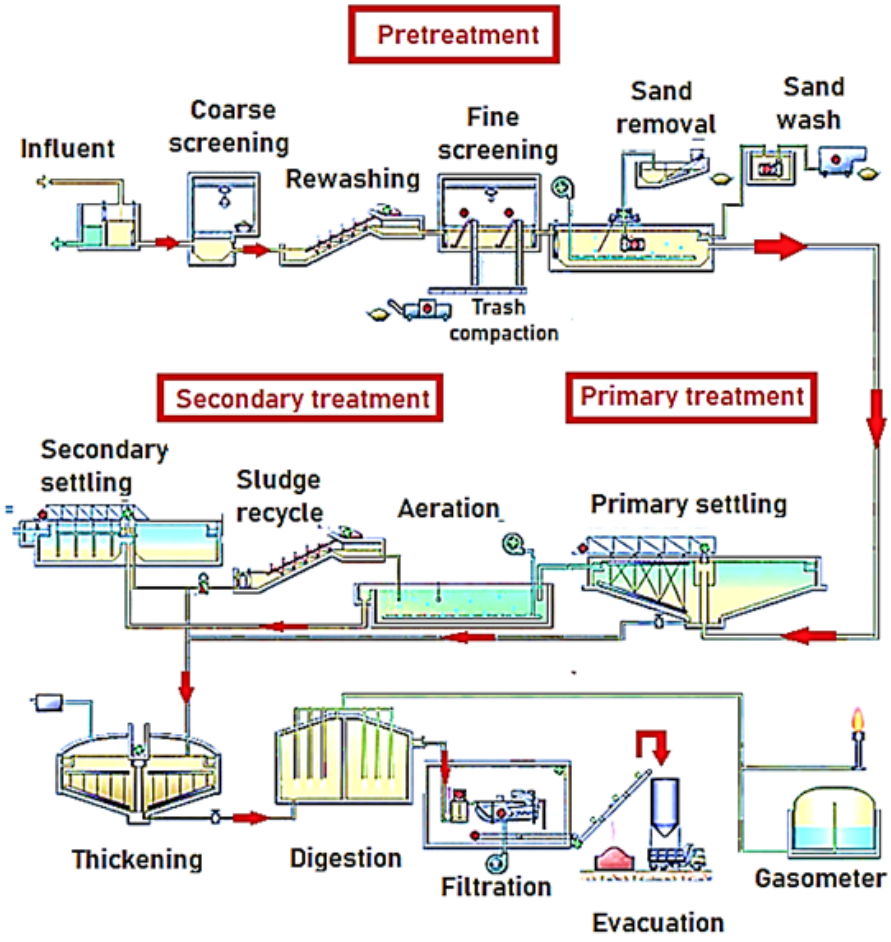

Figure 21: Oupeye process (Oupeye, n.d)

It is essential to highlight the differences in the treatment process between the different stations. As previously mentioned, the so-called sludge history or origin has a huge impact on sludge rheology, texture, and therefore on the drying behavior. To relate these differences, we relied on surveys, that unfortunately couldn't be obtained. Based on research, Table 7 highlights the characteristics believed to be relevant to a possible difference in the behavior and properties of the sample. Also, Figure 21 represents the actual process of S3 (Oupeye) found on the official station website (Oupeye, n.d), possibly, the figure also represents the five plants in question as well. The table shows no differences in terms of the treatments employed. Although, there might be huge differences in the technique or equipment used to perform treatments. However, the available resources show differences in capacity and commissioning year. Therefore, we seek to investigate whether they have a noticeable impact on the results.

Station	S1/SL1	S2	S3	S4	SL5
Capacity [habitants]	53,137	24,300	401,850	31,500	135,000
Commissioning	2002	1996	2007	2003	2001
Carbon treatment	✓	✓	✓	✓	✓
Nitrogen treatment	✓	✓	✓	✓	✓
Phosphorus treatment	✓	✓	✓	✓	✓
Bacteriological treatment (UV)	X	X	X	X	X

Table 7: Station characteristics (SPFG, n.d)

4 Materials and Methods

4.1 Dry matter content

To determine the dry matter content (DM) of the sludge, a specified amount of the sample is placed into pre-weighed crucibles. Subsequently, the sample is dried at a consistent temperature of 105°C until achieving a consistent mass, a process typically spanning around 24 hours.(Environment & Federation, 2019). Then, the dried residue in the crucible is weighed and subtracted from the initial crucible mass, leading to the pure dry residue mass. By measuring the sample's mass prior to and after the drying process, the division of the ultimate mass by the initial mass results in a fraction. When this fraction is expressed as a percentage, it represents the dry matter content, encompassing both suspended matter and dissolved salts present in the sludge. In order to ensure precise measurement, the procedure is iterated three times for each sample. The average outcome from these repetitions is then employed to attain a dependable depiction of the sludge's dry matter content.

This data holds significance for diverse applications, including the assessment of its viability for soil improvement or subsequent treatment, as well as gaining insights into its comprehensive composition;

$$DM[\%] = \frac{M_1}{M_2} \times 100\% \tag{7}$$

M_1: Wet Sludge mass [g](pre-drying)

M_2: Dry Sludge mass [g] (post-drying of 105°C)

4.2 Volatile matter content

The determination of volatile matter (VM) plays a significant role in understanding the organic composition of sludge samples. This analysis involves the utilization of dry residue [M_2] obtained while calculating the dry matter (DM) content. Initially, the specimens in the same crucibles are dried, ground, and then incinerated in a muffle furnace at a precisely controlled temperature of 550 °C for 2 hours. The organic components of the sludge are converted into gaseous products during this incineration process, leaving behind the inorganic ash. To quantify the VM content, the initial mass of the dry sample is compared to the remaining after incineration, using the formula mentioned in Equation 8 (Environment & Federation, 2019). To ensure accuracy, three separate analyses are made for each sample, and the average result is compelled. This process provides crucial information about the combustible or volatile components present in the sludge, offering valuable insights for various industries like agriculture, waste management, and environmental studies, where knowledge of sludge composition influences decision-making and treatment strategies.

$$VM[\%] = (1 - \frac{M_3}{M_2}) \times 100\% \tag{8}$$

M_3: Dry Sludge mass [g](post-incineration of 550°C)

4.3 Convective micro-drying

In their pursuit of understanding and optimizing the drying process for small extruded samples, researchers led by (Leonard, 2003) conducted a series of experiments using a specially designed convective "micro-dryer" (shown in Figure 22). In our study, we replicated this investigation by altering the sample dimensions and adjusting the air velocity, Table 8 presents the different parameters considered. The micro-dryer was carefully crafted to cater to the precise requirements. Tests are performed using a convective "micro-dryer", specially designed for handling small extruded samples ranging from 0.5 to 5 g. This micro-dryer operates conventionally, influenced by factors like relative humidity, temperature, and airspeed. Specifics about the micro-dryer are available in earlier research (Leonard et al., 2002). In this particular study, cylindrical

samples measuring around 18±1mm in diameter (D) and 15±1mm in height (h), with a mass of 4.3±0.2 g, were dried. The drying process occurred under these conditions: a temperature of 90°C, an air speed of 2 m/s, and a consistent absolute humidity of 0.005 kg water per kg of dry air. The sample in the micro-dryer hangs down on a sampling handler as shown in Figure 23. the air hit the sample horizontally in a one-way direction, causing uneven drying and shape deformation. The latter deformation is ignored in our study and the shape is assumed to remain cylindrical. The surface exchange and volume measurement is therefore estimated using the diameter and the height as described in the "H/D method". Although, the X-ray microtomography was used to calculate the surface exchange and the volume during micro-drying only for 'Sample 1 BL'. It is important to mention that unfortunately, the x-ray machine that provided more accurate measurement was out of commission before we could have used it for the remaining samples. Therefore, the so-called H/D method was used.

Parameter	Value	Unit
Airspeed	2	m/s
Air flow rate	144	Nl/min
Temperature	90	°C
Sample height	15	mm
Sample Diameter	18	mm
Humidity	uncontrolled	-

Table 8: Micro-dryer parameters

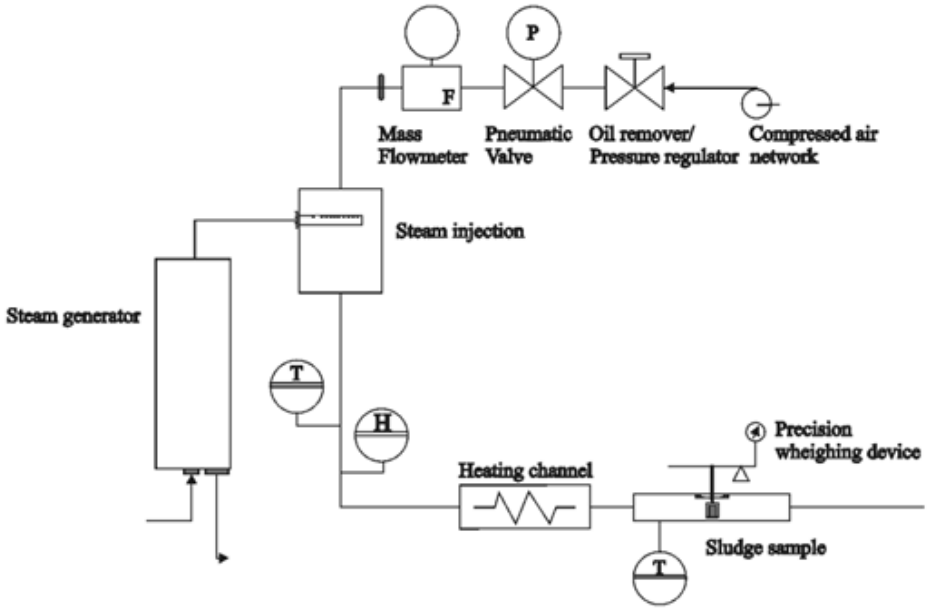

Figure 22: Convective micro-dryer (Leonard, 2003)

Figure 23: Convective micro-dryer handler

4.4 X-ray microtomography

The drying exchange surface and volume of sludge samples were measured using (Leonard, 2003). The drying process, which involved monitoring the samples' shrinkage, was conducted by removing the sludge samples from the dryer chamber and subjecting them to X-ray microtomography. This step allowed researchers to obtain images of multiple cross-sections before returning the samples to the micro-drier. The process was repeated approximately 10 times during the drying experiment. Previous studies have confirmed that these interruptions in the drying process do not affect the drying kinetics (Leonard et al., 2005; Leonard, 2003; Leonard et al., 2002). For the X-ray microtomography, a "Skyscan-1074 X-ray scanner" was used, operating at 40 kV and 1 mA. The X-ray source was accompanied by a 2D detector consisting of a 768 × 576-pixel, 8-bit X-ray camera, producing images with a pixel size of 41 μmm. Image reconstruction was performed using the supplied software (Skyscan / NRecon) that came with the machine. The quality of the reconstructed images depended on the amount of acquired data, with better image quality achieved through a higher number of projections. Subsequently, Matlab software was employed to analyze the microtomography-derived images and convert them into mathematical data suitable for generating the Krischer representation. Figure 24, illustrates the sequence of images, including raw tomography, a transversal cut from NRecon, and a processed black-and-white image from Matlab (Leonard, 2003).

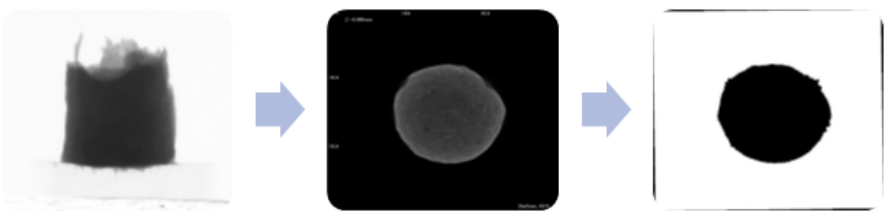

Figure 24: Sample shape image before and after image rebuild

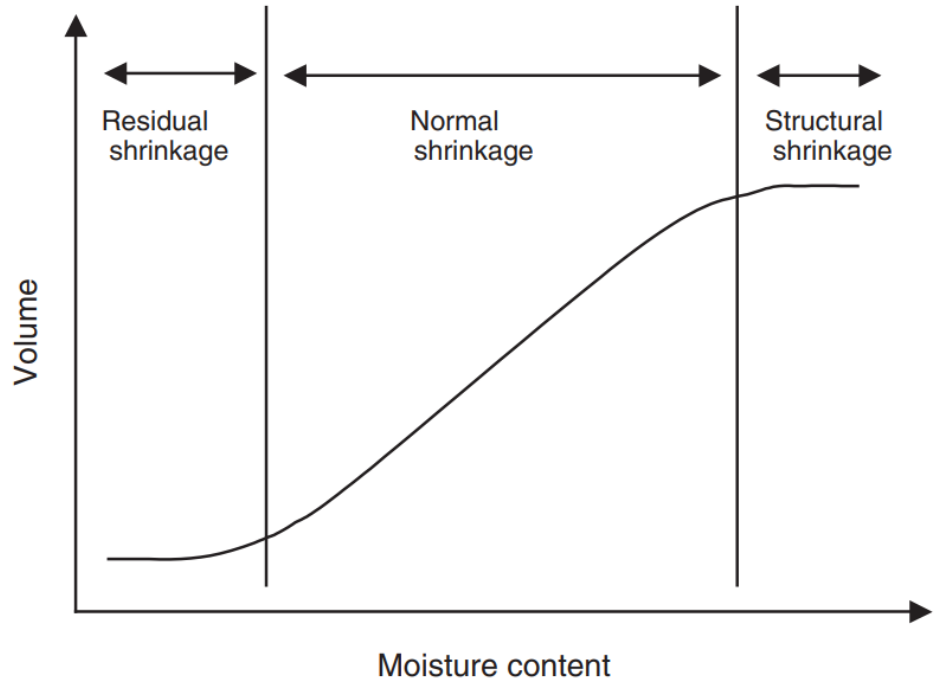

Figure 25: volume change with respect to moisture content, the shrinkage phenomena (Leonard, 2003)

During the drying process, we made interruptions to determine two important parameters of the sludge samples: the average equivalent diameter (d_{eq}, mm) and average height (h, mm). With this information, we calculated the surface area of each sample. In our study, we assumed the sludge samples to have a perfect cylindrical shape, with their entire surfaces in contact with the drying air. This allowed us to consider both the lateral area of the solid cylinder and the area of the two bases in our surface area calculations. By creating a correlation between the surface area (A, mm^2) and moisture content (X, kg_{water}/kg_{MS}), drying process became more clear. Figure 25 clearly illustrates the relationship between the evolution of surface volume (v) and moisture content (X) for the sludge, presenting a distinct trend. After that, We calculated the water flux, by using derived equations for each sample, and so, providing valuable information for the management. (Leonard, 2003).

4.5 H/D method

The height and diameter-based method is used in the scope of this study to estimate the shape change of samples during micro-drying. The original plan was to previously explain microtomography. However, as a result of the encountered technical issue, the H/D method came in handy. It consists of quickly retrieving the sample during micro-drying and measuring the height and diameter every 30 min. Assuming the specimen remains perfectly cylindrical, the area and volume can be calculated. Although this method allows us to get the area and volume only at a few points during drying, another assumption was employed; the shape dimensions are assumed constant between measurements, which results in a set of points representing the area and volume. By plotting the area (mm^2) and volume (mm^3) concerning the moisture content W (Kg_w/kg_s), a linear regression can be performed to check on the linearity of the shape change. A regression value higher than 0.95 implies a linear behavior.

4.6 Convective macro-drying

The convective macro-dryer operates similarly to the micro-dryer but allows for larger sample sizes, ranging from 0.6 to 5.5 kilograms. However, in this study, a sample mass of 1 Kg is considered. To carry out the drying experiments, a pilot-scale discontinuous dryer was used, specifically designed to replicate the conditions of a full-scale continuous belt dryer (as depicted in Figure 26). The drying process starts with an ambient air fan (a) drawing in the surrounding air, which is then heated to the desired temperature using electric resistances (b). If necessary, the air can be humidified after heating by introducing vapor from a vapor generator. The heated air then, passes through the bed of sludge extrudates (c), placed on a perforated grid (d) connected to weighing scales (e). The sample holder within the dryer has an inner diameter of 160 millimeters. Three operational parameters were controlled during the experiments: air temperature, superficial velocity, and humidity. For this particular study, the air temperature was set at 90°C, and the fixed air velocity was maintained at 2 meters per second, which was done by adjusting the built-in fan frequency at 18.2 Hz. No additional air humidification was carried out, and the ambient air humidity throughout the entire study remained at approximately 0.006 kilograms of water per kilogram of dry air (Fanara, 2020; Leonard, 2003). It is important to mention that the drying is considered terminated once a constant mass is reached (for a tolerance of 0.001). Also, a good built-in indicator of the drying progress is the temperature in and out, or before and passing through the material. It was remarked that at a temperature difference of [2-3] °C the sample mass becomes stable.

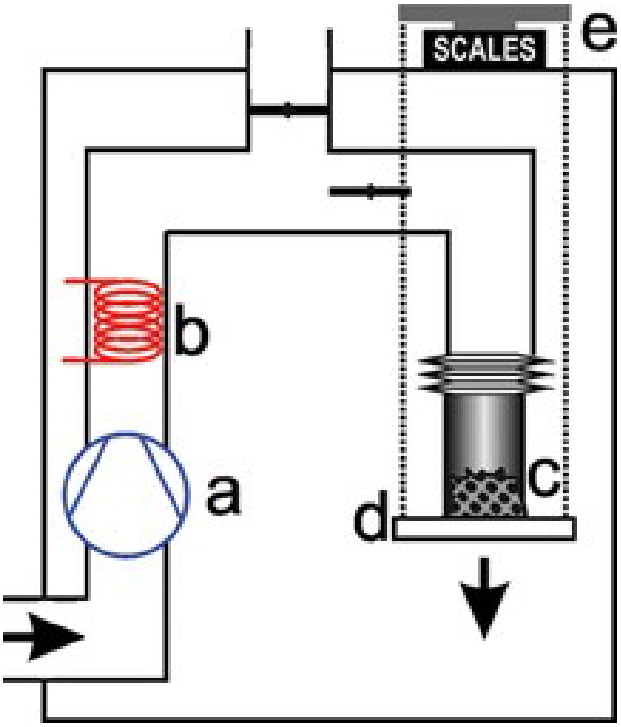

Figure 26: Convective macro-dryer schematic (Leonard, 2003)

4.7 Penetrometry

The instrument used for assessing the texture of the sludge is the LS1 penetrometer, a universal testing machine manufactured by AMETEK Lloyd Instruments in West Sussex, England. This advanced force sensor comes with a 30 mm diameter spherical probe, as depicted in Figure 27. The working principle involves applying a compressive force of 10 Newton (N) using the force sensor on a 60g sample of the sludge. The sample is placed on an aluminum capsule at the base of the machine and compressed to a depth of 10 mm at a constant speed of 1 mm/s, following the method proposed by (Pambou, 2016), ensuring consistency and accuracy.

Figure 27: LS1 AMETEK instrument

Each measurement takes approximately three minutes and consists of a cycle with compression and relaxation phases. This process provides valuable information about the sludge's compressive behavior and adhesiveness. Figure 28 shows a standard penetration curve for the sludge sample (Azeddine et al., 2023), illustrating key parameters. The highest positive peak, F_{max} (in N), represents the force required for the probe to penetrate the sample to its maximum depth and is related to its firmness or hardness. The area under the curve up to F_{max}, denoted as A^+ (in mJ/Nmm), quantifies the work done during the compression test, providing insights into the sample's behavior under compression.

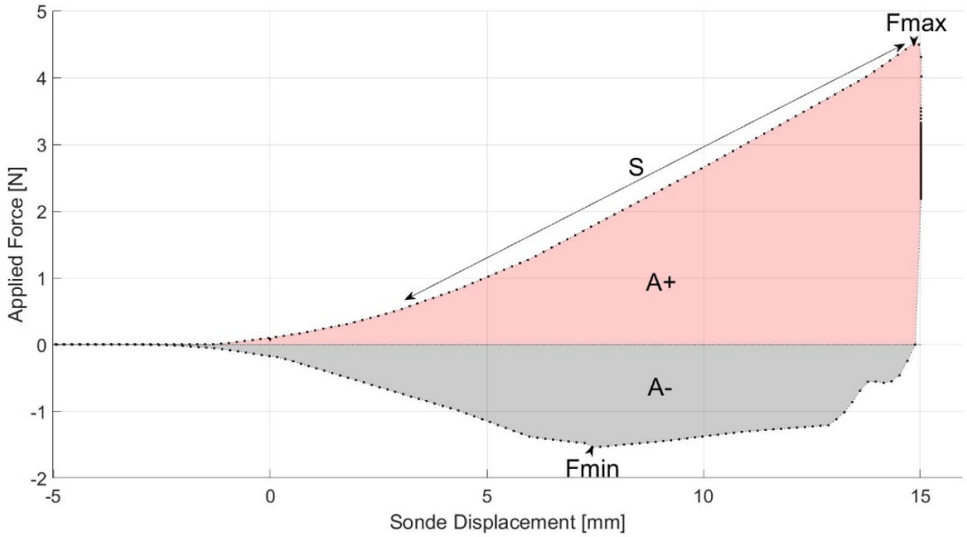

Figure 28: Hydroxide sludge experimental penetration curve (Azeddine et al., 2023)

Similarly, the lowest negative peak, F_{min} (in N), indicates the force needed to detach the sample from the probe and serves as an indicator of its adhesiveness. The negative area under the curve, A^- (in mJ/Nmm), represents the work required to remove the sample from the probe's surface, providing an adhesiveness index (A. Hil & Remy, 2005; Mezger, 2020). The initial slope of the positive part of the curve, S (in N/mm), reflects the sludge sample's rigidity (Rodríguez et al., 2010), while the cohesive load is obtained from the maximum load value recorded during the probe's penetration, expressed in kPa (Y. Liu et al., 2020; Pambou, 2016). To ensure accuracy and reliability in data analysis, all measurements were conducted at room temperature, and each sludge sample underwent three repetitions, with results averaged to minimize experimental variations and enhance the reliability of the derived parameters. This thorough approach ensures precise characterization of the sludge's instrumental texture properties, facilitating informed decision-making and effective applications. In the scope of this study, the properties calculated are adhesiveness and cohesiveness. Due to the inconsistency of the material, resulting in a huge variety of data, it was decided after observing results to rely on the following to calculate the properties in question:

- Adhesiveness [N]:

$$Adhesiveness = -F_{min} \tag{9}$$

F_{min} [N] represents the minimum force observed during penetrometry.

- Cohesiveness [N/mm^2]:

$$Cohesiveness = \frac{F_{max}}{Interface\ Area} \tag{10}$$

$$Interfacearea\ \ [mm^2] = 2x\pi xRxh \tag{11}$$

F_{max}: The maximum force [N]

R: The sphere head radius = 15 [mm]

h: The penetration depth = 10 [mm]

4.8 Texture profile analysis (TPA)

TPA is another method that can be used to study the texture of materials. It consists of using the same machine depicted in Figure 27. However this time the sample has a definite shape, a extruded cylinder of 18 mm diameter and 30 mm height. is subjected to compression using a flat circular head (Diameter = 60 mm) instead of the sphere used in penetrometry. The compression takes place over two rounds for a compression of 30% of the sample height, the first compression causes a material deformation that can be recognized in the second compression round (Liang et al., 2017). The measurements consist of the applied force over time, resulting typically in two significant peaks as depicted in Figure 29.

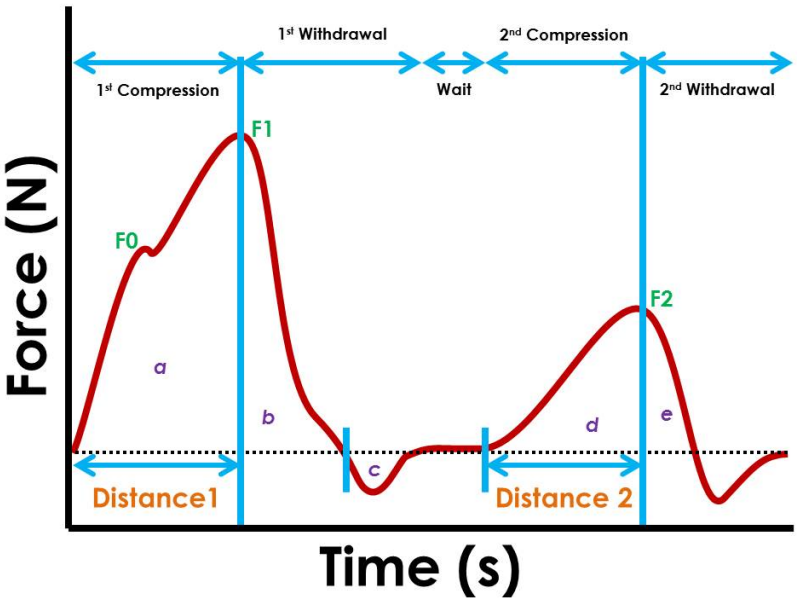

Figure 29: TPA typical result graph (Rheology-Lab, 2023)

The graphical representation allows us to estimate different characteristics, such as hardness, fracturability, springiness, adhesiveness, and cohesiveness. In the scope of this study, we focus on adhesiveness, cohesiveness, and hardness. These properties can be calculated as follows:

- Adhesiveness [N.s]:

$$Adhesiveness = Area(c) \tag{12}$$

shown in Figure 29, representing the area under the first negative peak. However, the unit, in this case, is Newton times seconds, different than the one utilized in penetrometry, thus each characteristic has the same terminology, but a different physical meaning. The adhesiveness calculated in the penetrometry represents the minimum force required to overcome the adhesive bond between the material surface and the device head surface. On the other hand, the adhesiveness estimated here in [N.s] is a unit of impulse usually employed in joules. It represents the change in momentum of an object subjected to a force for a duration of time. Both adhesiveness, although they show different meanings which can be useful depending on the specific application.

- Cohesiveness [No unit]:

$$Cohesiveness = \frac{(d+e)}{(a+b)} \tag{13}$$

(d + e) and (a +b), represents the area underneath the second and first compression curves shown in Figure 29. Also, different from the one calculated in penetrometry, here it is a dimensionless ratio that characterizes how the material held itself internally. However, cohesiveness in [N/mm^2], is a unit of force over area or mega-pascals [Mpa], and it represents the pressure or stress required to break apart a unit area of a material, therefore also reflecting the material internal strength.

- Hardness [N]:

$$Hardness = Force(F_1) \tag{14}$$

F_1 shown in the figure, represents the highest peak force during the first compression. It is a characteristic that gives an insight into the material's overall resistance to deformation. A Matlab code available in annex-11 is used to calculate the hardness.

The positive and negative areas are calculated using the trapezoidal numerical method on Matlab, the codes executed are available in annex-8 and annex-9 respectively.

4.9 Amplitude sweep

The rheological properties of materials are analyzed using an advanced modular MCR302e rheometer shown in Figure 30, manufactured by Anton Paar in Graz, Austria. This rheometer is equipped with a

serrated parallel plate geometry, featuring a 50mm diameter. Data collection and equipment control are managed through the Rheocompas 1.30 software. All measurements are conducted at a controlled temperature of 25°C to prevent moisture evaporation from the samples and ensure consistency. Also, the sample shape is prepared using an extruder to be 18 mm in diameter and 30 mm in height. To enhance accuracy and reliability, each sample and test is repeated three times, and the results are then averaged. Before each measurement, the sludge samples undergo a pre-shearing process lasting 1 minute, with a shear rate of 0.05% and a frequency of 1 Hz. This pre-shearing process, based on the method by (Mouzaoui et al., 2018), minimizes potential structural changes and flow history effects, resulting in consistent and repeatable rheological measurements. After pre-shearing, the samples are allowed to rest for 10 minutes to stabilize before the actual measurements, reducing any residual effects from the pre-shearing process. To identify the linear viscoelastic region (LVER) and assess the viscoelastic behavior of the samples, the "Amplitude Sweep" function of the Rheocompass software is employed. This involves using a 2 mm gap and a logarithmic shear strain ramp ranging from 0.01% to 130%, with a constant angular frequency of 1 Hz. This setup provides detailed data with 10 points per decade, enabling a comprehensive characterization of the samples' viscoelastic properties. The selection of parameters such as gap size, angular frequency, and range of shear strain rates is based on the established methodology (Mouzaoui et al., 2018), ensuring adherence to industry best practices and enhancing the reliability and comparability of the obtained rheological data.

Figure 30: MCR302e rheometer instrument by Anton Paar

The procedure followed in this experiment is explained in Figure 31. In some cases, the sludgy can

have alike solid behavior instead of moisture. The latter is due to a low moisture content, for this case, the methodology described will cause an area of interface destruction and will ruin the experiment. However, thanks to a study made by www, the issue can be resolved.

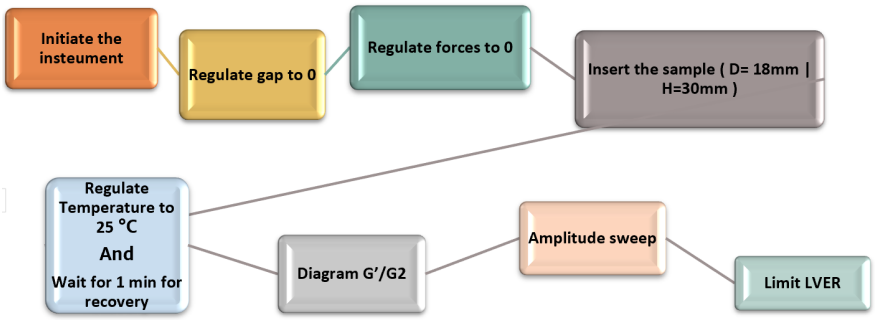

Figure 31: Amplitude sweep procedure

5 Drying results

5.1 Sludge TSC and TVC

Total solid content tests allow us to identify valuable characteristics of the material, namely the minimum achievable sample mass following the process of conductive drying, as well as the initial moisture content, or the initial humidity of the sample. Figure 32 shows the TSC of each station. The consequent initial humidity is represented in Figure 33. The experiments show that the total solid content for the 6 stations

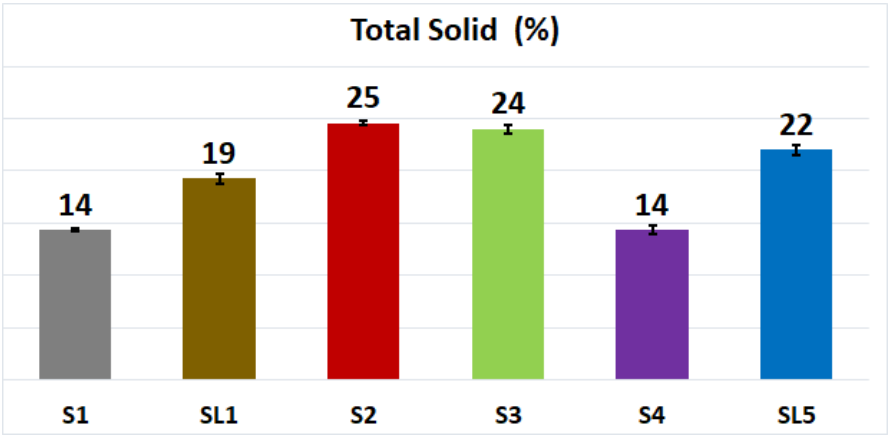

Figure 32: Total solid content (TSC)

is within the range of 14-25 %, and the initial moisture content is within the range of 75-86 % of the total sample mass. Samples from stations S1 and S4 show the highest humidity content and therefore the lowest TSC. It is remarkable for the samples coming from the same station S1 and SL1, the second being subjected to an extra additive (lime) during treatment, that it is possible to achieve a higher solid content when lime is added. As a result, the initial humidity of sample SL1 is lower than S1, which can probably lead to a

better drying performance and a less energy requirement to produce granular sludge. Sl5 is also subjected to liming. However, the latter shows even higher TSC and lower initial moisture content. The mentioned introduces the important argument of the study, being what characteristics, rheological, or texture properties resulting from different treatment histories can affect the solid to water content of sewage sludge, and possibly the drying behavior.

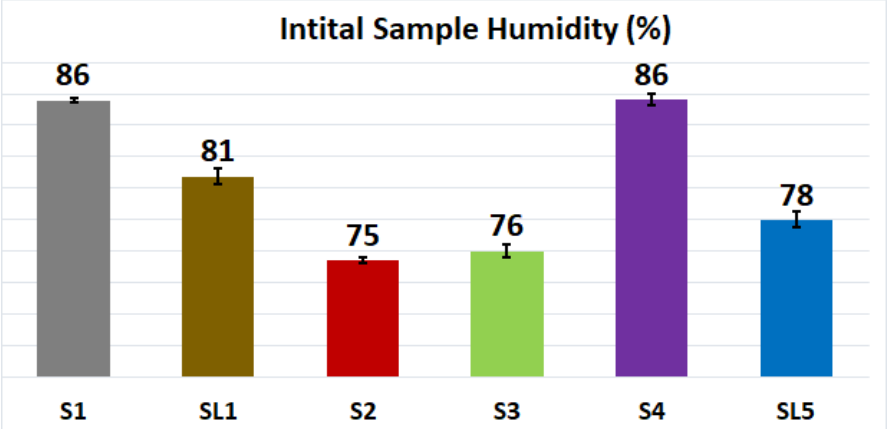

Figure 33: Initial moisture content of each station

The obtained results mash results of typical experiments seen in literature such as (Wang et al., 2016) where similar dewatered sludge samples recorded a TSC of $16 \pm 0.1\%$ and research values reached up to 20-25 %.

5.2 Sludge volatile solid content (TVC)

The volatile solids represent the organic sludge components, usually valorized for agricultural applications. Thus, the higher the volatile solid content in sludge the more effective it is for agricultural uses. These volatile solids usually evaporate at temperatures between 500-600 °C. The samples with higher TVC contain higher organic content and less water, resulting in a lower sample humidity after thermal drying (Moser et al., 2016). The mentioned can be observed in our results shown in Figure 34, as samples with lower humidity content such as S3, S2, and SL5 show higher volatile solid content, compared to S1 and S4 recording the lowest TVC and the highest Humidity. It seems like other factors can affect this analogy since sample SL1 has higher humidity than S3 and S2, but still has higher TVC. One can relate to the process of liming as it increases the TVC. The addition of lime for SL5 did not help enough as it still falls behind S3 and S2 in terms of TVC. The range of TVC is between 22 % and 60 % mashing literature divers values ranging between 15 % and 75 % as proved by (Moser et al., 2016). Finally, one should stop on the SL1 results, since they do not concede with the typical behavior of samples subjected to lime. According to the literature, liming causes TVC to be less important. In our case, SL1 TVC was higher than S1, which raises the question of whether the lime addition caused a certain chemical reaction, resulting in an organic compound formation or a compound that mimicked the same behavior during incineration (Abdel-Monem

et al., 2008).

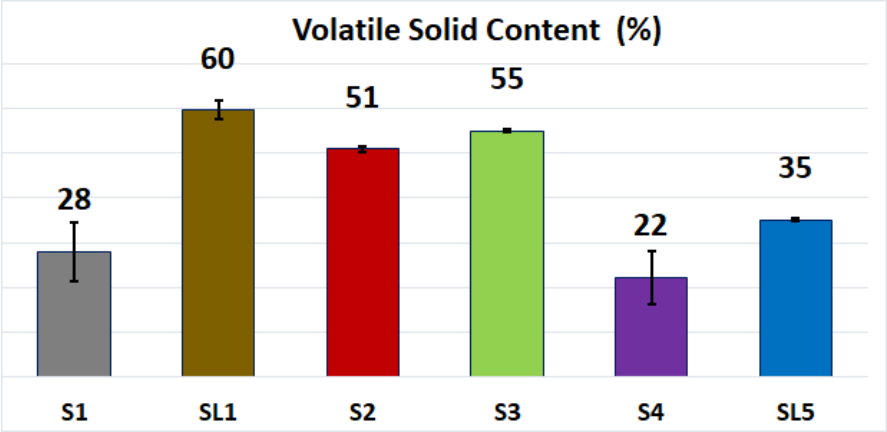

Figure 34: Total volatile solid content of each station

5.3 Macro-drying

Macro-drying experiments were conducted to study the behavior of 1 Kg of the dewatered sludge samples under conductive drying conditions at a temperature of 90°C and an air velocity of 2 m/s. In this section findings and insights gained from drying the different samples are represented:

- Temperature and velocity profiles: The "SEVAR" device utilized to perform the macro-drying allows us to measure the temperature and velocity profiles during drying. However, these insights are valuable when modeling and optimizing such a process, hence it does not have importance when it comes to studying the drying characteristics and rheology of dewatered sludge. In our study, the temperature and air velocity are standard and fixed in all the experiments. Although, observing the temperature profiles inside and outside the sample holder during drying helps us identify the progress as shown in Figure 64 (Annex-3). the outlet temperature represents the sample's internal temperature as the air passes through it, and the closer the outlet temperature is to the inlet temperature, the closer the end of the drying process, as depicted in the figures.

- Pressure drop: "SEVAR" also provides observation of the pressure during the drying process. Figure 61 (Annex 3) shows that for the 6 samples, the pressure during the whole process can be considered constant between 1-1.6 [mmbar], with a small pressure drop in the first 5-20 min of drying. The latter may be due to the crust formation during the early stages, that act as a barrier to the flow of air, causing a small pressure drop. The pressure drop stabilizes directly after for the whole drying period with the adaptation to the drying conditions point of view airflow resistance.

- Mass change over time: An essential aspect of understanding the conductive drying process is to analyze the overall mass change as drying progresses. Figure 35 illustrates the mass change curves for each sample over time.

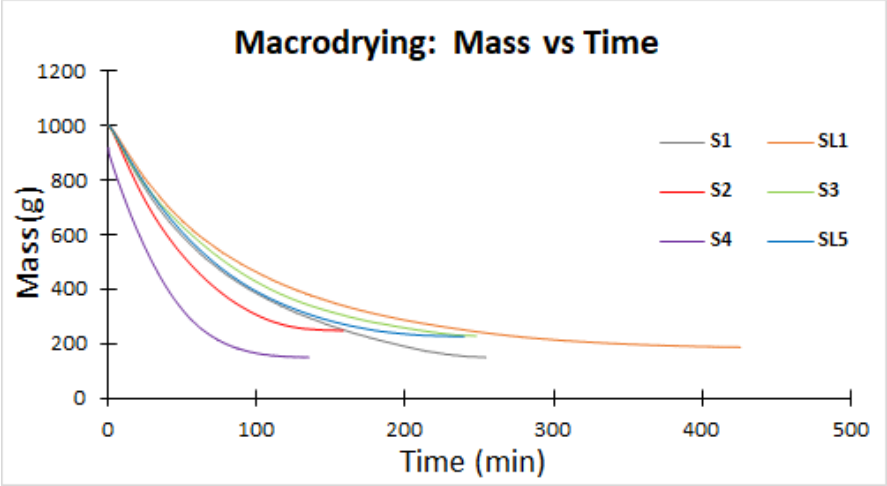

Figure 35: Mass change over time during macro-drying

The graph for each station separately is provided in (Annex 3) Figure 62. The results are valuable to have an idea of the mass change, drying duration, and minimum achievable mass. However, the comparison at that point is not extremely relevant, because each sample has a different initial mass, and even if we take the unitary mass depicted in Figure 36 it is still unfair to judge, because the samples have different initial water content as well. SL1 has the highest drying time and end-product mass, and S4 has the lowest drying time and end-product mass. Comparing the stations based on the unitary mass is not enough because the samples have different moisture content, which affects the conclusion, since of course the lower the moisture content, the lower the drying time. For that reason. We introduce the flux F [$Kg_w.h^{-1}.m^{-2}$]. and the moisture content [kg_w/kg_s]. F change with the introduced moisture content gives a better insight into the drying behavior.

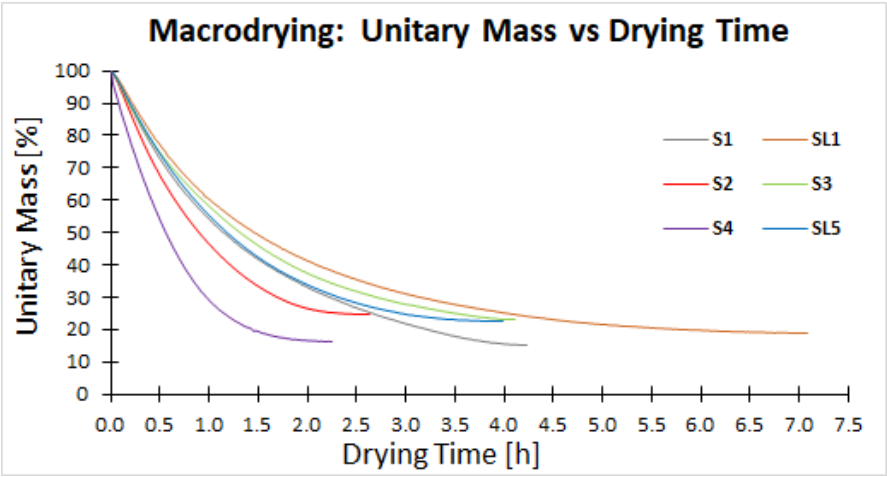

Figure 36: Unitary mass change over time during macro-drying

To calculate F, the area was considered; in the case of macro drying the area is considered constant for the whole drying period, being the cross-sectional area of the cylindrical container [A = 2x π x r^2 = 20106.19 mm^2], employed using the Matlab code in Annex-10 (Lanczos, 1956). The latter assumption

is so to speak acceptable since the air in "SEVAR" vertically hits the sludge, so the change in shape is assumed to be over the height and not the diameter of the extruded cylindrical sludge inside covering the whole horizontal plane surface.

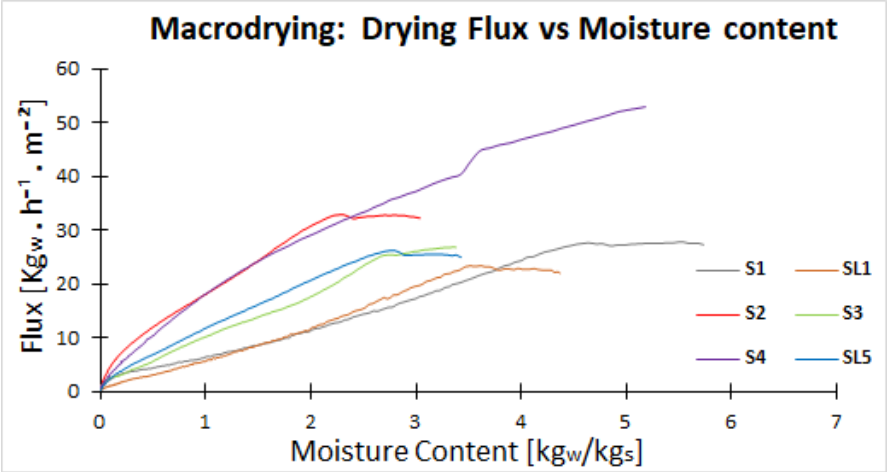

Figure 37: Flux change with moisture content during macro-drying

Figure 37 shows the flux variation that decreases as the moisture content decreases. To analyze the results it's important to look at the overall flux average to be able to judge the drying performance. S4 seems to have the highest Flux followed by S2, S1, SL5, S3, and lastly SL1. The results are quite complicated, it's however proved from the obtained that the initial content of water is not the only factor affecting the rate of drying. One can say that a significantly lower initial humidity leads to a better drying performance, this can be proved by looking at sample S2 being the one with high flux and the lowest moisture content. Similarly, SL1 has a low flux for high humidity, and SL5 medium flux for medium humidity. On the other hand, S4 seems to break the rule, having the highest flux and relatively high initial humidity. One can conclude as also mentioned by (Leonard, Vandevenne, et al., 2004) that the volatile solid content of S4 being the lowest can explain its high flux. As well as the highly volatile solid contained in SL1 and S3 explains the low consequent fluxes. The impact of volatile solid content can be explained by the fact that high TVC materials have lower thermal conductivity, leading to a less efficient heat transfer within the material, leading to a poorer drying performance (Deng et al., 2013).

Here comes the importance of the remaining experiments, explaining the odd behavior of samples that is not related to the moisture content, and checking if it can also be explained by the rheological and texture properties.

- Humidity change over time: The humidity trend over time for each station is shown in Figure 63

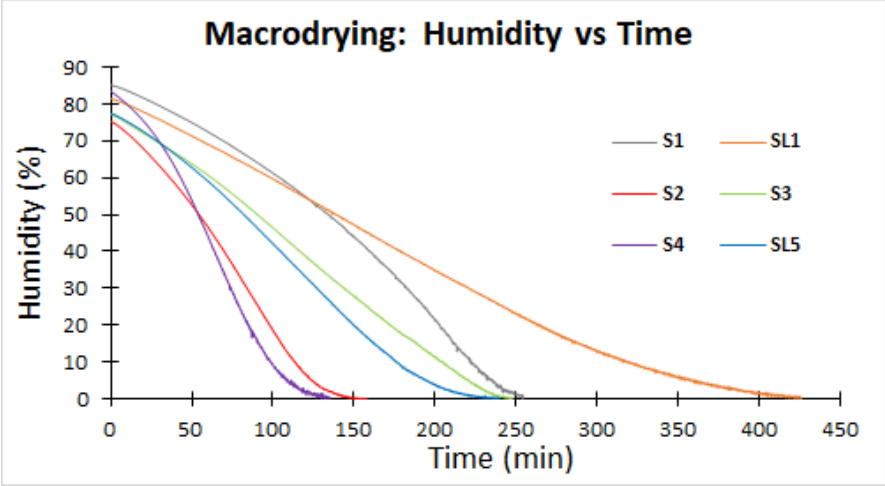

Figure 38: Samples humidity change with time during macro-drying

The results in the graphs mash the order of the previous section in terms of performance. It can be seen that S2 and S4 reach the minimum humidity level, followed by SL5, S3, S1, and lastly SL1.

- Drying duration: it is important to emphasize the importance of drying time in the context of sludge management since it relates to the energy and cost required to employ the treatment.

Sample	Drying time [h]
S1	4.2
SL1	7.1
S2	2.6
S3	4.1
S4	2.2
SL5	3.9

Table 9: Macro-drying time for each station

The lower the drying period the lower the energy consumption, the cost, and the environmental harm. Table 9 summarizes the drying time for each station, showing that indeed the higher the flux the faster the drying. Figure 39 neutralizes the effect of initial moisture content to better visualize, and compare the drying performance. This is done by considering the flux concerning the ratio of sample humidity over the initial humidity. The order of the faster drying rates is clearer and more convenient when using this representation.

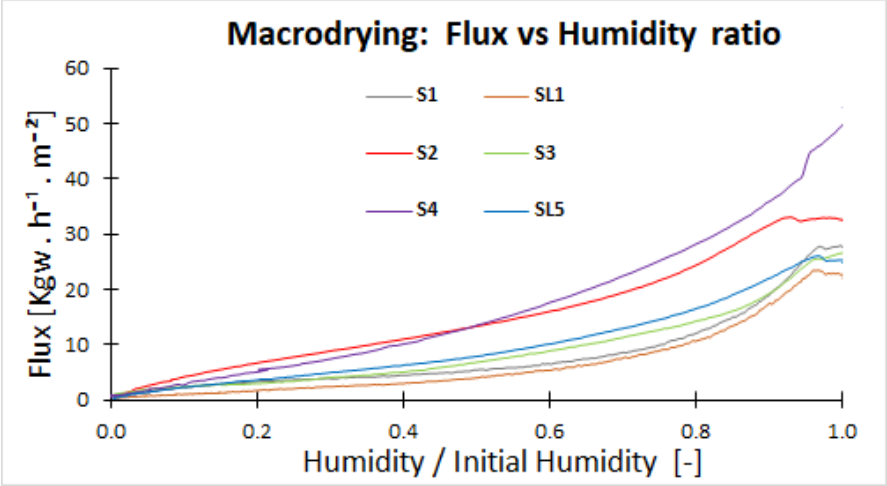

Figure 39: Flux vs humidity ratio during macro-drying

5.4 Micro-drying

Micro-drying is the second drying method that utilizes a smaller sample, keeping the same operating conditions. This method might be more accurate than macro drying because the area and volume changes are measured at several points during the process. However, the drawbacks of using this machine are oscillation and data fluctuation. Due to the smaller size compared to the macro-dryer, and the air direction being horizontally hitting the sample, its less stable and it results in oscillating data. Although, the obtained data are smoothed using the Matlab code in Annex-10 (Lanczos, 1956). The area as shown in Figure 68, and the volume in Figure 69 (Annex-4) follow a linear change with respect to the moisture content, which mashes similar experiments from the literature such as the study of (Leonard, Blacher, Marchot, Pirard, et al., 2003). The experiment results are as follows:

- Mass change with time:

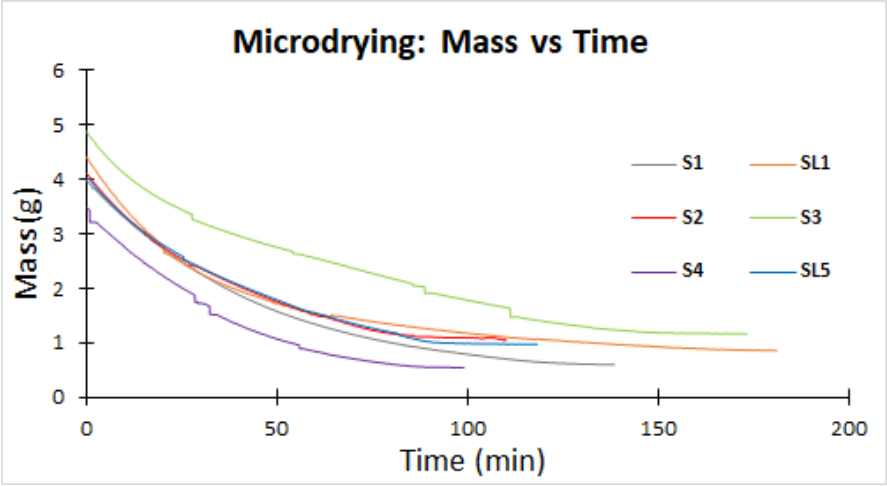

Figure 40: Mass change with time during micro-drying

The results obtained for micro-drying (Figure 66), mashes the ones obtained for macro-drying except for the S3 and SL1. During macro-drying SL1 had a lower mass at the end of the drying compared to

S3. Whereas, during micro-drying, it is the inverse. In terms of apparent drying duration, the results are similar to macro-drying with the following increasing order: S4, S2, SL5, S1, S3, and SL1. However, as mentioned earlier, it is not relevant to compare the drying performance based solely on the mass change with time, due to the difference in samples' initial mass and humidity.

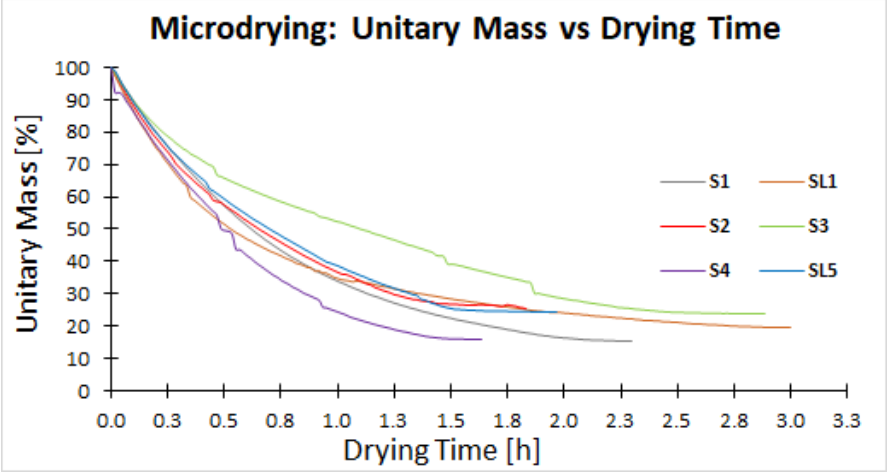

Figure 41: Unitary Mass change with time during micro-drying

- Unitary mass change with time: The unitary mass change with time (Figure 41), gives us a better observation of the evaporating behavior of the samples especially when coupled with the sample's humidity change with time (Figure 67). The results show that S4 and S1 give a lower end-product mass compared to Sl1, SL5, and S2. Also, S3 shows the highest end-product mass. The more mass is lost the more the water is removed, reducing the overall handling volume, which is important in sludge management.

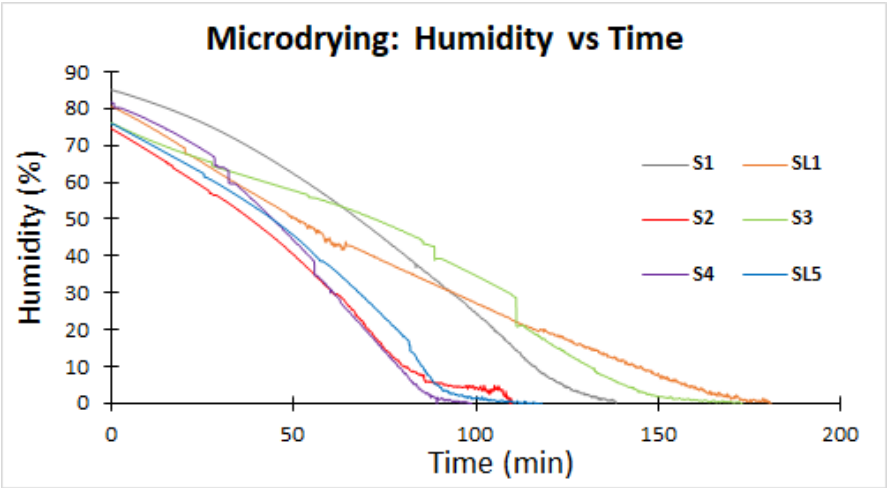

Figure 42: Samples humidity change with time during micro-drying

- The consequence of mass loss can be observed by the on-water evaporation can be seen in the humidity vs time graph. With different initial moisture content, it's not possible to compare the performance. Although, by looking at the slope of water loss, it can be seen that sample S1 shows a higher slope resulting in a relatively slow rate of change. Also, S3 shows a sudden increase in slope after 50 min of

drying affecting its performance and leading to a slow drying process that surely will be noticeable when looking at the flux change. S3 had a low initial moisture content and as can be seen the slope was quite steep like S4, S2, SL5, and SL1, till it suddenly change. The reason behind that may be related to factors other than drying characteristics. Comparing the mentioned with the macro-drying results, it appears that it's only during micro-drying that S3 shows an odd behavior.

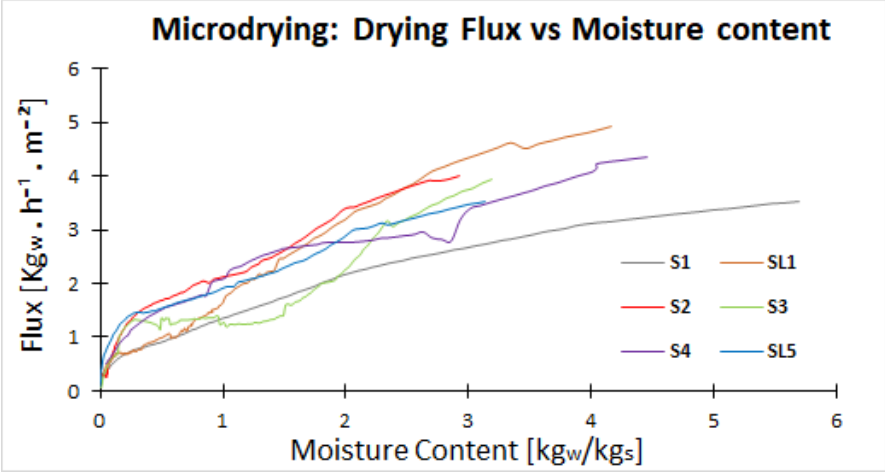

Figure 43: Flux change with moisture content during macro-drying

The Flux vs the moisture content (Figure 43) or the ratio of humidity over initial humidity (Figure 44) shows similar results to the one obtained during macro-drying, with only one difference. It is observed that samples subjected to liming perform slightly better in terms of flux change when the sample is smaller. SL1 and SL5 showed higher relative fluxes during micro-drying. The reason behind that is related to the differences in both devices, one employing vertical convective drying and the other horizontal convective drying. The airflow direction has an impact on the drying performance, but it depends on the material in question (EL-Mesery et al., 2023).

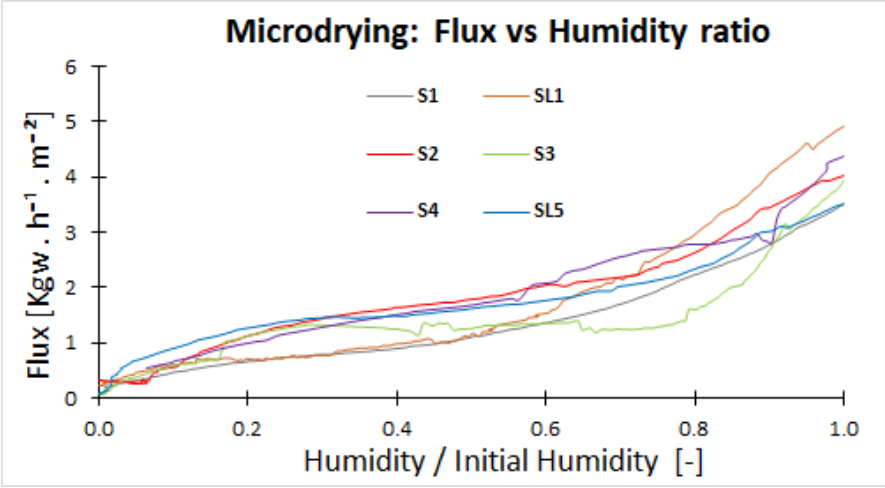

Figure 44: Flux vs humidity ratio during micro-drying

- Drying time: Once again, results for micro-drying and macro-drying appear to be similar with S4 being the fastest to dry and SL1 being the slowest. Table 10 presents the drying time for each sample.

Sample	Drying time [h]
S1	2.3
SL1	3
S2	1.8
S3	2.8
S4	1.6
SL5	1.9

Table 10: Micro-drying time for each station

- Volume and area change during micro-drying

Sample	Area reduction [%]	Volume reduction [%]
S1	47	62
SL1	76	87
S2	44	58
S3	34	48
S4	54	68
SL5	47	62

Table 11: Volume and area reduction during micro-drying

The volume and area of sludge decrease during conductive drying causing cracks and shrinkage to the samples as proved also by (Leonard, Blacher, Pirard, et al., 2003) and illustrated in Figure 57. The size reduction is proportional to the initial moisture content (MC), the higher the MC the higher the size reduction. All the samples shown in Table 11 follow this rule except for SL1. SL1 if compared with the S1 being sampled from the same treatment plant, shows a lower moisture content as expected due to the addition of lime, increasing the TSC, and therefore decreasing the water for a specific mass of sample. This lower initial moisture content did not translate into a lower volume reduction after drying. But, on the contrary, SL1 recorded the highest decrease in volume. (X. Liu et al., 2012) experimentally proves that the higher the liming dosage the lower the moisture content. On the other hand, it has been proven that the higher the liming dosage the more the volume is reduced following a drying process (Teleshova & Petuhova, 2021). This proves that our results mash the literature. Although, We rely on the later experiments to possibly explain the reason why lime addition leads to reduced after-drying specimen volume compared to non-limed samples.

5.5 Drying conclusion

In order, to visualize the differences, and be able to relate the different drying characteristics to the rheological and texture properties of the samples in question, Table 12, illustrate the order in term of the rank ranging from 1 to 6, with a low rank signifying a low value, and a high rank signifying a high value. The value ranges and units are also represented in the illustrative table, to summarize the important characteristics. The parameters of choice are chosen based on their relevancy such as TSC, TVC, unitary mass, flux, and drying time.

		RANK (Increasing value →)						Range	Unit
		1	2	3	4	5	6		
ALL	TSC	S1	S4	SL1	SL5	S3	S2	[14 - 25]	%
	TVC	S4	S1	SL5	S2	S3	SL1	[22 - 60]	%
	Initial Humidity	S2	S3	SL5	SL1	S4	S1	[75 - 81]	%
MACRO	Unitary Mass (Macro)	S4	S1	S2	SL5	S3	SL1	[0 - 100]	%
	Flux (Macro)	SL1	S3	SL5	S1	S2	S4	[0.1 - 53]	$Kg_w.h^{-1}.m^{-2}$
	Drying Time (Macro)	S4	S2	SL5	S3	S1	SL1	[2.2 - 7.1]	Hours
MICRO	Unitary Mass (Micro)	S4	S1	SL1	S2	SL5	S3	[15 - 100]	%
	Flux (Micro)	S3	SL1	S1	SL5	S2	S4	[0.07 - 5]	$Kg_w.h^{-1}.m^{-2}$
	Drying Time (Micro)	S4	S2	SL5	S1	S3	SL1	[1.6 - 2.8]	Hours
	Volume lost	S3	S2	SL5	S1	S4	SL1	[48-87]	%

S1
SL1
S2
S3
S4
SL5

ALL: Samples characteristics
MACRO: Macro-drying results
MICRO: Micro-drying results

Table 12: Drying characteristics summary

Firstly, Sample S1 has low TSC and TVC percentages, consequently, a high initial moisture content, the overall drying period for S1 is considered slow, and the end-product mass achieved for this sample is quite low for a moderated overall flux and moderated to high volume reduction. S4 shows similar specs, except that it has the highest flux rate leading to a very fast drying time. At this point, further investigations and comparison of S1 and S4 in terms of rheology can help us identify what could have caused the higher flux in S4 that led to faster and more economical drying.

Secondly, samples S2 and S3 both have recorded high TSC, and moderated to high TVC. As previously explained, high TSC means low initial moisture content, therefore low volume reduction, and low to moderated end-product mass. Nevertheless, S2 shows higher flux than S3, which makes S2 dry faster than S3.

Finally, SL1 and SL5 both have a moderated TSC, and initial moisture content. These two samples are the only samples subjected to liming. Therefore, and as shown by (Teleshova & Petuhova, 2021), they translate height to moderated volume reduction; with SL1 shrinking 15 % more than SL5. SL1 has a smaller flux rate than SL5, making the drying time longer. Moreover, TVC is higher for SL1, and as observed for all the samples, TVC correlates perfectly with the minimum achievable mass after convective drying. The

impact of TVC on the end-product mass seems more important than the effect of initial humidity.

In general, findings concede with literature experiments such as the one made by (Bennamoun et al., 2013; X. Liu et al., 2012; Teleshova & Petuhova, 2021). It can be concluded that the higher the TSC, the lower the initial moisture content. Also, the lower TVC, the lower the after-drying mass. Additionally, limning results in lower humidity and higher shrinkage. Finally, the flux determines the drying quality, and the required duration, which directly relates to the cost, and energy requirements to handle sludge. Apparently, other aspects control the flux intensity, we believe that the subsequent experimentation help in completing the picture.

6 Texture results

6.1 Penetrometry

Penetrometry gives us an insight into the sample's texture properties such as "cohesion": The internal capability of the material particles to hold together when subjected to stress, and "adhesiveness": The ability to adhere to a surface. The 6 samples involved in this study show penetrometry results:

- Applied force vs the sonde displacement: Figure 72 (Annex-6) illustrates the 3 trials of each sample using the pentameter. The resulting is an applied force [N] vs sonde displacement [mm] graph, characterized by a maximum and minimum force, and positive and negative areas under the curves. It is remarked that, the samples are not extremely consistent. All samples have similar behavior, with different positive and negative areas, as well as different maximum and minimum peaks.

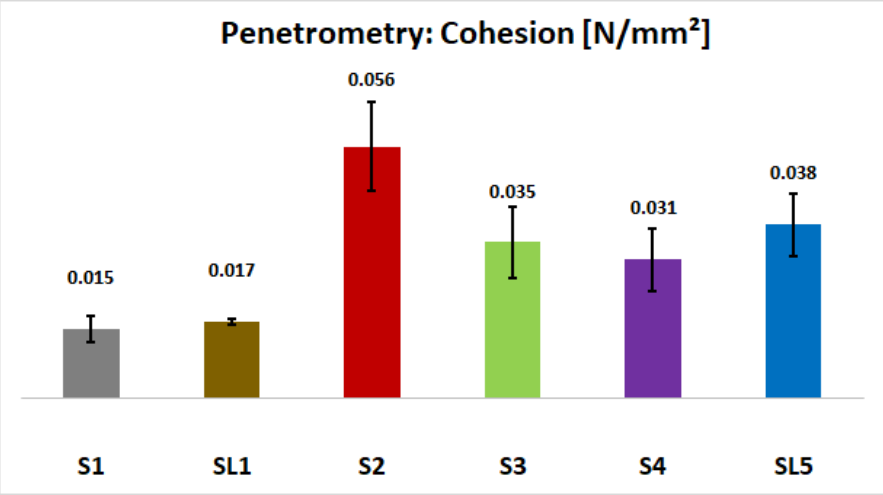

Figure 45: Penetrometry cohesiveness results

- Cohesion: The cohesiveness results for the samples are shown in Figure 45. The cohesion in this test is calculated as a pressure unit, describing the pressure needed to break the internal bonds of the materials apart. It is observed that S2, the sample that is having the lowest moisture content, have the highest cohesiveness. Whereas, S1, the sample with the highest initial humidity, shows the lowest cohesion pressure. However, one can say that cohesion is inversely proportional to the initial moisture content. Although, samples recording cohesiveness between S2 and S1 appear to not ideally follow this conclusion.

- Adhesiveness: Figure 46, shows that the adhesiveness of samples S2 and SL5 is greatly higher than the remaining ones, with sample S1 recording the lowest adhesiveness. It is important to mention that results obtained are in the same order of magnitude, but lower than the one found in literature such as (Azeddine et al., 2023). Also, cohesion results were of the same order of magnitude, but higher than the ones seen in the literature. The reasons behind the differences are typical, since the sludge as we have seen so far, is very wide in terms of characteristics, and properties; with multiple influencing parameters. More specifically, the study made by (Azeddine et al., 2023) analyzed samples from a different country, with higher TSC, and lower TVC.

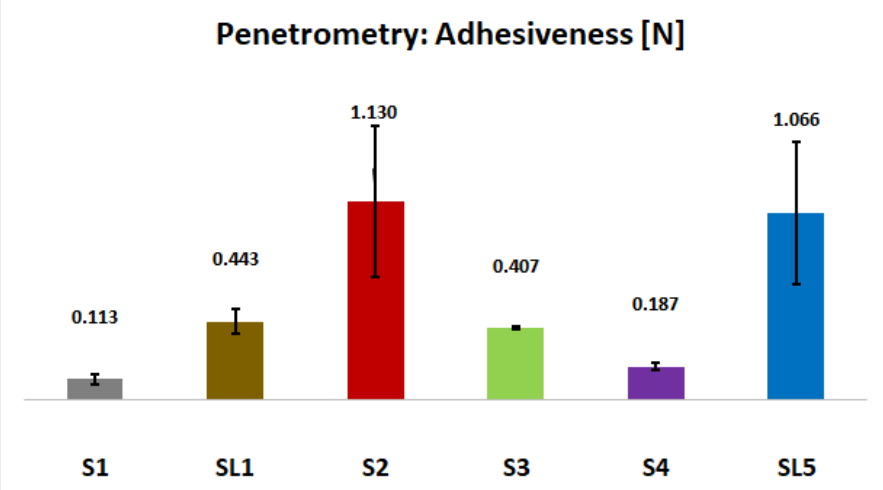

Figure 46: Penetrometry adhesiveness results

6.2 Texture profile analysis

- Force vs time: Figure 29 (Annex-7), shows the different samples applied force vs time results. The peaks explained in the literature can be seen. Some of the peaks are higher for samples and lower for others. In all the samples first compression peak is bigger than the second compression peak, with different intensities between samples, which indeed shows that the material in question is a viscoelastic solid that doesn't recover the full shape after being subjected to stress, but it persists in a deformation. The order of magnitude of the peak forces is validated, as it concedes with results found in literature such as (Liang et al., 2017).

- Cohesiveness: The cohesiveness ratio calculated in TPA shows different order than the one observed in the penetrometry. As explained earlier, both have different physical meanings. In analyzing the data, the cohesion expressed in [N/mm^2] or [MPa] will be used as it concedes with the unit, and physical representation found in the literature for pasty sludge materials (Azeddine et al., 2023). Although, TPA cohesiveness may be better than penetrometry cohesion.

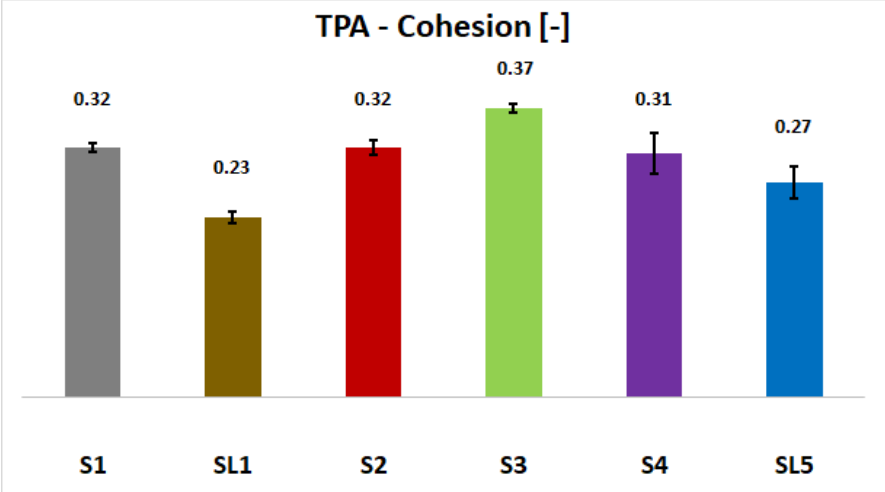

Figure 47: TPA cohesion results

it can be seen that, the cohesiveness values don't vary much between samples, whereas the maximum difference is 14 % (Figure 47). Nevertheless, for standardizing a pasty sludge with different histories, and influencing factors; the cohesion ratio appears to be a good way to identify the type of material in use, as it considers the ratio of the second over the first compression peak.

- Adhesiveness: The adhesiveness found in literature is expressed mainly in [N] the one estimated here is in [N.s], which gives an insight into how big the negative area under the curve after the first compression, may describe the momentum of adhesiveness recovery following stress. SL1 shows an extremely higher value in a different magnitude order compared to the other samples (Figure 48), which urged further investigations. The answer was found in a study made by (Deng et al., 2020) as the article demonstrates that for any pasty sludge material cohesiveness, stickiness and adhesiveness follow a pattern with respect to the moisture content. The study shows that, the adhesiveness increase with the decrease in moisture content, until it reaches a maximum at a certain moisture content range, then it decreases gradually with further humidity decrease. This may imply that the moisture content in SL1 may be in the optimal maximum range of this specific sample. Whereas, all the others may be in the early or later ranges.

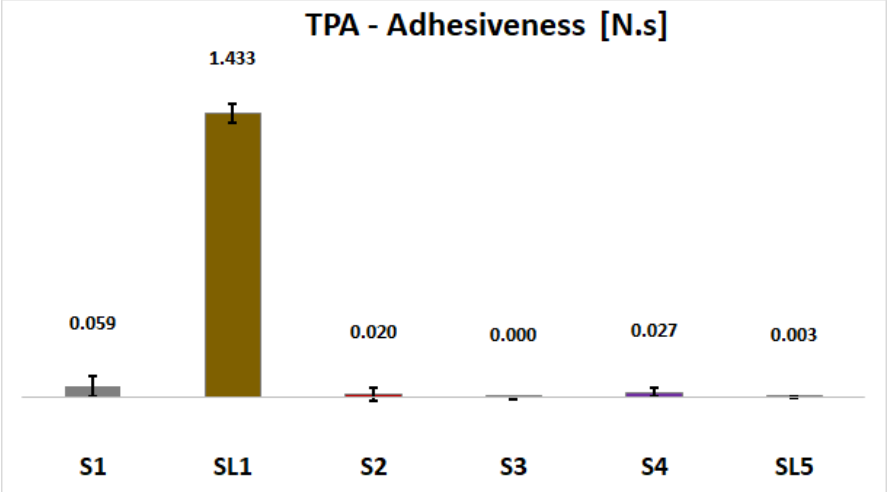

Figure 48: TPA adhesiveness results

- Hardness: Figure 49, shows that SL1 and S3 have the highest hardness value, which is the highest peak and the maximum load observed during the compression test. This parameter, represents how hard a material is.Moreover, The harder the material, the more solid-like behavior it possesses (Kirby et al., 2015)

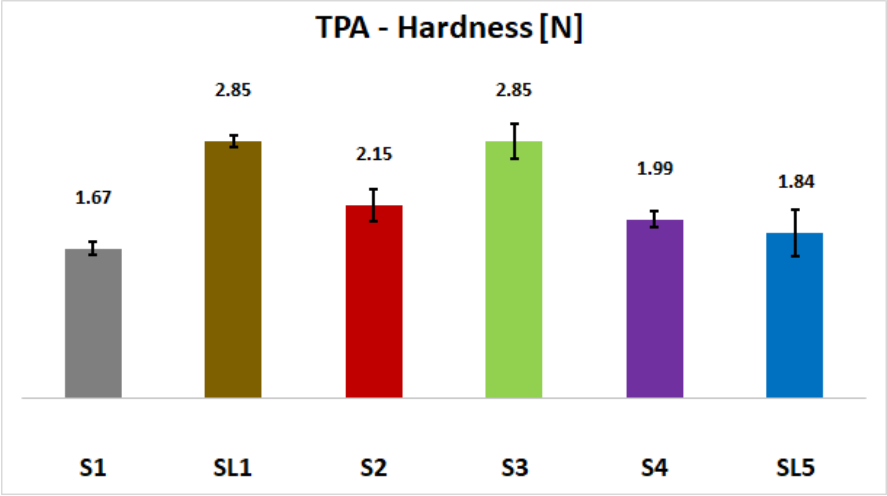

Figure 49: TPA hardness results

6.3 Amplitude sweep

- Storage, loss modulus vs shear strain:

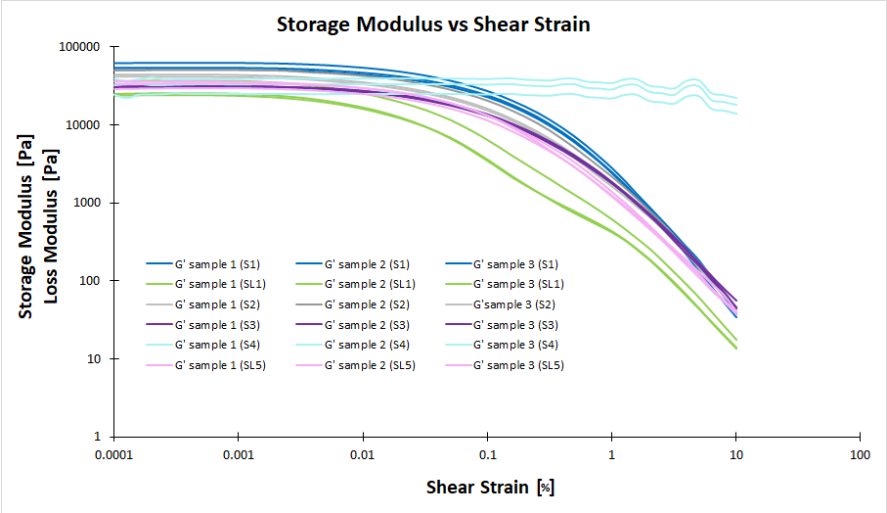

Figure 50: Storage modulus vs shear strain for all samples

The storage modulus is a key parameter to understand the ability of the material to store elastic energy when subjected to stress. Figure 50, shows the behavior of all 3 samples of the 6 stations considered in this study. It can be observed that sample S1 has the highest storage modulus G', and SL1 has the lowest G'. This means that S1 is less prone to deformation than SL1, and the ability of the remaining sample to stay elastic falls between these two samples. However, sample S4 seems to be an exception, during the experiments S4 showed a very solid-like behavior, it breaks and forms cylinders during the amplitude sweep. A corrected methodology was used for this sample and proposed by (Mouzaoui et al., 2018). All the samples had a storage modulus higher than the loss modulus G". G" represents the ability of the material to dissipate energy as heat. As long as G' > G", the material is considered solid or gel, once G' < G" it means that the material is in the liquid state (Thiedeitz et al., 2022). Figure 71, shows the behavior of G' and G" with respect to the the shear strain separately for each station.

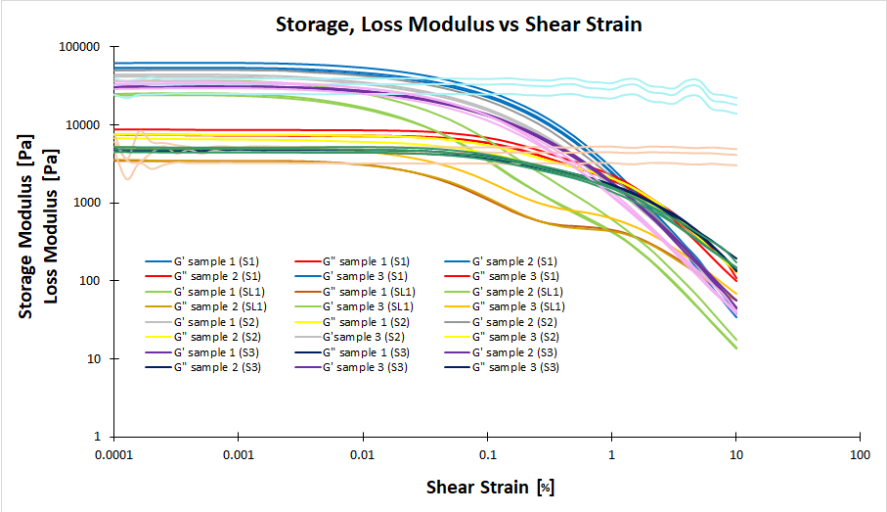

Figure 51: Storage, shear modulus vs shear strain

- Limit of the viscoelastic solid region (limit LVE): The samples can be characterized by the LVE limit. The higher the viscoelastic limit, the longer the sample exhibits a linear viscoelastic behavior before deforming. Figure 52 shows the different shear strain values at the LVE limit. Also, Figure 53 shows the corresponding storage modulus values at which the viscoelastic regime ends.

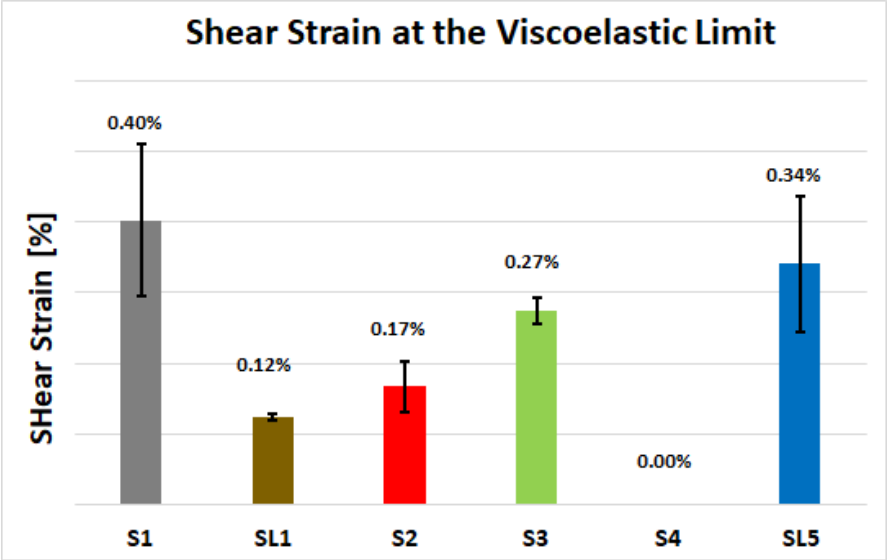

Figure 52: Shear strain at the LVE limit

Sample S4 has the highest strain at the LVE limit, which means it may showcase significant deformation potential under viscoelastic conditions. Also, S4 shows a low storage modulus at the same LVE limit indicating a relatively lower stiffness. In other words, S4 show more prone to deformation. In contrast, sample SL1, with the second-highest Strain value at the LVE limit, also holds the highest storage modulus at the LVE limit. This combination implies a material that can follow important deformation while being stiff.

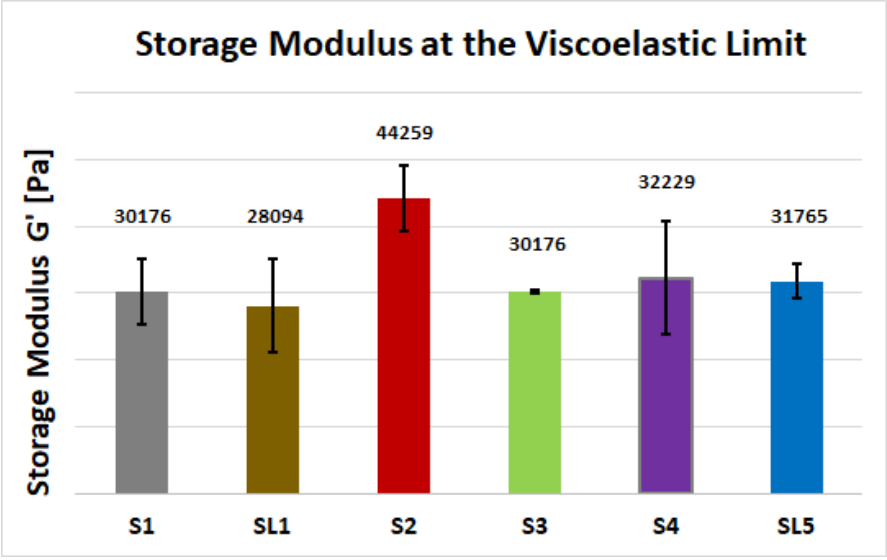

Figure 53: Storage modulus at the LVE limit

Moreover, sample S2, is the third in strain and the sixth in storage modulus, which gives it moderate

deformation potentials, low stiffness, and flexible behavior (Huron et al., 2010; Liang et al., 2017). For sample S3, it has the fourth most high strain and second most high storage modulus making it moderately prone to deformation and high on stiffness. In contrast, samples SL5 and S1 exhibit relatively similar order in strain and storage modulus, reflecting high viscoelastic responses (Thiedeitz et al., 2022).

6.4 Texture and Rheology Conclusion

The analysis of the viscoelastic limits (LVE) of the samples, holds indications for important parameters, such as drying flux, cohesion, and adhesiveness. A higher LVE limit, reflects more stability under stress and could correlate with longer drying times caused by delayed transition into the viscoelastic regime (Liang et al., 2017), probably resulting in slower drying flux. Higher LVE limits, leads to slower drying rates, and associated with stronger particle interactions or cohesiveness and therefore a slower duration and a higher cost. Conversely, lower LVE limits apparently indicate higher adhesiveness and faster drying rates. To sum up, the LVE limit results, provide a lens to understand the connection of rheology with the drying flux, cohesion, and adhesiveness.

7 Overall conclusion

The interplay of various parameters and characteristics are explored for the 5 treatment plants in Liege, Table 13 summarizes the findings and provides the range in which the studied parameters fall.

The experimental data analysis reveals a complex relationship between parameters. Firstly, a higher initial moisture content usually to contributes usually to longer drying times, due to the need to evaporate more water. This connection has been well explained in the literature (Madan et al., 2014). However, this didn't correlate accordingly with drying fluxes, revealing that other characteristics may have a greater impact on the drying time. Moreover, higher adhesiveness corresponds to a shorter drying time for some samples and a higher drying time for other samples, which means that adhesiveness has an effect that is not straightforward. Although, literature shows that less adhesive samples have a reduced drying rate (Mert et al., 2007). additionally, the cohesive interactions between particles cause the formation of a more solid-like structure, accordingly, the elevated adhesiveness can be linked to increased cohesion and hardness, which is observed by a high storage modulus for sample S2 and SL5. Also, less cohesiveness and adhesiveness lead to a larger viscoelastic regime in which the material responds linearly and elastically to the force applied. Interestingly, the unitary mass serves as an indicator of the drying efficiency, since a lower mass reflects a more effective drying and a higher flux. This observation is manifested in the case of samples S4, S2, and SL1.

The correlation between hardness and drying flux show that an optimal hardness can be found for dewatered sludge, since moderated hardness lead to higher drying fluxes and lower drying time (S4 and S2). This can be also proved by looking at sample sL1 which records a high hardness and a long drying period. The study sheds light on the role of cohesion in shaping drying behaviors. Higher cohesion appears to lead to slower drying times, aligning with the well-established understanding that stronger particle bonding impedes moisture movement. The connection between cohesion and hardness is evident, indicating that materials with stronger cohesive forces exhibit greater hardness.The comparison between sludge samples S1 and SL1 provides valuable insights into the influence of lime addition on the various parameters studied. Notably, the addition of lime has led to discernible changes in the drying and rheological characteristics of the samples. In terms of moisture content, SL1 records higher initial moisture content compared to S1, indicating that lime addition increased water retention in this case. The addition of lime also appears to speed up the drying process, as evidenced by SL1's higher drying flux. However, this hasn't translated to a shorter drying time. Also, SL1 displays greater adhesiveness and hardness than S1, possibly indicating altered surface properties due to the lime treatment. Therefore, the addition of lime helps in increasing the flux but not in enhancing the drying due to the alteration of texture properties that impact the overall drying. Additionally, SL1's higher strain at the viscoelastic limit and storage modulus suggests enhanced mechanical strength and deformability after liming. The percentage of lost volume is also higher for SL1, suggesting potential changes in volume reduction during the drying process caused mainly by the higher moisture content.

Overall, the comparison underscores the multifaceted impact of lime on sludge characteristics, affecting parameters related to moisture retention, drying kinetics, rheological behavior, and mechanical properties. The comparison between SL1 and other samples, such as S4 and S2, reveals intriguing insights into the impact of liming on the drying characteristics of sludge. Despite SL1's higher drying flux and volatile solid content, its longer drying time stands out as an exception. This discrepancy can be attributed to a combination of factors, including SL1's higher cohesion and strain at the viscoelastic limit, lower storage modulus, and softer texture. These properties, most likely influenced by the liming treatment, have seemingly counteracted the expected benefits of higher drying flux. While SL1 demonstrates enhanced drying flux, its unique rheological and textural attributes have contributed to a prolonged drying time. This underscores the importance of considering multiple parameters when evaluating drying efficiency. Consequently, S4 and S2 emerge as more energy-efficient samples due to their faster drying times and higher flux, showcasing their potential for cost-effective drying processes. Contributing to the conclusion that low initial moisture content samples show high adhesiveness and cohesiveness, and the contrary for the samples with high moisture content. Texture and rheology play a pivotal role in determining the energy efficiency of drying processes. While parameters like drying flux and volatile solids content are critical indicators, the unique characteristics of sludge samples, such as cohesion, strain at the viscoelastic limit, storage modulus, and hardness, can significantly influence drying times and energy requirements. The case of SL1 highlights that a comprehensive understanding of texture and rheology is essential to fully comprehend drying behavior. Thus, considering these factors alongside traditional indicators is imperative for optimizing energy-efficient drying strategies and reducing operational costs. The mentioned comparisons are pretty much confusing because of the various interconnection between the parameters. For that reason, it is relevant to compare S1 to S4. Both samples have similar TVC and moisture initial content, hence can be better referred to emphasize the importance of texture and rheology. Sample S1, with its higher adhesiveness, cohesion, and hardness values, has a more cohesive and compact structure. On the other hand, sample S4 exhibits lower adhesiveness, cohesion, and hardness, indicating a more porous and less cohesive structure. This porous nature can enhance water evaporation and facilitate a faster drying process. When considering rheology, sample S1's higher storage modulus at the viscoelastic limit implies a stiffer structure, potentially hindering water release during drying. In contrast, S4's lower storage modulus suggests a more flexible structure, allowing for better water movement and evaporation. While both S1 and S4 have similar initial moisture content and volatile solids, their differing texture and rheology properties play a crucial role in energy-efficient drying. S4's less cohesive and more porous structure, along with its more flexible rheological properties, promote faster water evaporation and a shorter drying time. This comparison highlights how texture and rheology can contribute to enhanced energy efficiency during the drying process, even for samples with similar initial moisture content and TVC.

Finally, it's important to note that while these observed trends provide valuable insights, the uniqueness of

your samples and experimental conditions may introduce variations from generalized expectations.

		RANK (Increasing value →)						Range	Unit
		1	2	3	4	5	6		
ALL	TSC	S1	S4	SL1	SL5	S3	S2	[14 - 25]	%
	TVC	S4	S1	SL5	S2	S3	SL1	[22 - 60]	%
	Initial Humidity	S2	S3	SL5	SL1	S4	S1	[75 - 81]	%
MACRO	Unitary Mass (Macro)	S4	S1	S2	SL5	S3	SL1	[0 - 100]	%
	Flux (Macro)	SL1	S3	SL5	S1	S2	S4	[0.1 - 53]	$Kg_w.h^{-1}.m^{-2}$
	Drying Time (Macro)	S4	S2	SL5	S3	S1	SL1	[2.2 - 7.1]	Hours
MICRO	Unitary Mass (Micro)	S4	S1	SL1	S2	SL5	S3	[15 - 100]	%
	Flux (Micro)	S3	SL1	S1	SL5	S2	S4	[0.07 - 5]	$Kg_w.h^{-1}.m^{-2}$
	Drying Time (Micro)	S4	S2	SL5	S1	S3	SL1	[1.6 - 2.8]	Hours
	Volume lost	S3	S2	SL5	S1	S4	SL1	[48-87]	%
PEN	Cohesiveness	S1	SL1	S4	S3	SL5	S2	[15 - 56]	KPa
	Adhesiveness	S1	S4	S3	SL1	SL5	S2	[0.113 - 1.113]	N
TPA	Cohesiveness	SL1	SL5	S4	S1	S2	S3	[0.23 - 0.37]	-
	Adhesiveness	S3	SL5	S2	S4	S1	SL1	[0 - 1.433]	N.s
	Hardness	S1	SL5	S4	S2	S3	SL1	[1.666 - 2.852]	N
RHEO	Strain at LVE limit	S4	SL1	S2	S3	SL5	S1	[0 - 0.41]	%
	Storage Modulus at LVE limit	SL1	S3	S1	SL5	S4	S2	[28 - 45]	KPa

S1 SL1 S2 S3 S4 SL5

ALL: Samples characteristics — *PEN: Penetrometry results*
MACRO: Macro-drying results — *TPA: Texure profile analysis results*
MICRO: Micro-drying results — *RHEO: Rheology results - Amplitude sweep*

Table 13: Rheology, texture and drying characteristics of pasty sludge in the region of Liege

Bibliography

A. Hil, E. J., & Remy, M. (2005). The effect of lime treatment on sludge rheological properties. Technology, no, (1-6), 59. https://www.mdpi.com/2571-8797/5/1/15

Abdel-Monem, M., Al-Zubeiry, A., & Al-Gheethi, E. I. A. (2008). Elimination of salmonella and faecal indicator bacteria in sewage sludge by quick lime stabilization. J Environ Sci, Al- Mansoura Univ. Egypt, 36, 281–297.

Andreoli, C. V., von Sperling, M., & Fernandes, F. (2007). Sludge Treatment and Disposal. IWA Publishing. https://doi.org/10.2166/9781780402130

Azeddine, F., Sergio, P. A., Angélique, L., El Khadir, L., Ali, I., & El Houssayne, B. (2023). Rheological behavior and characterization of drinking water treatment sludge from morocco. Clean Technologies, 5(1), 259–273. https://doi.org/10.3390/cleantechnol5010015

Baudez, J.-C. (2002). Rhéologie et physico-chimie des boues résiduaires pâteuses pour l'étude du stockage et de l'épandage. 88. https://doi.org/10.1051/lhb/2002091

Bennamoun, L., Arlabosse, P., & Leonard, A. (2013). Review on fundamental aspect of application of drying process to wastewater sludge. Renewable and Sustainable Energy Reviews, 28, 29–43. https://doi.org/https://doi.org/10.1016/j.rser.2013.07.043

Brinker, C., & Scherer, G. (1990). Sol-gel science: The physics and chemistry of sol-gel processing. Elsevier Science. https://books.google.be/books?id=V2vRvsTaCwMC

Cabral, F., Vasconcelos, E., Goss, M. J., & Cordovil, C. M. (1998). The value, use, and environmental impacts of pulp-mill sludge additions to forest and agricultural lands in europe. 6(1), 55–64. https://doi.org/10.1139/a98-004

Cao, X., Jiang, Z., Cui, W., Wang, Y., & Yang, P. (2016). Rheological properties of municipal sewage sludge: Dependency on solid concentration and temperature [Selected Proceedings of the Tenth International Conference on Waste Management and Technology]. Procedia Environmental Sciences, 31, 113–121. https://doi.org/https://doi.org/10.1016/j.proenv.2016.02.016

Deng, W., Li, X., Yan, J., Wang, F., Chi, Y., & Cen, K. (2011). Moisture distribution in sludges based on different testing methods. Journal of Environmental Sciences, 23(5), 875–880. https://doi.org/https://doi.org/10.1016/S1001-0742(10)60518-9

Deng, W., Su, Y., & Yu, W. (2013). Theoretical calculation of heat transfer coefficient when sludge drying in a nara-type paddle dryer using different heat carriers [2013 International Symposium on Environmental Science and Technology (2013 ISEST)]. Procedia Environmental Sciences, 18, 709–715. https://doi.org/https://doi.org/10.1016/j.proenv.2013.04.096

Deng, W., Xiao, J., Lai, Z., & Su, Y. (2020). A new method to characterize sludge stickiness during drying: Effects of sludge temperature and calcium oxide (cao) on stickiness. Drying Technology, 38(9), 1107–1120. https://doi.org/10.1080/07373937.2019.1615938

Dorn, C., Reddy, C. S., Lamphere, D. N., Gaeuman, J. V., & Lanese, R. (1985). Municipal sewage sludge application on ohio farms: Health effects. 38(2), 332–359. https://doi.org/https://doi.org/10.1016/0013-9351(85)90097-0

Đurđević, D., Žiković, S., & Blecich, P. (2022). Sustainable sewage sludge management technologies selection based on techno-economic-environmental criteria: Case study of croatia. Energies, 15(11). https://doi.org/10.3390/en15113941

EL-Mesery, H. S., Tolba, N. M., & Kamel, R. M. (2023). Mathematical modelling and performance analysis of airflow distribution systems inside convection hot-air dryers. Alexandria Engineering Journal, 62, 237–256. https://doi.org/https://doi.org/10.1016/j.aej.2022.07.027

Environment, W., & Federation, A. (2019). Standard methods for the examination of water and wastewater. Scientific e-Resources. https://www.wef.org/publications/publications/books/StandardMethods/

Eshtiaghi, N., Markis, F., Yap, S. D., Baudez, J.-C., & Slatter, P. (2013). Rheological characterisation of municipal sludge: A review. Water research, 47. https://doi.org/10.1016/j.watres.2013.07.001

European-Comission, European-Environmental-Agency, Wise-Marine, Biodiversity-information-system, Climate-ADAPT, & Forest-information-system-for-Europe. (2019). Wise freshwater information system for europe - belgium. https://water.europa.eu/freshwater/countries/uwwt/belgium

European-Environment-Agency & ISWA, I.-S.-W.-A. (1998). Sludge treatment and disposal: Management approaches and experiences. Office for Official Publications of the European Communities. https://books.google.be/books?id=9J3eAAAAMAAJ

Eurostat. (2023). Sewage sludge production and disposal. https://ec.europa.eu/eurostat/web/products-datasets/-/env_ww_spd

Fanara, A. (2020). Modelling of drying phenomena in concrete with recycled aggregates. University ofLiege. https://matheo.uliege.be/bitstream/2268.2/9028/10/TFE_FANARA_Arthur.pdf

Grekhova, I., & Gilmanova, M. (2016). The usage of sludge of wastewater in the composition of the soil for land reclamation [15th International scientific conference “Underground Urbanisation

as a Prerequisite for Sustainable Development" 12-15 September 2016, St. Petersburg, Russia]. Procedia Engineering, 165, 794–799. https://doi.org/https://doi.org/10.1016/j.proeng.2016.11.777

Hovey, G., Allen, D., & Tran, H. (2017). Drying characteristics of biosludge from pulp and paper mills. TAPPI Journal, 16, 465–473. https://doi.org/10.32964/TJ16.8.465

Huiliñir, C., & Villegas, M. (2015). Simultaneous effect of initial moisture content and airflow rate on biodrying of sewage sludge [Special Issue on Sludge Research]. Water Research, 82, 118–128. https://doi.org/https://doi.org/10.1016/j.watres.2015.04.046

Huron, Y., Salmon, T., Crine, M., Blandin, G., & Léonard, A. (2010). Effect of liming on the convective drying of urban residual sludges. Asia-Pacific Journal of Chemical Engineering, 5(6), 909–914. https://doi.org/https://doi.org/10.1002/apj.421

Insel, G., Kendir, E., Ayol, A., Erdinçler, A., Arıkan, O., Imamoglu, I., Alagöz, A., Gençsoy, E., Sanin, D., Büyükkamacı, N., Karataş, Ö., Saygılı, G., Şener, G., Cokgor, E., & Filibeli, A. (2013). Current situation and future perspectives in municipal wastewater treatment and sludge management in turkey. Journal of Residuals Science and Technology, 10, 133–138. https://avesis.metu.edu.tr/

Kemp, I., Fyhr, B., Laurent, S., Roques, M., Groenewold, C., Tsotsas, E., Sereno, A., Bonazzi, C., Bimbenet, J.-J., & Kind, M. (2001). Methods for processing experimental drying kinetics data. Drying Technology - DRY TECHNOL, 19, 15–34. https://doi.org/10.1081/DRT-100001350

Kirby, F., Nieuwelink, A.-E., Kuipers, B. W. M., Kaiser, A., Bruijnincx, P. C. A., & Weckhuysen, B. M. (2015). Cao as drop-in colloidal catalysts for the synthesis of higher polyglycerols. Chemistry – A European Journal, 21(13), 5101–5109. https://doi.org/https://doi.org/10.1002/chem.201405906

Kneule, F. (1964). Le sechage. Eyrolles Paris.

Kocbek, E., Garcia, H. A., Hooijmans, C. M., Mijatović, I., Lah, B., & Brdjanovic, D. (2020). Microwave treatment of municipal sewage sludge: Evaluation of the drying performance and energy demand of a pilot-scale microwave drying system. Science of The Total Environment, 742, 140541. https://doi.org/https://doi.org/10.1016/j.scitotenv.2020.140541

Lanczos, C. (1956). Applied analysis. Prentice-Hall. https://books.google.be/books?id=V%5C_hQAAAAMAAJ

Leonard, A., BLACHER, S., MARCHOT, P., PIRARD, J.-P., & CRINE, M. (2005). Image analysis of x-ray microtomograms of soft materials during convective drying: 3d measurements. Journal of Microscopy, 218(3), 247–252. https://doi.org/https://doi.org/10.1111/j.1365-2818.2005.01485.x

Leonard, A., Vandevenne, P., Salmon, T., Marchot, P., & Crine, M. (2004). Wastewater sludge convective drying: Influence of sludge origin [PMID: 15515271]. Environmental Technology, 25(9), 1051–1057. https://doi.org/10.1080/09593330.2004.9619398

Leonard, A. (2003). Étude du séchage convectif de boues de station d'épuration (Doctoral dissertation). ULiège - Université de Liège. http://bictel.ulg.ac.be/ETD-db/collection/available/ULgetd-06222007-101214/

Leonard, A., Royer, S., Blandin, G., Salmon, T., Fraikin, L., & Crine, M. (2011). Importance of mixing conditions during sludge liming prior to their convective drying. European Drying Conference - EuroDrying. https://orbi.uliege.be/bitstream/2268/29989/1/IADC2009_Leonard.pdf

Leonard, A., Blacher, S., Marchot, P., & Crine, M. (2002). Use of x-ray microtomography to follow the convective heat drying of wastewater sludges. Drying Technology, 20, 1053–1069. https://doi.org/10.1081/DRT-120004013

Leonard, A., Blacher, S., Marchot, P., Pirard, J.-P., & Crine, M. (2003). Image analysis of x-ray microtomograms of soft materials during convective drying. Journal of microscopy, 212, 197–204. https://doi.org/10.1046/j.1365-2818.2003.01242.x

Leonard, A., Blacher, S., Marchot, P., Pirard, J.-P., & Crine, M. (2004). Measurement of shrinkage and cracks associated to convective drying of soft materials by x-ray microtomography. DRYING TECHNOLOGY Vol. 22, No. 7, 1695–1708. https://doi.org/10.1081/DRT-200025629

Leonard, A., Blacher, S., Pirard, R., Marchot, P., Pirard, J.-P., & Crine, M. (2003). Multiscale texture characterization of wastewater sludges dried in a convective rig. Drying Technology, 21, 1507–1526. https://doi.org/10.1081/DRT-120024490

Liang, F., Sauceau, M., Dusserre, G., & Arlabosse, P. (2017). A uniaxial cyclic compression method for characterizing the rheological and textural behaviors of mechanically dewatered sewage sludge. Water Research, 113, 171–180. https://doi.org/https://doi.org/10.1016/j.watres.2017.02.008

Liu, X., Shi, J., Zhao, Y., Li, Z., & Zhang, J. (2012). Experimental research on lime drying process of mechanical dewatered sludge from a wastewater treatment plant in beijing. Procedia Environmental Sciences, 16, 335–339. https://doi.org/10.1016/j.proenv.2012.10.047

Liu, Y., Zhuge, Y., Chow, C., Keegan, A., Li, D., Pham, P., Huang, J., & Siddique, R. (2020). Utilization of drinking water treatment sludge in concrete paving blocks: Microstructural analysis, durability and leaching properties. Journal of Environmental Management, 262, 110352. https://doi.org/10.1016/j.jenvman.2020.110352

Macosko, C. (1994). Rheology: Principles, measurements, and applications. VCH. https://books.google.be/books?id=XXspAQAAMAAJ

Madan, A., Pare, A., & N.A, N. (2014). Mathematical modelling of thin-layer drying process of bamboo (bambusa bambos) shoots at varying temperature. Research Reviews: Journal of Botany, 3, 1–9.

Manchester, S. (2017). The fire and explosion hazards of dried sewage sludge. IChemE. https://www.icheme.org/media/10163/xvi-paper-18.pdf

Mert, B., Gonzalez, D., & Campanella, O. H. (2007). A new method to determine viscoelastic properties of corn grits during cooking and drying. Journal of Cereal Science, 46(1), 32–38. https://doi.org/https://doi.org/10.1016/j.jcs.2006.10.009

Mezger, T. (2020). For users of rotational and oscillatory rheometers. Vincentz Network. https://doi.org/doi:10.1515/9783748603702

Mihelcic, J. (2019). Sludge management: Biosolids and fecal sludge. https://doi.org/10.14321/waterpathogens.48

Moser, B., Water, V., Tomaro, D., Bertolas, N., Ohm, S., Hegeman, F., Luke, D., & Saltes, J. (2016). Biological solids and sludges – handling, processing, and reuse study guide. Wisconsin Department of Natural Resources. https://dnr.wisconsin.gov

Mouzaoui, M., Baudez, J., Sauceau, M., & Arlabosse, P. (2018). Experimental rheological procedure adapted to pasty dewatered sludge up to 45 percent dry matter. Water Research, 133, 1–7. https://doi.org/https://doi.org/10.1016/j.watres.2018.01.006

Ofei, T., & Saasen, A. (2019). A new approach to dynamic barite sag analysis on typical field oil-based drilling fluid.

Oupeye. (n.d). Station d'epuration hermalle. http://www.oupeyeinfo.be/Page039.html

Pambou, Y.-B. (2016). Influence du conditionnement et de la déshydratation mécanique sur le séchage des boues d'épuration. https://api.semanticscholar.org/CorpusID:99248002

Peeters, B. (2010). Mechanical dewatering and thermal drying of sludge in a single apparatus. Drying Technology - DRY TECHNOL, 28, 454–459. https://doi.org/10.1080/07373930903155614

Peeters, B., Dewil, R., Van Impe, J., Vernimmen, L., & Smets, I. (2011). Using a shear test based lab protocol to map the sticky phase of activated sludge. https://kuleuven.limo.libis.be/discovery/search?query=any,contains,LIRIAS466938&tab=LIRIAS&search_scope=lirias_profile&vid=32KUL_KUL:Lirias&offset=0

Rheology-Lab. (2023). Texture analysis and texture, profile analysis. https://www.rheologylab.com/

Rodríguez, N., Martínez-Ramírez, S., Blanco-Varela, M., Guillem, M., Puig, J., Larrotcha, E., & Flores, J. (2010). Re-use of drinking water treatment plant (dwtp) sludge: Characterization and technological behaviour of cement mortars with atomized sludge additions. Cement and Concrete Research, 40, 778–786. https://doi.org/10.1016/j.cemconres.2009.11.012

Ruiz, T., & Wisniewski, C. (2008). Correlation between dewatering and hydro-textural characteristics of sewage sludge during drying. Separation and Purification Technology - SEP PURIF TECHNOL, 61, 204–210. https://doi.org/10.1016/j.seppur.2007.07.054

Schlichting, H., & Kestin, J. (1961). Boundary layer theory (Vol. 121). Springer.

Shariff, Z. A., Fraikin, L., Bogdan, A., Léonard, A., Meers, E., & Pfennig, A. (2023). Pulse process: Recovery of phosphorus from dried sewage sludge and removal of metals by solvent extraction

[PMID: 36912280]. Environmental Technology, 0(0), 1–13. https://doi.org/10.1080/09593330.2023.2191221

SPFG. (n.d). Liste des stations d'épuration. Société Publique de La Gestion de l'Eau. http://www.spge.be/fr/

Tao, T., Peng, X., & Lee, D. (2006). Skin layer on thermally dried sludge cake. Drying Technology, 24, 1047–1052. https://doi.org/10.1080/07373930600776258

Tao, T., Peng, X., & Lee, D. (2005). Thermal drying of wastewater sludge: Change in drying area owing to volume shrinkage and crack development. Drying Technology - DRY TECHNOL, 23, 669–682. https://doi.org/10.1081/DRT-200054164

Teleshova, E. N., & Petuhova, E. A. (2021). Study of the effect of quicklime on the sludge treatment and dehydration. IOP Conference Series: Earth and Environmental Science, 852(1), 012103. https://doi.org/10.1088/1755-1315/852/1/012103

Thiedeitz, M., Kränkel, T., & Gehlen, C. (2022). Viscoelastoplastic classification of cementitious suspensions: Transient and non-linear flow analysis in rotational and oscillatory shear flows. Rheologica Acta, 61, 3. https://doi.org/10.1007/s00397-022-01358-9

Turovskiy, I., & Mathai, P. (2006). Wastewater sludge processing. Wiley. https://books.google.be/books?id=DwMWvTki7h8C

United-Nations. (2022). World population prospects. Department of Economic and Social Affairs and Population Division. https://population.un.org/dataportal/home

Vaxelaire, J., & Cézac, P. (2004). Moisture distribution in activated sludges: A review. Water Research, 38(9), 2215–2230. https://doi.org/https://doi.org/10.1016/j.watres.2004.02.021

Wang, T., Chen, J., Shen, H., & An, D. (2016). Effects of total solids content on waste activated sludge thermophilic anaerobic digestion and its sludge dewaterability [Special Issue on Bioenergy, Bio-products and Environmental Sustainability]. Bioresource Technology, 217, 265–270. https://doi.org/https://doi.org/10.1016/j.biortech.2016.01.130

Zheng, Q., Hu, Z., Li, P., Ni, L., Huang, G., Yao, Y., & Zhou, L. (2021). Effects of air parameters on sewage sludge drying characteristics and regression analyses of drying model coefficients. Applied Thermal Engineering, 198, 117501. https://www.sciencedirect.com/science/article/pii/S1359431121009339

8 Annex-1- Moisture profile and texure change

Moisture Profile

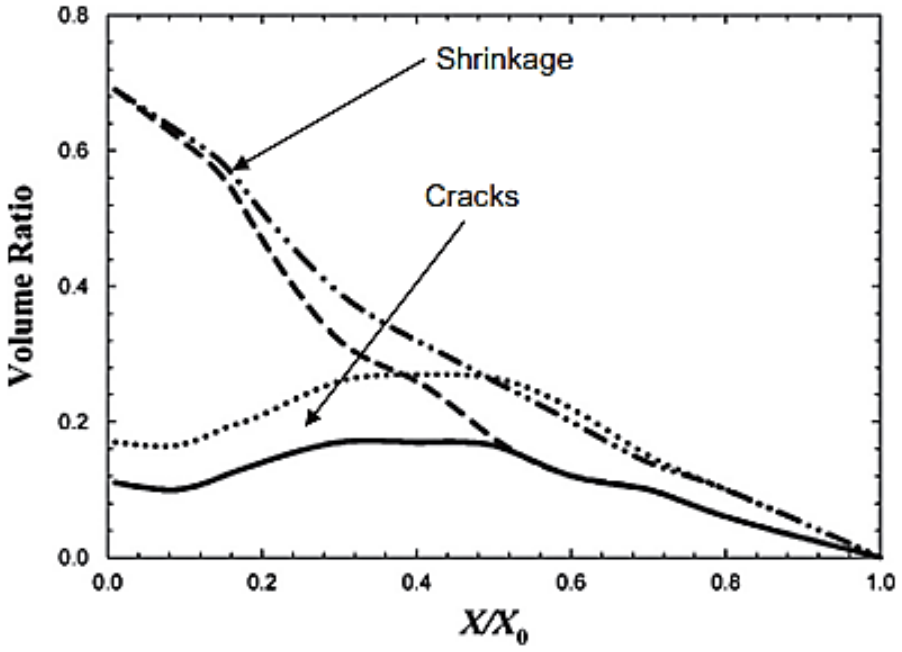

Figure 54: Sludge shrinkage and cracks and structure changes during convective drying (Tao et al., 2005)

The utilization of imaging techniques has facilitated the distinction of two significant phenomena occurring during the convective drying of wastewater sludge: shrinkage and cracks. (Leonard, 2003) then, (Tao et al., 2005) employed a camera and an X-ray micro-computerized tomography scanner to study the impact of artificial cracks on sludge samples' shrinkage. The outcomes, depicted in Figure 55, clearly reveal a difference in product diameter before and after 181 minutes of drying. Figure 54 illustrates the variation of shrinkage concerning moisture content, showing a substantial reduction in volume, around 70% of the initial total volume. Additionally, X-ray microtomography scanning reconstructions demonstrate the formation of cracks, depicted in Figure 55 through white zones representing airflow inside the product. Figure 54 indicates that with imposed cracks, the change in volume is not significant, reaching a maximum value of approximately 30% of the total volume. Notably, after 151 minutes, the X-ray scanned photo exhibits a darker surface contour compared to the core, suggesting the formation of the skin. Furthermore, using the same imaging technique, the authors (Tao et al., 2006) reconstructed the evolution of skin formation during convective drying. These reconstitution results are presented in Figure 56. (Bennamoun et al., 2013). (Leonard et al., 2002; Leonard, Blacher, Marchot, Pirard, et al., 2003, 2004; Leonard, Blacher, Pirard, et al., 2003) also utilized X-ray microtomography during convective drying to observe shrinkage and cracks. They systematically scanned the sample, providing detailed information about these phenomena during the drying process, without affecting the product's behavior. Figure 57 shows that shrinkage initiates early in the process, with a constant drying rate, while the appearance of cracks occurs later during the falling dry-

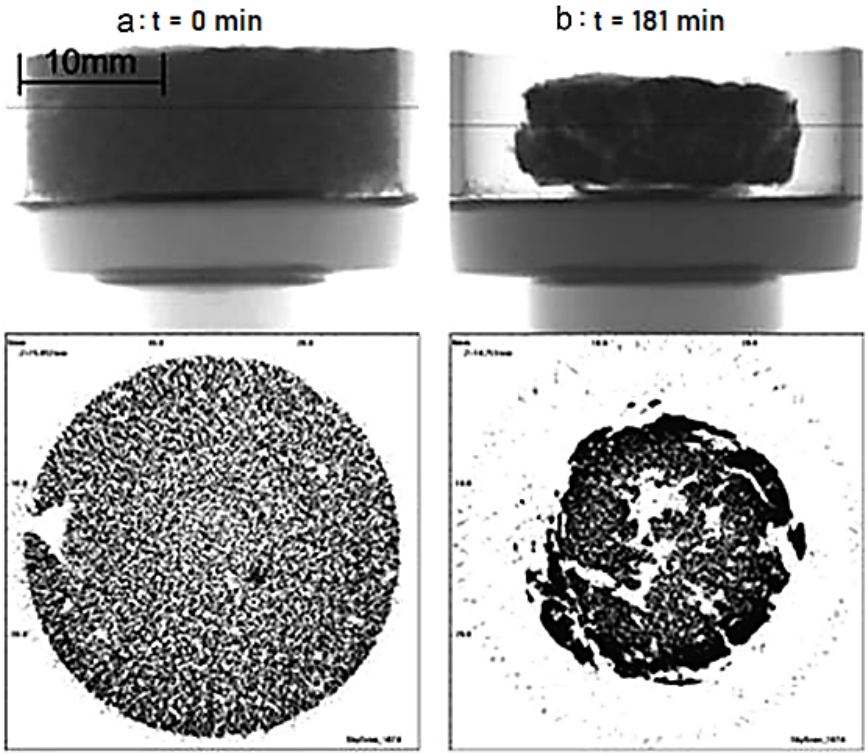

Figure 55: Sludge shrinkage during convective drying (Tao et al., 2005)

ing rate (illustrated by the white zones). The authors discovered that the origin of the sludge influences shrinkage (ranging from 60% to 80%) and cracks (ranging from 30% to over 50%) by the end of the drying process, as shown in Figure 58 (a) and (b) (Leonard, Blacher, Marchot, Pirard, et al., 2003). Additionally, the applied operating conditions, particularly air velocity, can influence these phenomena (Figure 58 (c)) (Leonard, Blacher, Marchot, Pirard, et al., 2004). Moreover, (Bennamoun et al., 2013) used the same imaging technique and a calibration curve relating grey level to moisture content (Figure 59 (c)) to determine the moisture profile distribution inside the product. From these curves, they calculated the internal diffusion coefficient as a function of product moisture content. (Ruiz & Wisniewski, 2008) conducted studies providing further insights into the rheological behavior of wastewater sludge during convective drying and after mechanical dewatering. Figure 60 summarizes and schematizes their findings. After mechanical dewatering, the product had a liquid form with a funicular hydric aspect and around 383% moisture content (wet basis). Upon convective drying, the material exhibited a plastic tendency with the same funicular hydric aspect, a constant drying evaporated flux, and constant deformation marked as "ε" in the figure, until reaching a moisture content of about 164%. After this phase, the material transitioned to a solid form, still with a funicular hydric aspect and constant drying rate, but with a decrease in deformation. Subsequently, the product underwent a phase change from funicular hydric with free water to hygroscopic aspect with bound water, during which the evaporated flux decreased. Finally, the last registered phase was the solid phase without shrinkage and deformation (at W=40%, wet basis), with a hygroscopic hydric aspect and a continuous decrease in the evaporated flux. (Peeters et al., 2011) utilized an innovative drying system called centri-dry, comprising both a centrifuge and a flash dryer. They observed a reduction in dryer perfor-

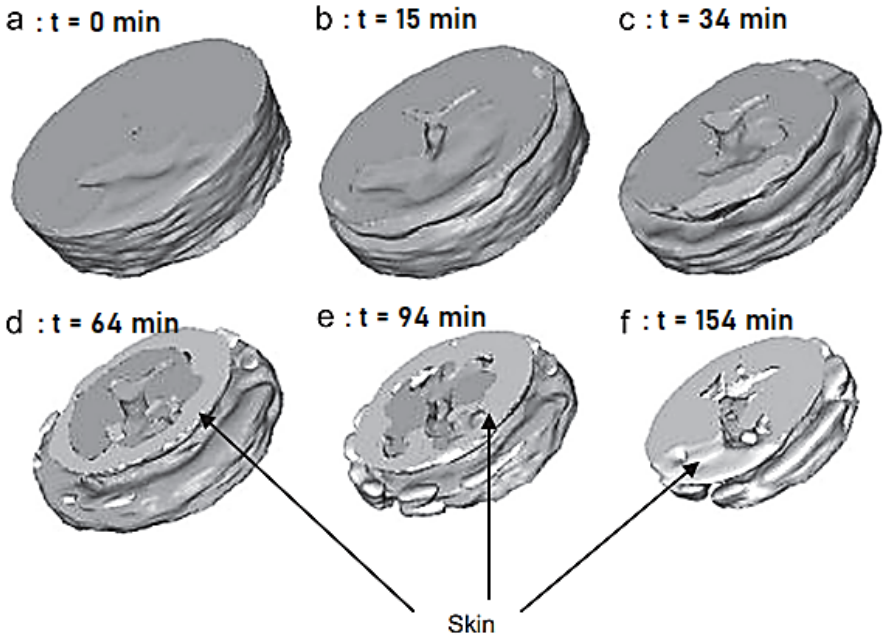

Figure 56: Sludge skin variation with respect to time during convective drying(Tao et al., 2006)

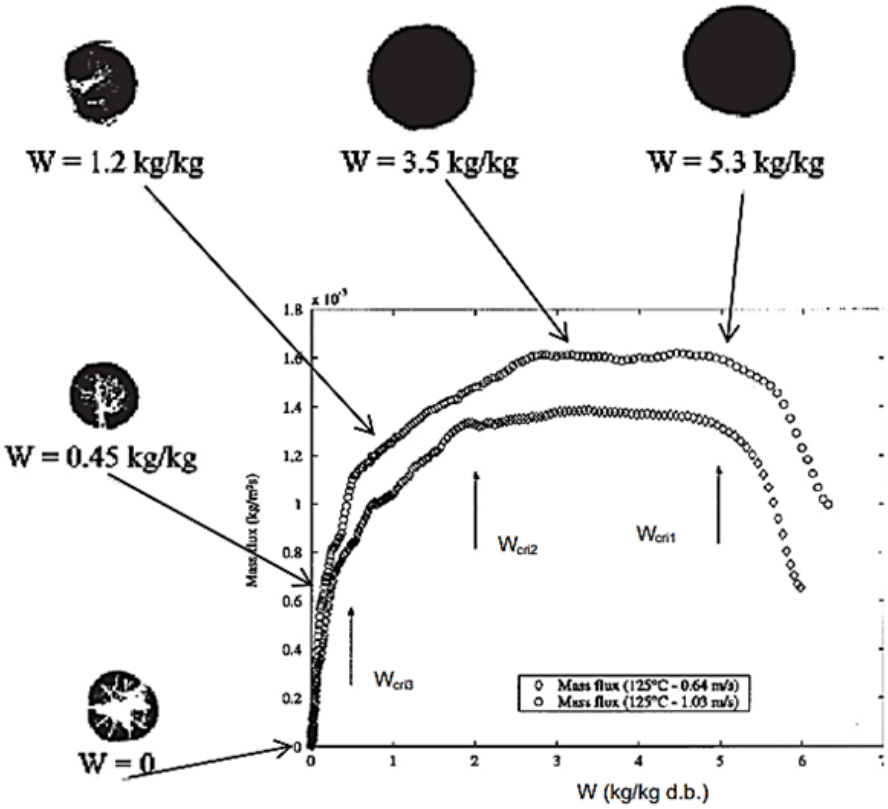

Figure 57: Sludge Shrinkage and cracks during the convective drying process (Leonard, Blacher, Marchot, Pirard, et al., 2003)

mance during the sticky phase. To address this, they developed a specific laboratory device to plot the shear stress against the product's dry solid percentage. The sticky phase was identified based on the highest shear stress values. (Peeters, 2010) resolved this issue by considering the hypothesis of modifying the moisture content temperature conditions of the product that contacts the drying chamber walls. They confirmed this by reducing the cake dryness after centrifugation through adjustments in the clay to biosolids feed ratio

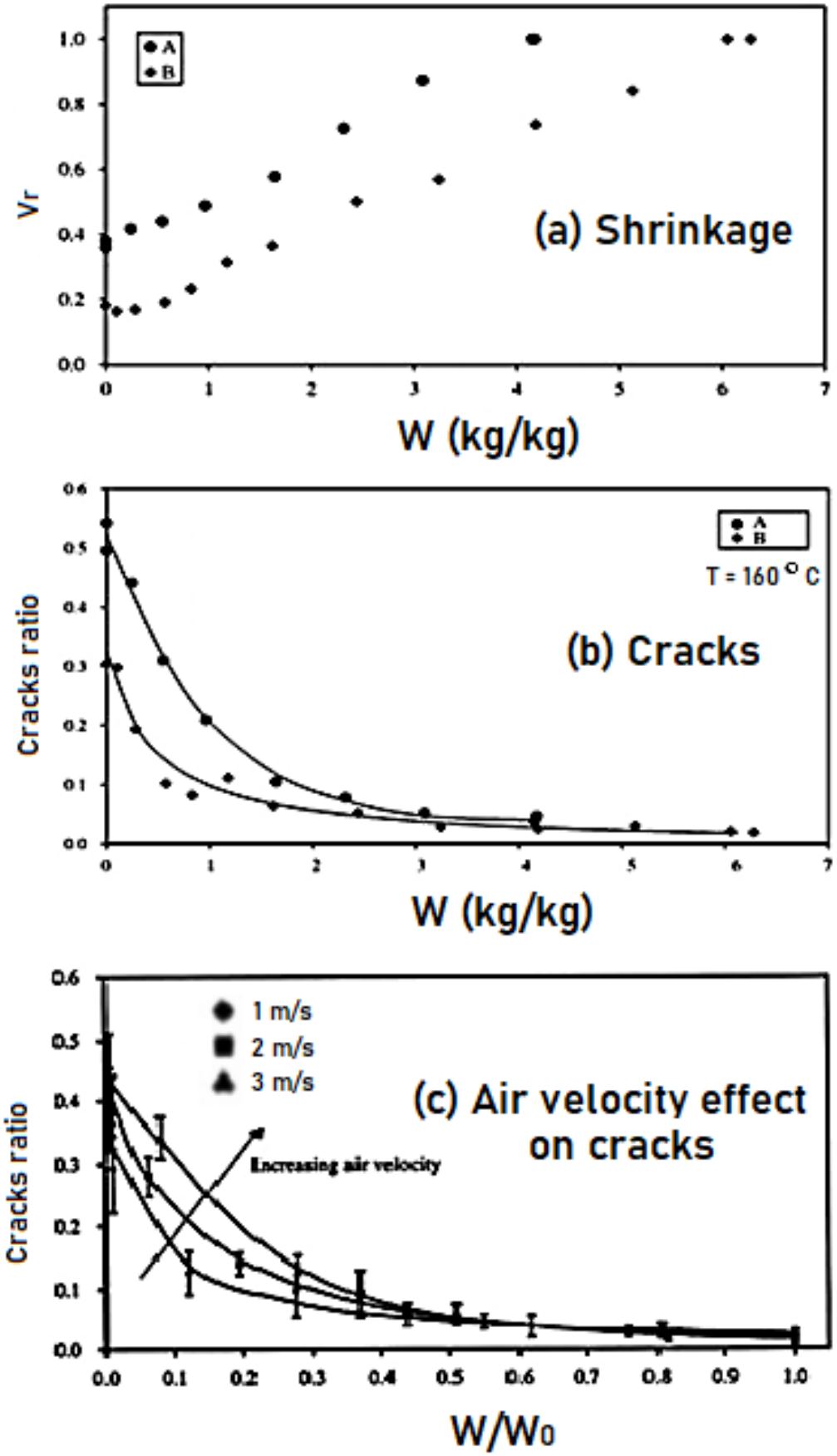

Figure 58: Sludge origin and operation conditions influence on the shrinkage and cracks (Leonard, Blacher, Marchot, Pirard, et al., 2003)

and centrifuge bowl speed, resulting in remarkable performance improvement and a significant decrease in dryer interruptions.

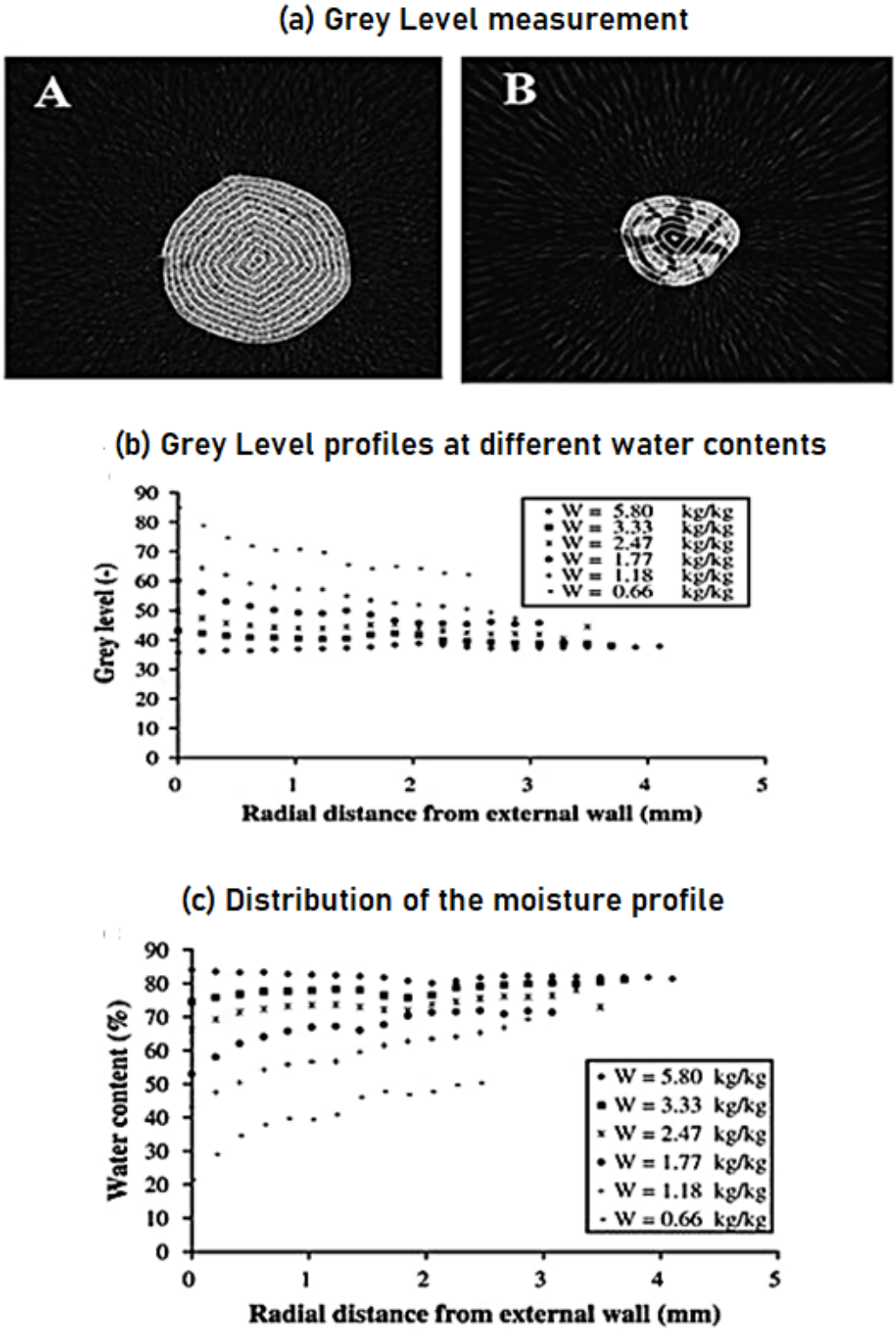

Figure 59: The grey level sludge measurements (Leonard, Blacher, Marchot, Pirard, et al., 2003)

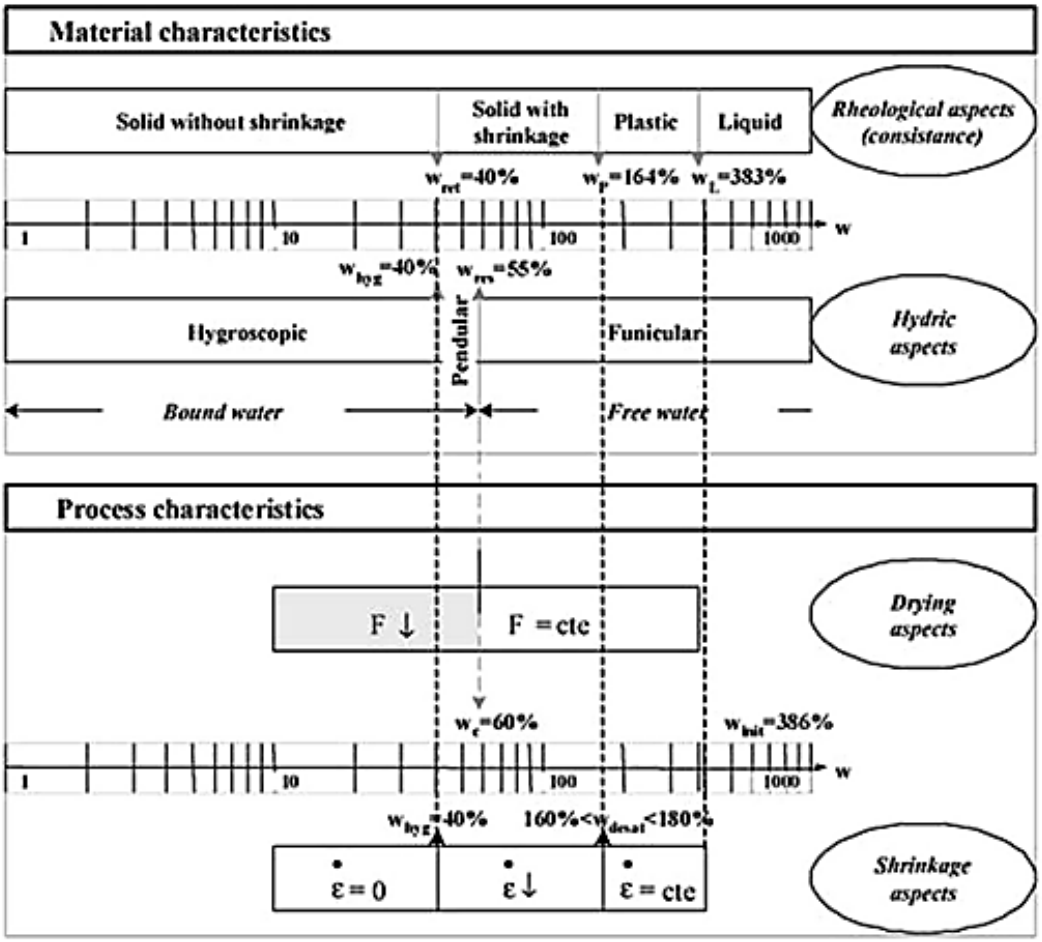

Figure 60: The grey level sludge measurements (Ruiz & Wisniewski, 2008)

9 Annex-2- Rheology theory

Rheology is a scientific discipline that illustrates how materials flow and deform when subjected to shear stresses. It primarily focuses on investigating viscoelastic materials, which exhibit characteristics of both elastic solids and Newtonian fluids. These materials encompass a range of substances, such as pastes, sludge, suspensions, and emulsions. The rheology of liquid sludge has been extensively studied, with particular emphasis on understanding their conditioning efficiency and mechanical dehydration (Cao et al., 2016), as well as designing pumping systems that require accurate pressure loss calculations. In contrast, investigations into the rheological properties of pasty sludge have been relatively scarce. Notably, a significant contribution to this field is the thesis of (Leonard, 2003), which extensively explores rheology and physio-chemical characteristics of mud sludge, with specific applications in storage and spreading (Baudez, 2002). To dive deeper the thesis made by (Leonard, 2003) comes in handy:

When a solid is subjected to shear stress, represented by (in Pascals), it undergoes a deformation denoted as (dimensionless). The primary objective of rheology is to experimentally determine the behavioral law or rheological equation, = f(τ), which establishes the relationship between this shear deformation and the stress that caused it. This connection relies on the specific properties and characteristics of the material being studied. In fact, sludge similarly to many other materials, exhibits behavior that falls between two

extreme cases: that of a perfectly viscous liquid and a perfectly elastic solid. A perfectly viscous liquid maintains a constant viscosity represented by μ $(Pa.s)$, regardless of the deformation rate, γ (s^{-1}). Such a fluid follows Newton's law as shown in Equation 15:

$$\mu = \mu_0 = \frac{\tau}{\gamma} => \frac{d\gamma}{dt} = \frac{\tau}{\mu_0} \tag{15}$$

By Integrating Equation 15, we arrive at Equation 16. This equation reveals that a liquid has the ability to retain all the stresses it experiences, and the resulting deformation persists even when the stress diminishes to zero. Additionally, if the liquid is subjected to constant stress, the material will continue to flow without any constraints indefinitely.

$$\gamma(t) = \frac{1}{\mu_0} \int_0^t \tau(t^{'}) dt^{'} \tag{16}$$

For a perfectly elastic solid, when stress is applied, the deformation increases linearly, as stated in Equation 17. J (Pa^{-1}) represents the elastic compliance, a constant. However, it is common to use G (Pa) instead which is equal to $1/J$, referring to the shear modulus or rigidity modulus. The relation leads to the formulation of Hooke's law shown in Equation 18. The deformation occurs immediately upon the application of stress. Unlike liquids, solids do not retain any memory of previous stresses. Once the stress is removed, the deformation completely reverses and disappears.

$$\gamma(t) = J.\tau(t) \tag{17}$$

$$\tau(t) = G.\gamma(t) \tag{18}$$

Several techniques exist to analyze the characteristics of viscoelastic materials. Creep and relaxation curves, involving the application of constant stress or strain, are commonly utilized in polymers and suspensions. Alternatively, dynamic measurements, which subject the material to oscillating deformations such as "amplitude sweep" can be used. The benefit of the latter is to gain insights into the viscous and elastic properties of the material. When the material gets subjected to a sinusoidal deformation (Equation 19), the measured stresses follow a sinusoidal pattern likewise. However, with a phase shift angle δ (Equation 20). To ensure accurate results, the deformation should stay small enough to fall within the linear viscoelastic range of the material. Within this range, the Boltzmann superposition principle holds, which means that the total deformation resulting from a combination of stresses is the sum of deformations caused by each stress applied individually. The phase angle δ is zero for a perfect solid (deformation occurs in sync with stress), is 90° for an ideal liquid (stress aligns with the shear rate), and takes intermediate values for a viscoelastic material.

$$\gamma(t) = \gamma_0.cos(\omega.t) \tag{19}$$

$$\tau(t) = \tau_0.cos(\omega.t + \delta) \tag{20}$$

In experimental settings, we determine the stress that aligns with the deformation $(\tau^{'}(t))$and the stress that is 90° out of phase $(\tau^{''}(t))$ (Equation 21). With the experimental measurements, the elastic modulus $(G^{'})$ and the viscous modulus $(G^{''})$ can be calculate (Equation 22). The elastic modulus is zero for a Newtonian liquid, whereas the viscous modulus is zero for a completely elastic solid.

$$\tau(t) = \tau^{'}(t) + \tau^{''}(t) = \tau_0^{'}.sin(\omega t) + \tau_0^{''}.cos(\omega t) \tag{21}$$

$$\tau = G^{'}\gamma_0.sin(\omega t) + G^{''}\gamma_0.cos(\omega t) \tag{22}$$

To simplify computations, we utilize the framework of complex numbers. We assign the following complex quantities to the real quantities $\tau(t)$ and $\gamma(t)$:

$$\bar{\tau} = \tau_0.e^{i(\omega t+\delta)} \tag{23}$$

$$\bar{\gamma} = \gamma_0.e^{i\omega t} \tag{24}$$

we introduce a complex module $\bar{G}$, denoted as $\bar{\tau} = \bar{G}(\omega).\bar{\gamma}(t)$. Like any complex value, $\bar{G}$ can be broken down into two components: its real and imaginary parts (Equation 25). It is possible to demonstrate that the tangent of the phase angle (or loss tangent) is equivalent to the ratio of viscous and elastic modules (Equation 26). Therefore, determining $\bar{G}$ is all that is needed to fully characterize the material.

$$\bar{G}(\omega) = G^{'}(\omega) + i.G^{''}(\omega) \tag{25}$$

$$tg(\delta) = \frac{\tau_0^{''}}{\tau_0^{'}} = \frac{G^{''}(\omega)}{G^{'}(\omega)} \tag{26}$$

The Complex viscosity is also defined in Equation 27:

$$\bar{\mu}(\omega) = \frac{\bar{\tau}}{\bar{\gamma}} = -\frac{i.\bar{\tau}}{\omega.\bar{\gamma}} = -i\frac{\bar{G}(\omega)}{\omega} \tag{27}$$

Various cells consisting of both a stationary and rotating part can be employed for measurement purposes.

These include the Couette geometry with coaxial cylinders, the plane-plane geometry using parallel disks, and the plane-cone geometry. Coaxial cylinders are not suitable for studying pasty materials; hence, the plane-plane geometry, enabling easy placement of a sample of soft material, is usually selected (Macosko, 1994). A rheological analysis may entail investigating how viscoelastic properties are influenced by deformation (or stress) amplitude, deformation frequency, or temperature.

10 Annex-3- Macrodrying data

10.1 Pressure drop

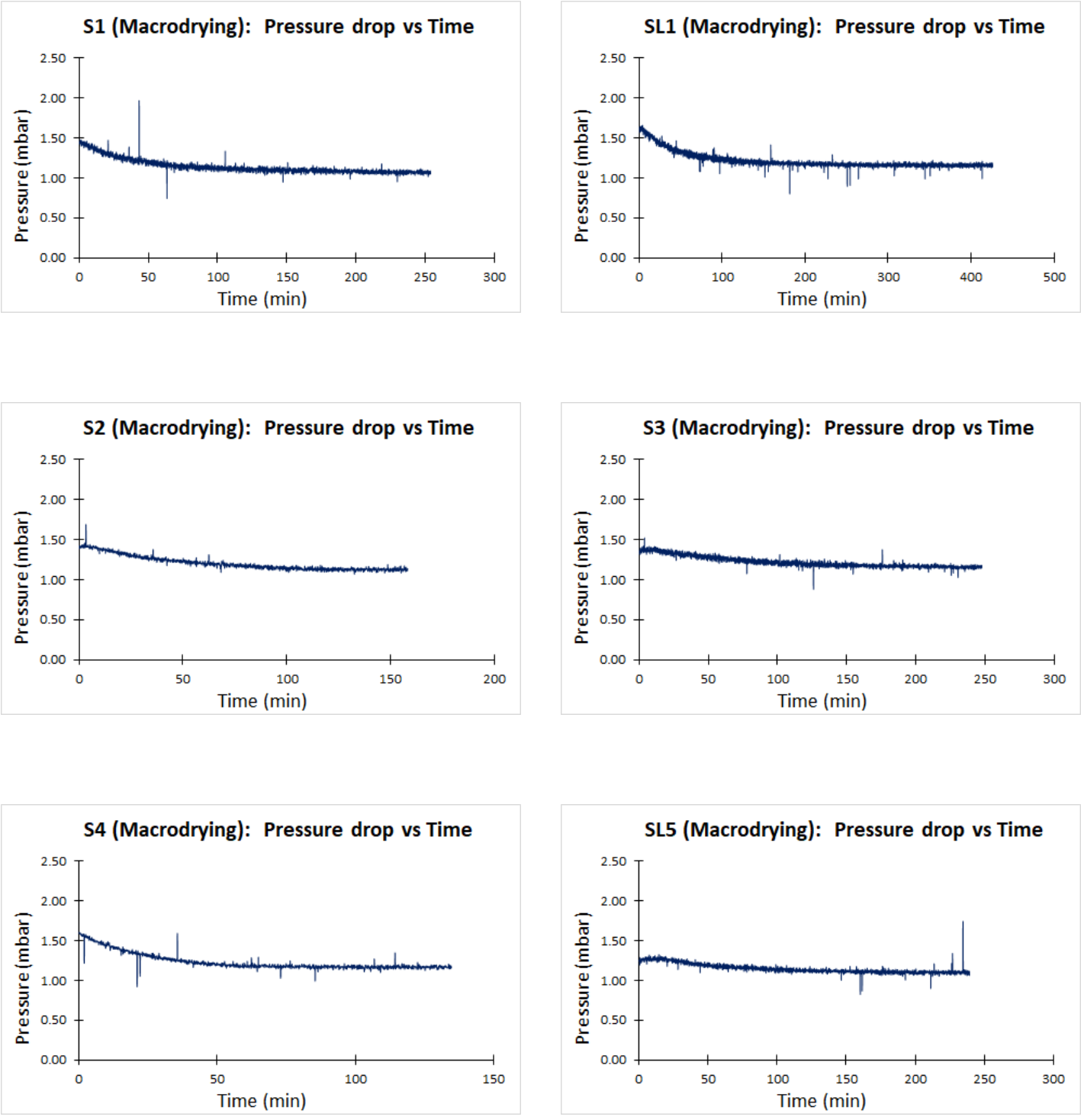

Figure 61: Pressure Drop during macro-drying for each station

10.2 Mass change over time

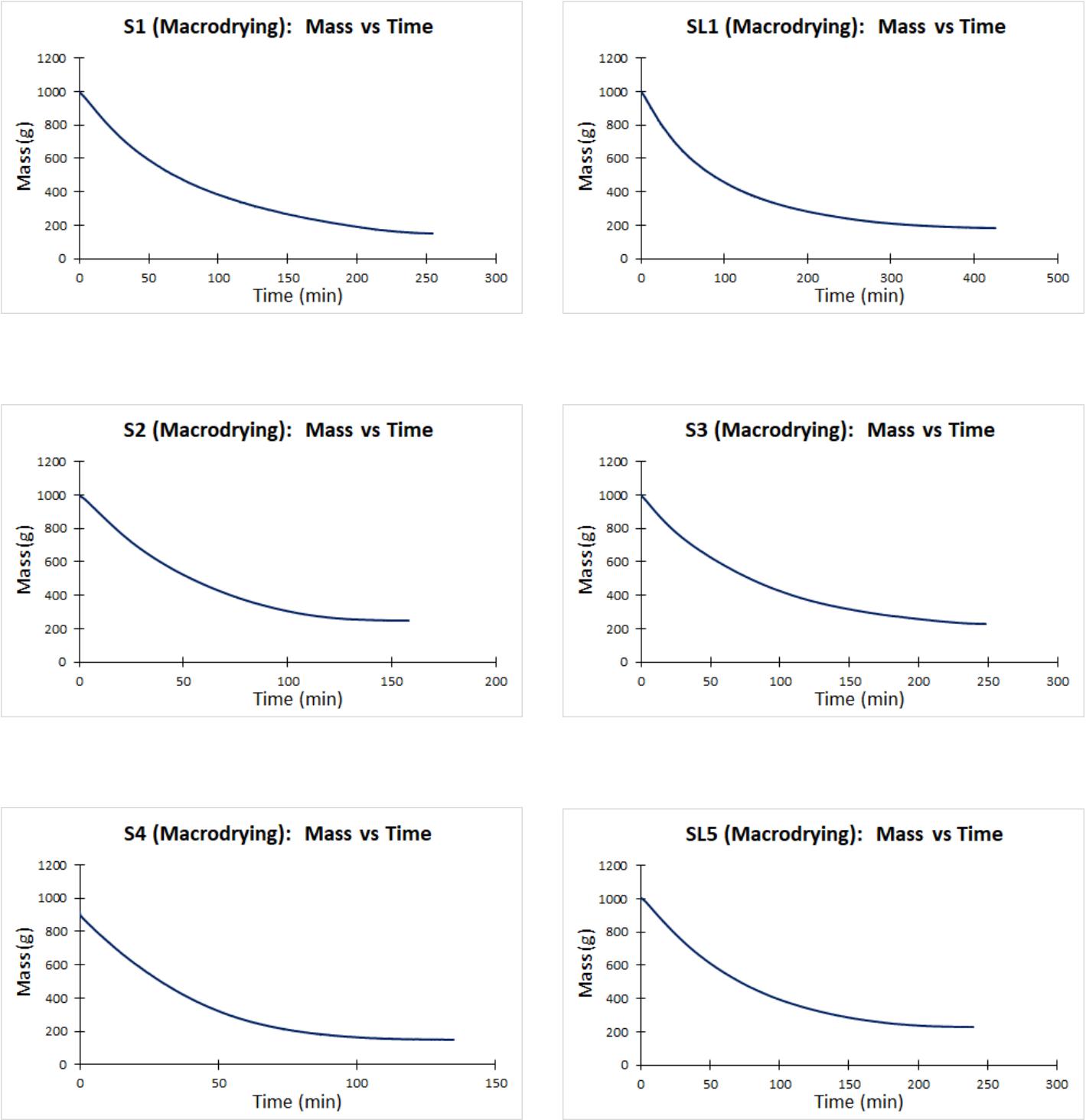

Figure 62: Mass change over time during macrodrying for each station

10.3 Samples humidity change over time

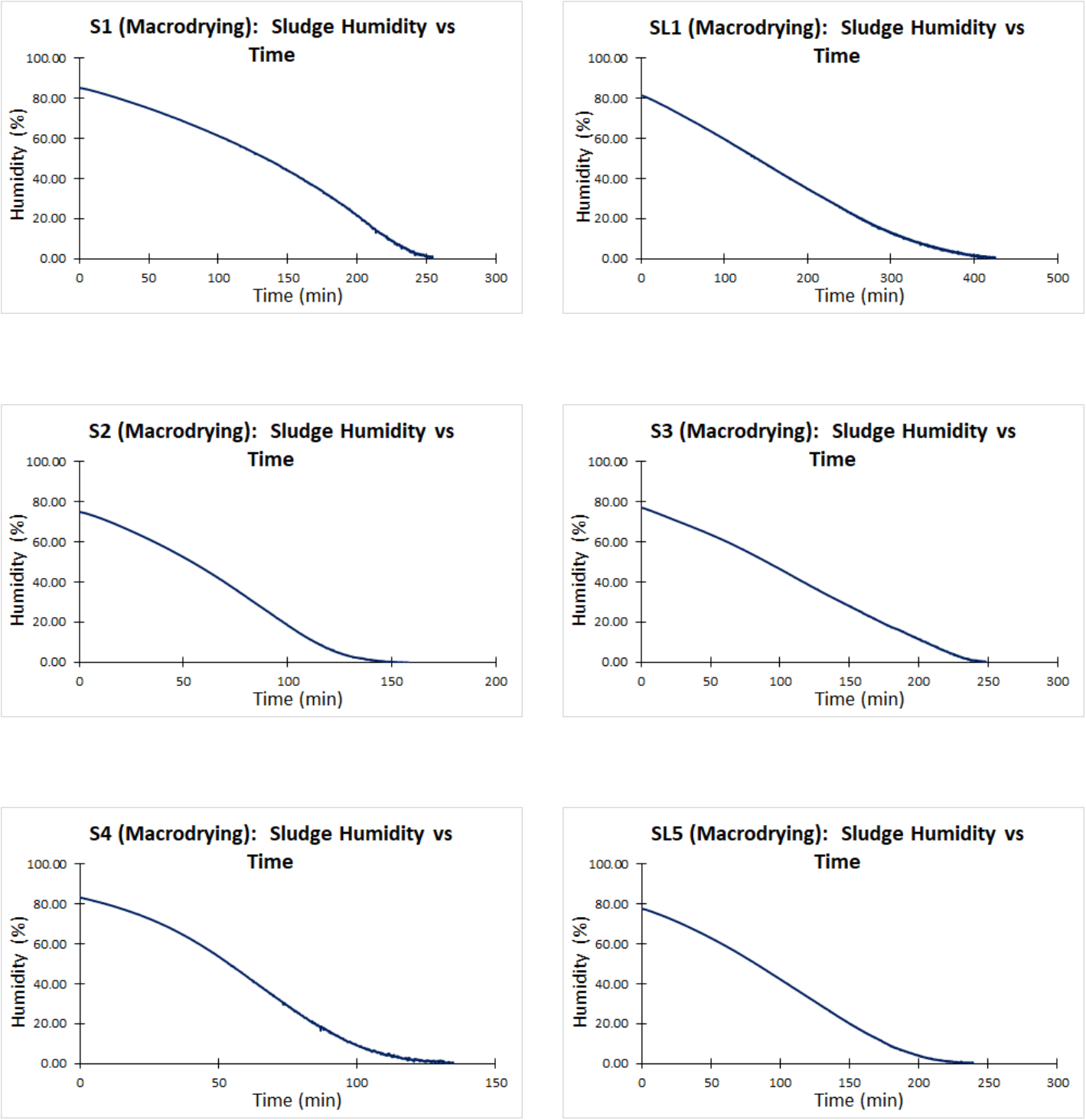

Figure 63: Samples humidity change over time during macrodrying for each station

10.4 Samples temperature and velocity profiles

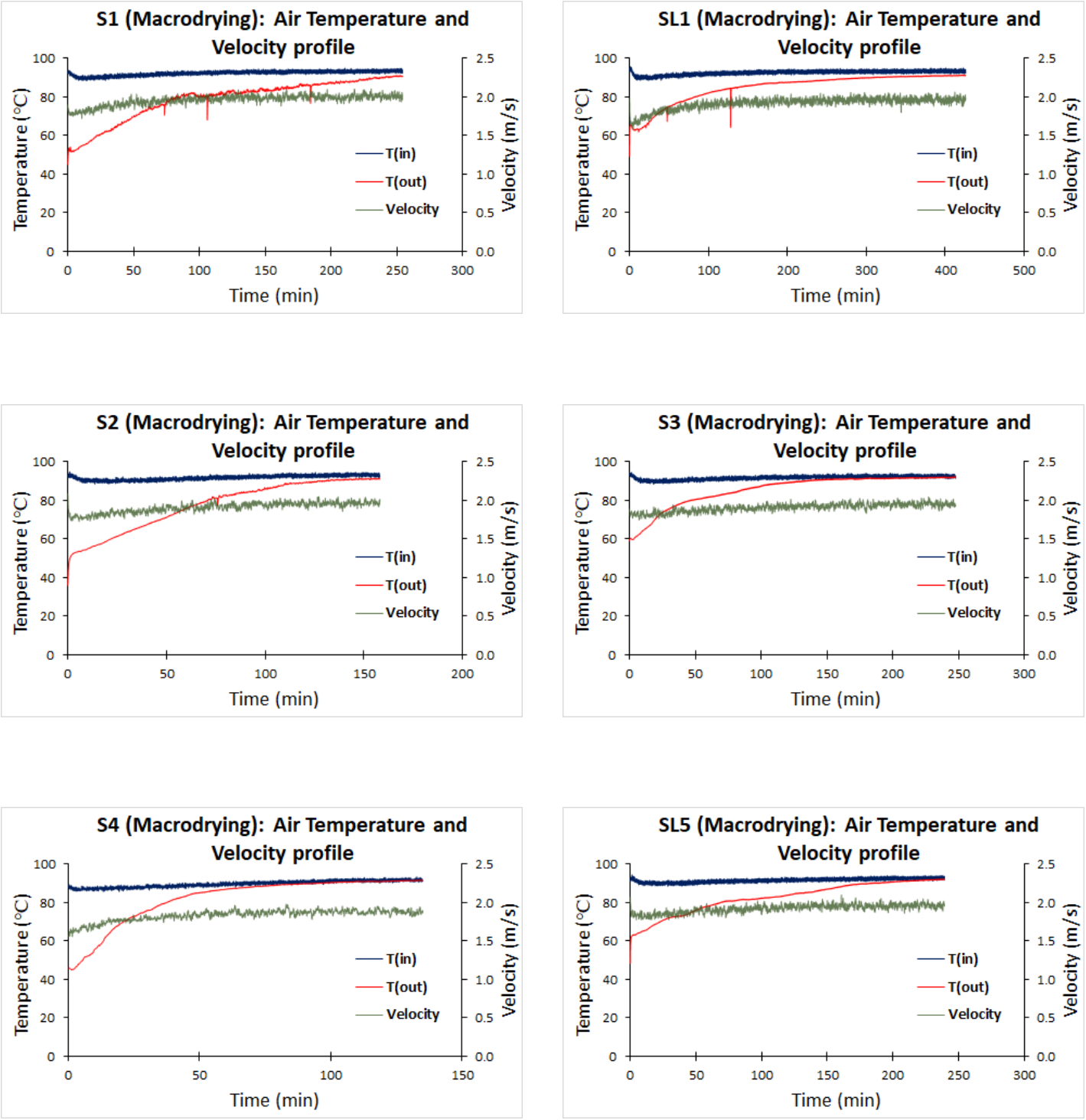

Figure 64: Samples temperature and velocity profiles during macrodrying for each station

10.5 Drying rate vs moisture content before smoothening

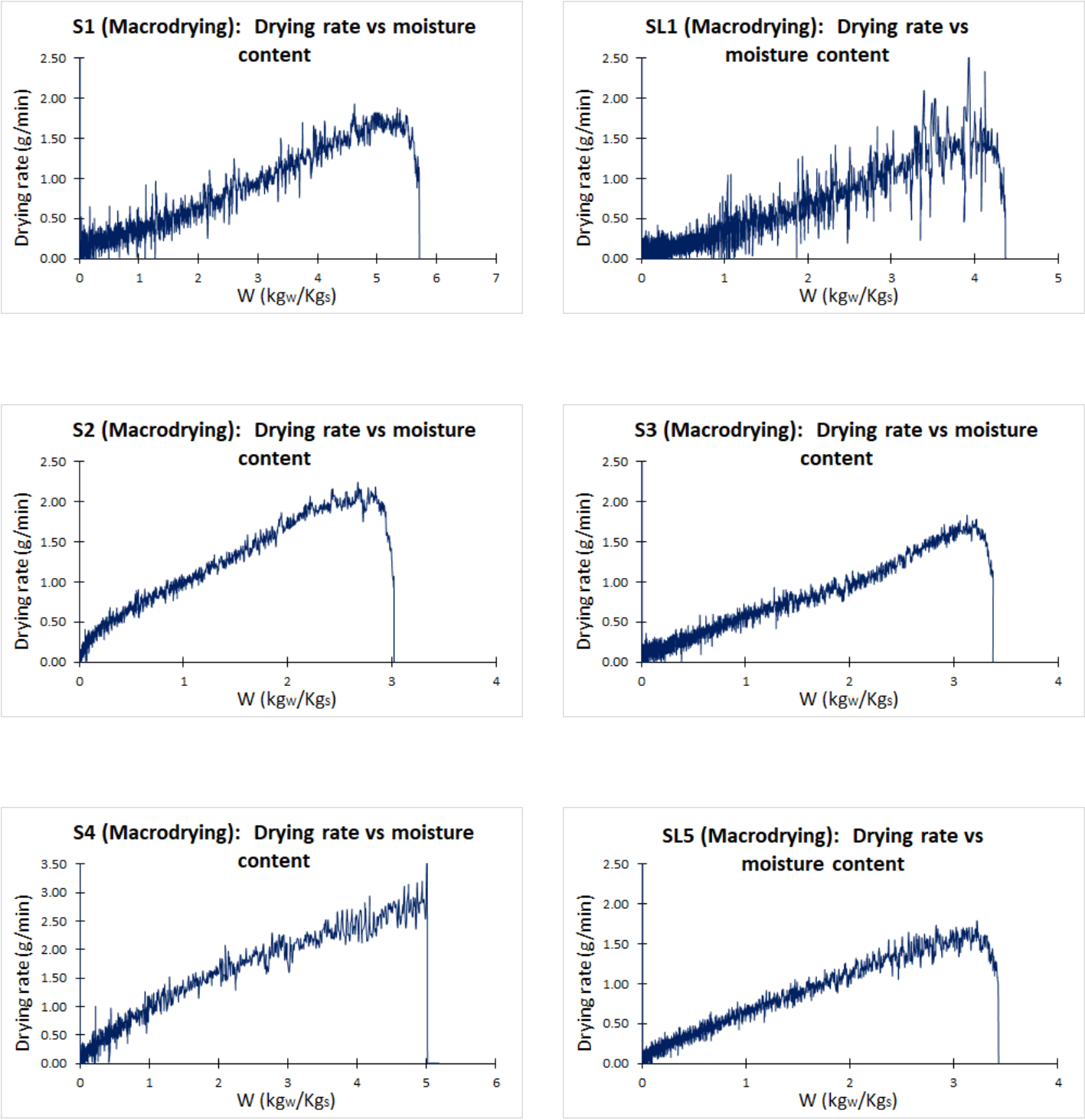

Figure 65: Drying rate vs moisture content before smoothening during macrodrying for each station

11 Annex-4- Microdrying data

11.1 Mass change over time

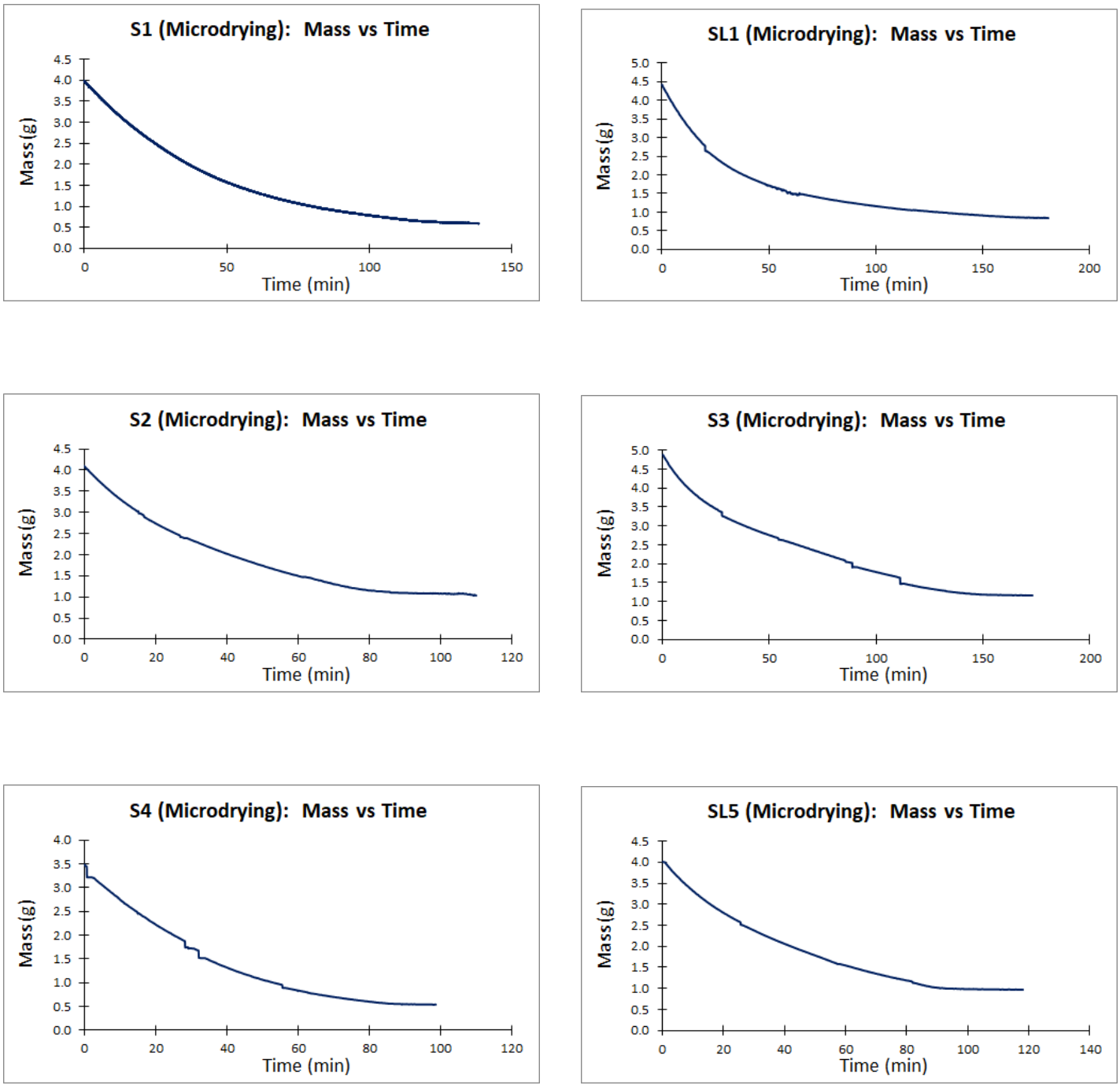

Figure 66: Mass change over time during micro-drying for each station

11.2 Samples humidity change over time

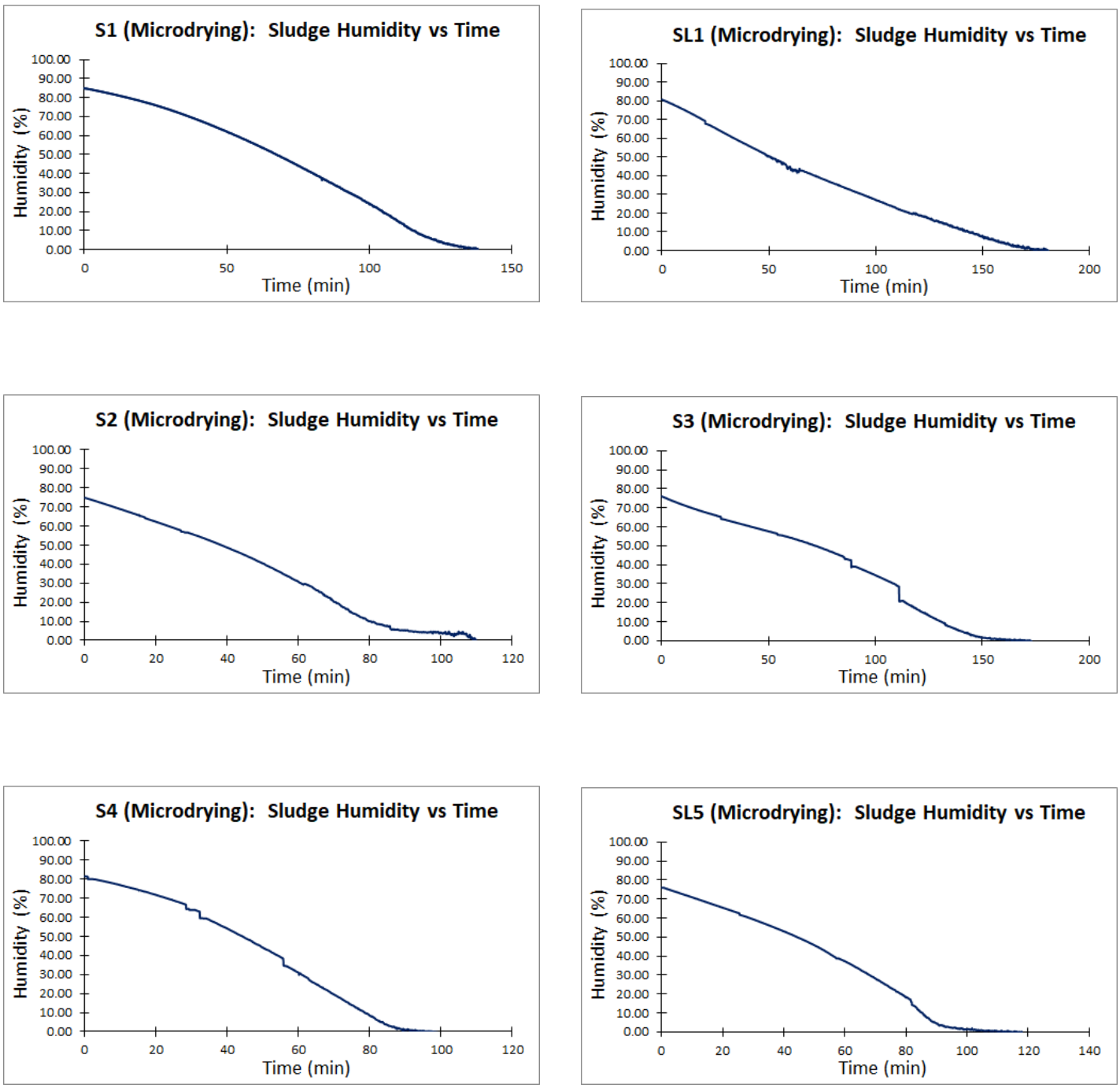

Figure 67: Samples humidity change over time during microdrying for each station

11.3 Samples linear area change with moisture content

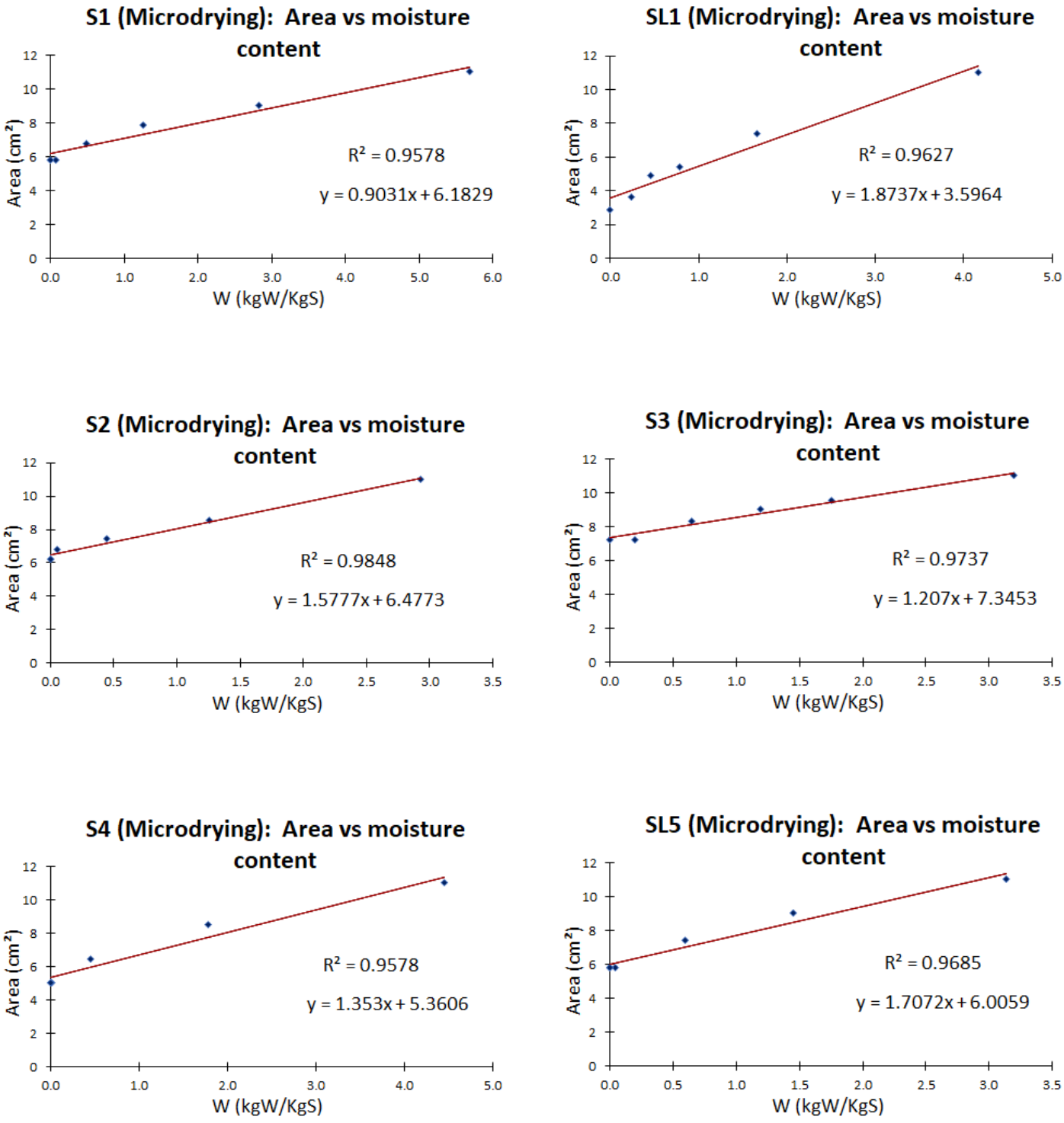

Figure 68: Samples area change with moisture content during microdrying for each station

11.4 Samples linear volume change with moisture content

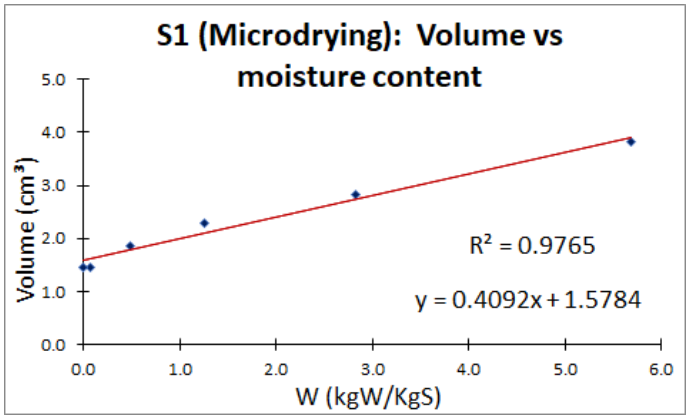

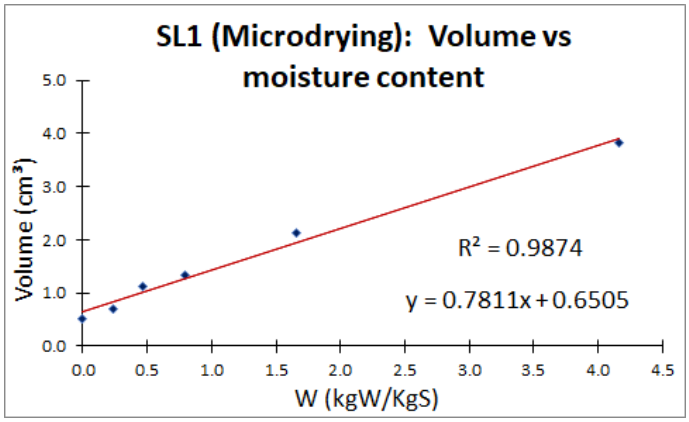

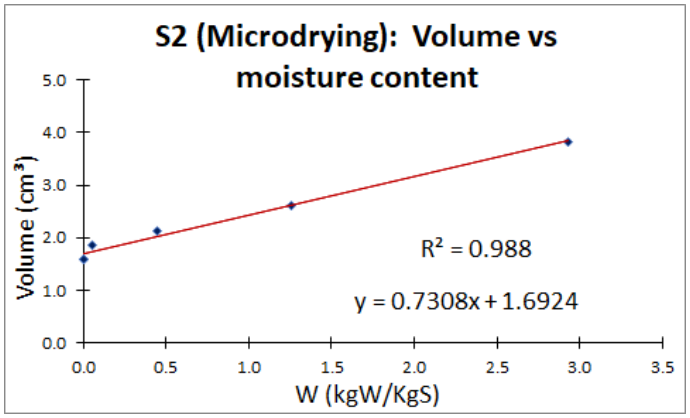

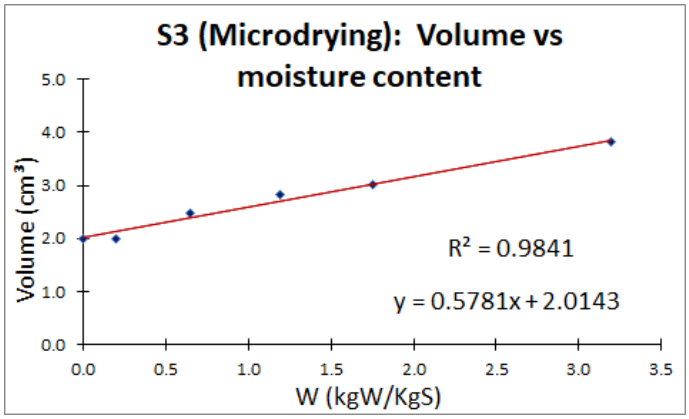

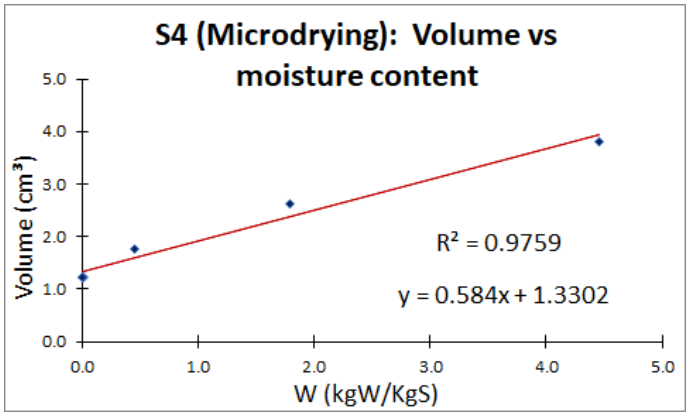

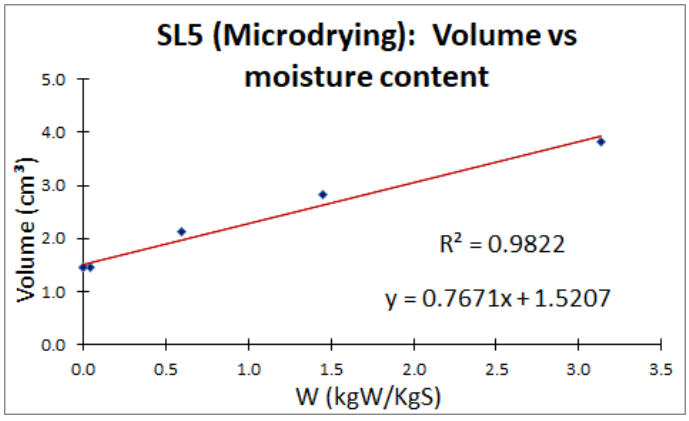

Figure 69: Samples volume change with moisture content during microdrying for each station

11.5 Drying rate vs moisture content before smoothening

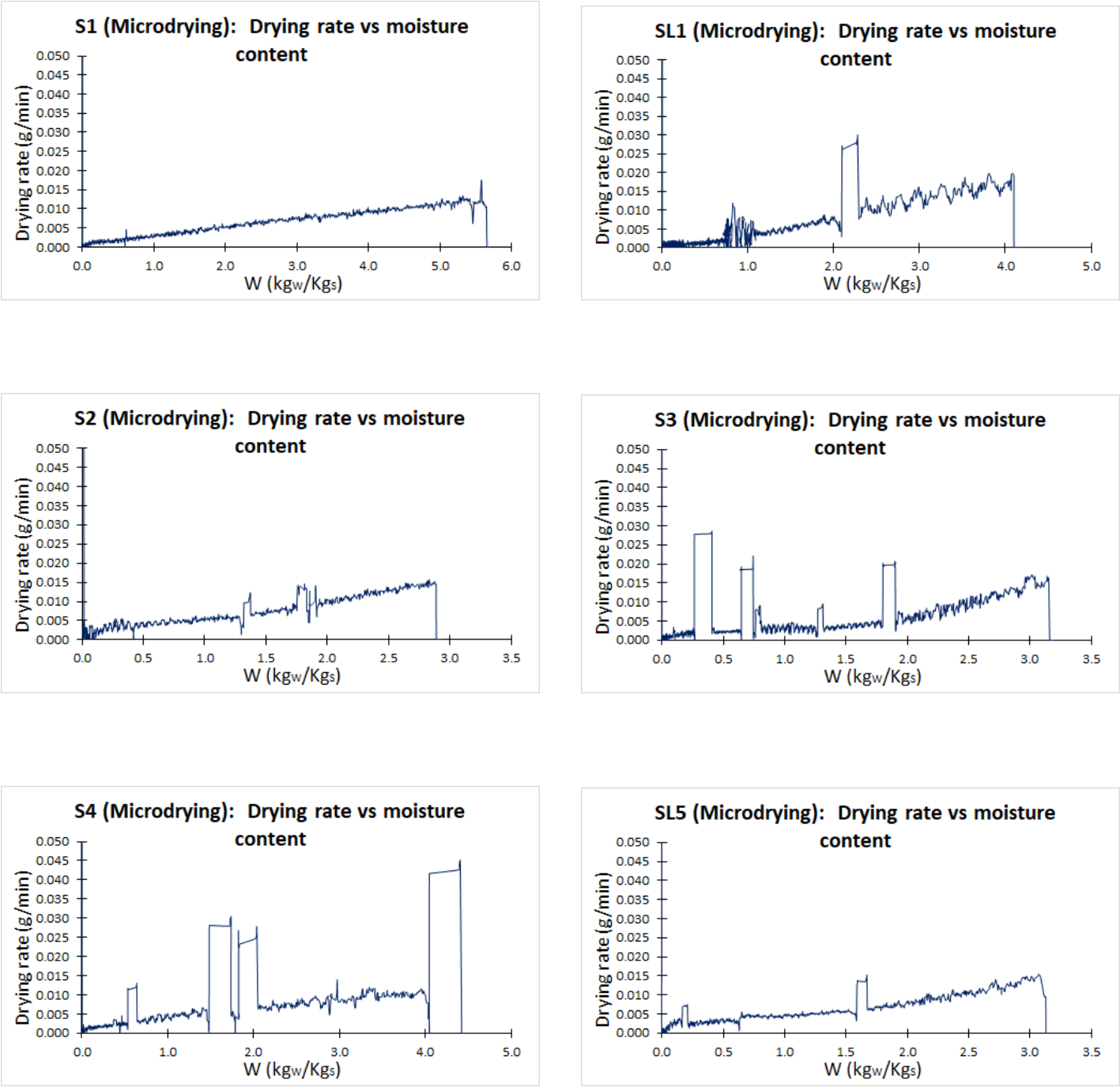

Figure 70: Drying rate vs moisture content before smoothening during microdrying for each station

12 Annex-5- Rheometer-Amplitude Sweep data

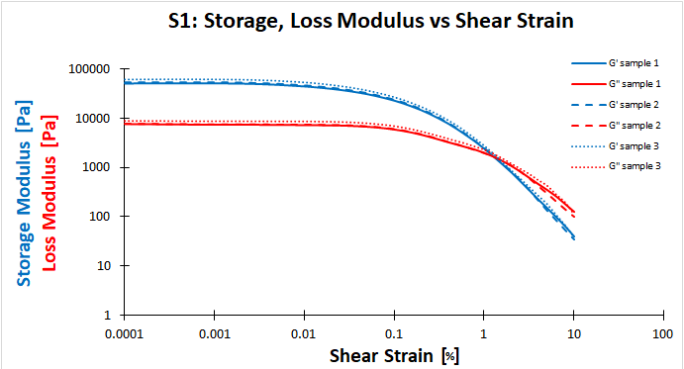

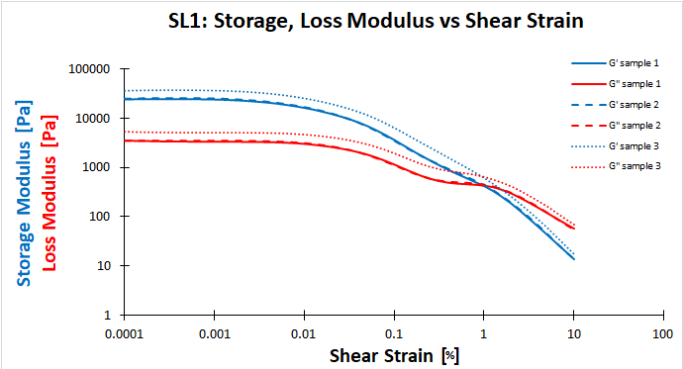

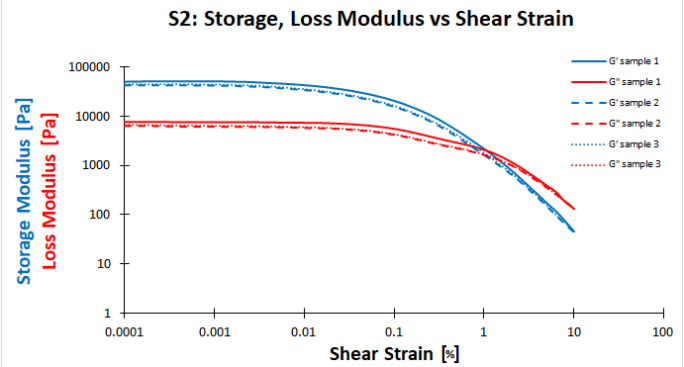

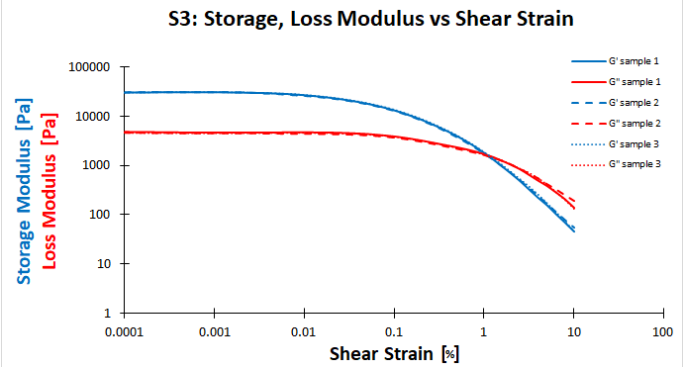

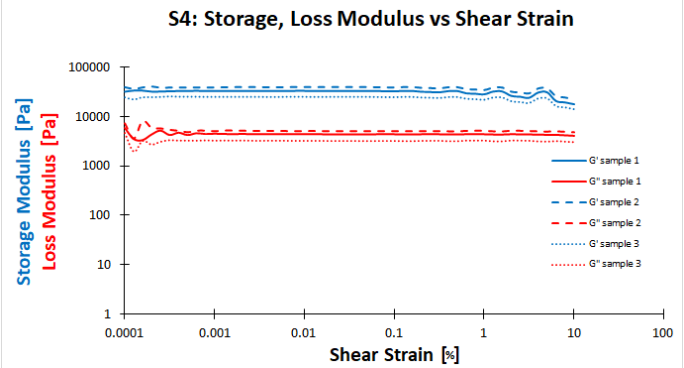

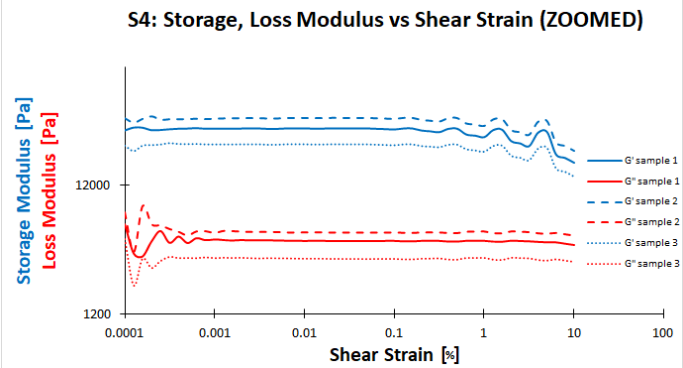

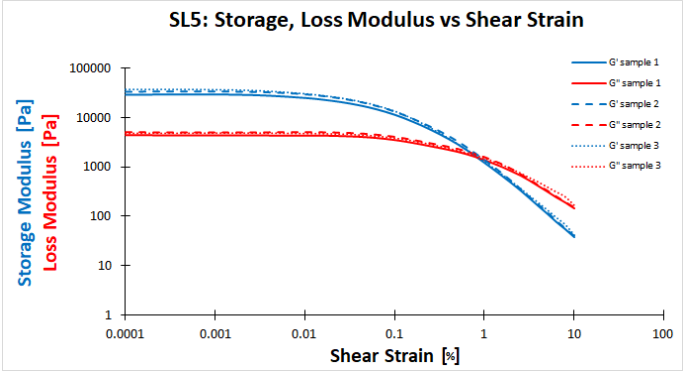

Figure 71: Storage modulus vs shear strain for each station

13 Annex-6- Penetrometry data

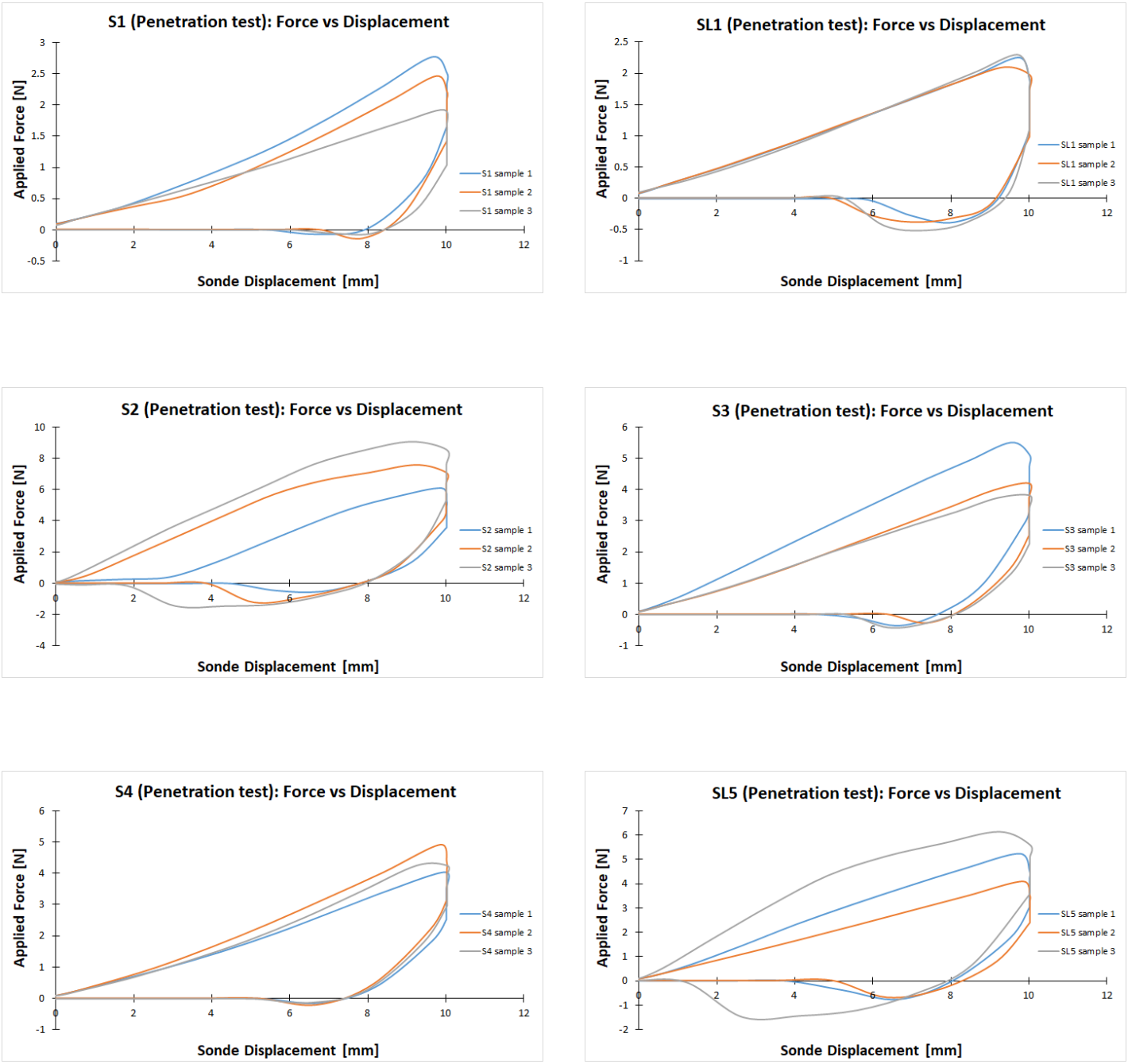

Figure 72: Penetrometry: force vs sonde displacement for each station

14 Annex-7- Texture profile analysis data

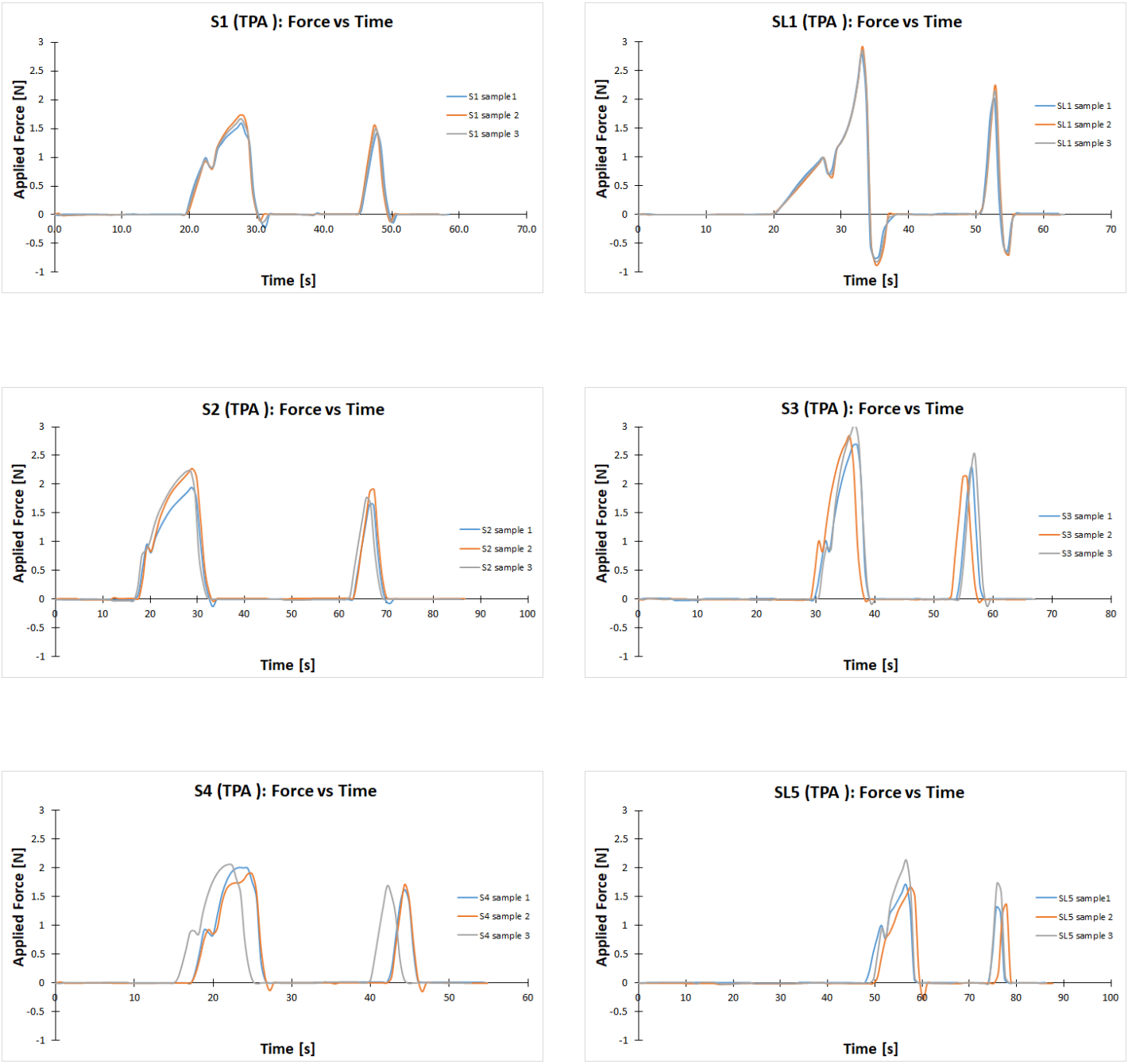

Figure 73: Texture profile analysis: force vs time for each station

15 Annex-8- Matlab code for positive area calculation

```
%import our data
Mr=readmatrix('S1')
Mrr=readmatrix('S2')

x_vals = Mrr(:,??);
y_vals = Mr(:,??);

%%%%%%%%%%%%%%%%%%%%%%%%%%%%%%%%%%%%%%%%%%%%%%%%%%%%%%%%%%%%%%%%%%%%%%% EDIT ME
x_range_start = ??; %  start of the x-range
x_range_end = ??;   %  end of the x-range
%%%%%%%%%%%%%%%%%%%%%%%%%%%%%%%%%%%%%%%%%%%%%%%%%%%%%%%%%%%%%%%%%%%%%%% EDIT ME


 positive_area = 0;

for i = 1:length(x_vals) - 1
    if x_vals(i) >= x_range_start && x_vals(i) <= x_range_end
        if y_vals(i) > 0 && y_vals(i + 1) > 0
            base = min(x_vals(i + 1), x_range_end) - max(x_vals(i),
               x_range_start);
            avg_height = (y_vals(i) + y_vals(i + 1)) / 2;
            area = base * avg_height;
            positive_area = positive_area + area;
        end
    end
end

disp(['Positive area under the specified x-range: ', num2str(
   positive_area)]);
```

16 Annex-9- Matlab code for negative area calculation

```
%import our data
Mr=readmatrix('??')
Mrr=readmatrix('??')

x = Mrr(:,??);
y = Mr(:,??);

%%%%%%%%%%%%%%%%%%%%%%%%%%%%%%%%%%%%%%%%%%%%%%%%%%%%%%%%%%%%%%%%%%%%%%% EDIT ME
x_range_start = ??; %  start of the x-range
x_range_end = ??;   %  end of the x-range
%%%%%%%%%%%%%%%%%%%%%%%%%%%%%%%%%%%%%%%%%%%%%%%%%%%%%%%%%%%%%%%%%%%%%%% EDIT ME

%% Calculate the negative area within the specified range
negative_area = 0;

for i = 1:length(x)-1
    if x(i) >= x_range_start && x(i+1) <= x_range_end
        if y(i) < 0 && y(i+1) < 0
            x_range = [x(i), x(i+1)];
            y_range = [y(i), y(i+1)];

            interp_func = @(xx) interp1(x_range, y_range, xx, 'linear')
                ;

            area_segment = quad(@(xx) -interp_func(xx), x_range(1),
                x_range(2));
            negative_area = negative_area + area_segment;
        end
    end
end
disp(['Negative Area:', num2str(negative_area)]);
```

17 Annex-10- Matlab code for curve smoothening

```
clc
close all
clear all
%%Constantes PARA TODAS LAS PRUEBAS

%% experimental Variables
Mr=readmatrix('?');
ti=Mr(?,?); %time [s]
T=Mr(?,?);%[ C ]
mi=Mr(:,?);%mass [g]
Ai=Mr(:,?);%area [mm2]
xi=Mr(:,?);%humidity [kgw/kg]


%% calculated Variables
tcal=60;%time calculation [s]
int=tcal/ti; % Time interval
m=mi(1:int:end)/(1000);
A=Ai(1:int:end)*(1e-6);
mun=m/m(1)*100;
t=[0:1:(length(m)-1)]*tcal/3600;% Drying time [s]
x=xi(1:int:end); %Sample's  mouisture
ms=-(x-1); %Sample's solid content mouisture
w= x./ms; %Sample's Water-Solid ratio


%% Results
for i=2:1:(length(m))
        F(i,1)=(m(i-1)-m(i))/(tcal/3600);
end
F(1)=F(2)*6/7;
F=F./A;
% F1= smooth(W,F,0.1,'loess');
```

```
34
35 % Par metros de suavizado
36 window_size = 15;
37 s = 5; % Par metro de forma de la ventana de interpolaci n
38
39
40 F1 = zeros(size(F));
41 for i = 1:numel(x)
42     indices = max(i - window_size + 1, 1):min(i + window_size - 1,
       numel(x));
43     weights = sinc((x(i) - x(indices)) * s) .* sinc((x(i) - x(indices))
        / window_size);
44     F1(i) = sum(F(indices) .* weights) / sum(weights);
45 end
46
47 F2 = zeros(size(F));
48 for i = 1:numel(w)
49     indices = max(i - window_size + 1, 1):min(i + window_size - 1,
       numel(w));
50     weights = sinc((w(i) - w(indices)) * s) .* sinc((w(i) - w(indices))
        / window_size);
51     F2(i) = sum(F(indices) .* weights) / sum(weights);
52 end
53
54 Fmax=max(F1)
55 %% Graphics
56
57 hold on
58 subplot(3,1,1)
59 plot(t,mun,'b-')
60 %xlim([0 (3600/ti)])
61 title('Mass loss')
62 ylabel('Unitary mass  (%)')
63 xlabel('Drying time [h]')
64
```



```
65 hold on
66 subplot(3,1,2)
67 plot(t,x,'b-')
68 %xlim([0 (3600/ti)])
69 title('Drying Curve')
70 ylabel('Moisture (KgH2O/Kgs)')
71 xlabel('Drying time [h]')
72
73 hold on
74 subplot(3,1,3)
75 plot(w,F1,'b')
76 %xlim([0 (3600/ti)])
77 title('Drying Curve')
78 xlabel('Moisture wet basis (KgH2O/Kgh)')
79 ylabel('Drying Rate KgH2O/s*m2')
80 %
81 T=table(w,F1,t',mun,x);
82 writetable(T,'SS.xlsx')
```


18 Annex-11- Matlab code to calculate the hardness

```
%import our data
Mr=readmatrix('?')


% Sample force-time data
force_newtons = Mr(:,?);  %applied force in newton
time = Mr(:,?);           % Time values in seconds



max_force = max(force_newtons);      % Maximum force (hardness)


disp(['Max force (hardness): ', num2str(max_force), ' N']);
```